CENTER *for* MUSCULOSKELETAL RESEARCH

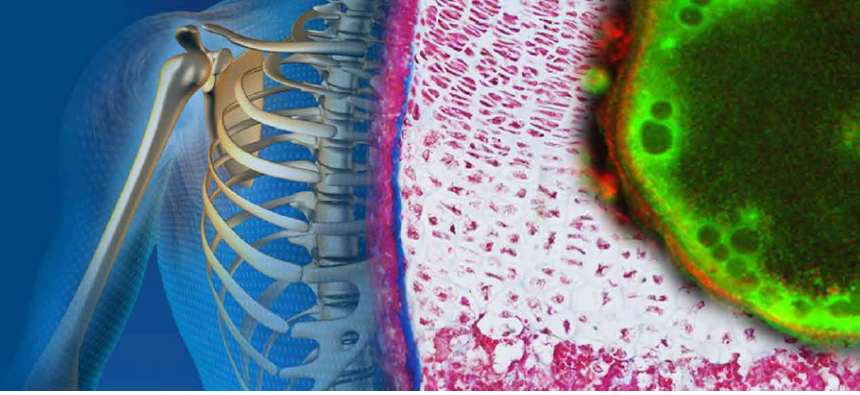

# 13th Annual CMSR Symposium

Thursday, October 26, 2023

## Sponsored By

Department of Orthopaedics and Rehabilitation
University of Rochester Medical Center
&
National Institute of Arthritis and Musculoskeletal and Skin Diseases (NIAMS) Grant T32 AR076950

MEDICINE *of* THE HIGHEST ORDER

UR MEDICINE

# *ROCMSK Training Program*

The Annual Center for Musculoskeletal Research (CMSR) Symposium is the centerpiece of the NIH/NIAMS funded T32 program entitled "Rochester Musculoskeletal (ROCMSK) Training Program" at the University of Rochester Medical Center. This program is designed to provide interdisciplinary didactic and research training in musculoskeletal science.

The overarching goal of ROCMSK Training Program is to develop future generations of interdisciplinary musculoskeletal scientists and leaders of innovations. The program is administered in the CMSR at the University of Rochester and integrates 21 highly collaborative faculty with primary appointments in seven academic and clinical departments.

The CMSR and associated training faculty represent a highly integrated group of mentors that provide research training opportunities in the following disciplines, highlighted by abstracts featured in this Symposium:

- Bone Biology and Disease
- Cartilage Mechanobiology
- Arthritis and Regenerative Therapies
- Tendon Development, Repair, and Regenerative Engineering
- Muscle Biology and Disease
- Drug Delivery
- Fracture Repair and Bone Tissue Engineering
- Musculoskeletal Infection, Stem Cells, and Musculoskeletal Development
- Skeletal Cancer Biology and Therapeutics

The education program ensures a comprehensive understanding of musculoskeletal science that is seamlessly accessible to all CMSR trainees at every academic level. ROCMSK training emphasizes basic and translational science education. The training experience aims to build competency in areas ranging from the most basic molecular and genetic studies to the design and execution of human clinical trials. This year, ROCMSK awarded two pre-doctoral and one post-doctoral training seats.

This Symposium is a celebration of the trainees' accomplishments.

# 13th Annual Center for MusculoSkeletal Research Symposium

**Thursday, October 26, 2023**

Zoom Link

https://urmc.zoom.us/j/97236329590

## Clinical Hour Presentations

**School of Nursing (SON) Auditorium, 1W-304, Helen Wood Hall**

| | | |
|---|---|---|
| 7:00 am | *Welcome & Introduction* | ***Paul Rubery, MD*** |
| 7:02 am | *Intramedullary Nail Versus Plate Fixation for Diaphyseal Humerus Fractures: A Retrospective Comparative Analysis* | ***Urvi Patel, MD***<br>*John Ketz, MD* |
| 7:10 am | *Determining the Role of Posterior Pelvic Ring Fixation Density in Post-operative Pelvic Ring Displacement* | ***James Brodell, MD***<br>*Sandeep Soin, MD* |
| 7:18 am | *Outcomes Following Cubital Tunnel Release With and Without Ulnar Nerve Transposition* | ***Dominique Rinfret, MD Student***<br>*Constantinos Ketonis, MD, PhD* |
| 7:26 am | *New York's opioid restriction law and disparities in opioid fills after total hip/knee arthroplasty* | ***Derek Schloemann, MD***<br>*Caroline Thirukumaran, PhD* |
| 7:34 am | *Phenotyping 1-year Dissatisfaction and Poor Outcomes in Primary TKA Patients with PAM, PROMIS, and OSPRO-YF: Baseline Data Results from 267 Consecutive TKA Patients* | ***Mina Botros, MD***<br>*Thomas Myers, MD* |
| 7:42 am | *Concordance of patient-perceived sports bra size with objective measurement* | ***Elaine Xu, MD Student***<br>*Katherine Rizzone, MD* |
| 7:50 am | *The UR Medicine's Motion Analysis Laboratories - What can be expected?* | ***Ram Haddas, PhD*** |

## Rosier Award Trainee Presentations

**School of Nursing (SON) Auditorium, 1W-304, Helen Wood Hall**

| | | |
|---|---|---|
| 9:00 am | *Welcome & Introduction* | ***Paul Rubery, MD***<br>***Hani Awad, PhD*** |
| 9:05 am | *Why I chose to become the Chairman of the URMC MSKI Council* | ***Sam Guerrieri (UR Alum '87)*** |
| 9:15 am | *We are the CMSR* | ***Jennifer Jonason, PhD*** |
| **Post-Doctoral Fellows** | | |
| 9:15 am | *Mitochondrial genetics influences osteogenic potential of mesenchymal stem cells and bone phenotype in a sex-dependent manner* | ***Sarah Catheline, PhD***<br>*Eliseev Lab* |
| 9:30 am | *TriNetX Analytics Network analyses of the USA population reveals bidirectional associations between Achilles tendinopathy and hypertension mediated by voltage-gated Ca2+ channel CaV1.2* | ***Haiyin Li, PhD***<br>*Cao Lab* |
| 9:45 am | *CCL20/CCR6 limits the disease severity in Staphylococcus aureus osteomyelitis by increasing Th17 and macrophage recruitment at the site of inflammation* | ***Himanshu Meghwani, PhD***<br>*Muthukrishnan Lab* |
| 10:00 am | *Real-Time Fluorescent Microscopy Assessment of PAD4-Mediated NETosis and NET Degradation by S. aureus Nuclease During Nidus Formation on Metal Implants* | ***Youliang Ren, PhD***<br>*Xie/Schwarz Labs* |
| 10:15 am | *Break* | |
| **Pre-Doctoral Trainees** | | |
| 10:30 am | *Tendon-Targeted delivery of drug-loaded nanoparticles to modulate healing* | ***Emmanuella Adjei-Sowah***<br>*Loiselle/Benoit Labs* |
| 10:45 am | *Neurological Markers of Pain and Functional Disability during Romberg's Test in Patients with Lower Back Pain* | ***Justin Jablonski***<br>*Haddas Lab* |
| 11:00 am | *Localized Knee Irradiation Creates Persistent DNA Damage in Chondrocytes and Promotes Joint Hyperalgesia* | ***M. Nick James***<br>*Jonason Lab* |
| 11:15 am | *Ablation of Tumor Derived IGFBP-3 Attenuates Cancer-Associated Skeletal Muscle Wasting via Downregulation of the Ubiquitin Proteasome Pathway* | ***Zachary Sechrist***<br>*Cole Lab* |
| 11:30 am | *The Role of PRDM16 in Craniofacial Development* | ***Eliya Tazreena Tashbib***<br>*Wu Lab* |
| 11:45 am | *3D printed PCL scaffolds containing amorphous calcium phosphate nanoparticles promote long bone regeneration through osteoimmunomodulation* | ***Ming Yan***<br>*Awad Lab* |
| 12:00 pm | *Three-Minute Teasers (3MT) – Finalists for Best Poster Presentations* | |

**12:45 pm** **Lunch & Poster Session** — **Saunders Research Building (SRB) Atrium**

**2:15 pm** **Annual CMSR Photo** — **Saunders Research Building (SRB) Atrium**

## Plenary Session

**School of Nursing (SON) Auditorium, 1W-304, Helen Wood Hall**

### CMSR Faculty Spotlight

2:30 pm **Anne Nichols, PhD**
*Defining the role of the epitenon in tendon health and healing*

3:00 pm **Ram Haddas, PhD**
*Technology & tools for assessing patient's disability and function*

3:30 pm **Sandeep Mannava, MD, PhD**
*Clinical Orthopaedics Update: What is new in training, clinical practice, and patient outcomes*

### Keynote Presentation

**4:00 pm** **Hicham Drissi, PhD**
*Advances in cell and molecular approaches for skeletal tissue preservation and repair*

**5:30 pm** ***Dinner and Rosier Awards Presentation*** — **Evarts Lounge, 1W-133, Helen Wood Hall**

## Keynote Speaker: Hicham Drissi, PhD

**Professor and Vice Chair for Research**
**Department of Orthopaedics**
**Emory University**

Hicham Drissi, PhD is a Professor and Vice Chair for Research in the Department of Orthopaedics at Emory University. Additionally, he leads the Emory University Musculoskeletal Research Center. Dr. Drissi is also a research scientist at the Atlanta VA Medical Center. His federally funded research program has been focused on defining the transcriptional mechanisms that govern skeletal development, homeostasis, and repair. In doing so, Dr. Drissi utilizes a variety of genetic and surgical models, stem cells, and human tissues with a goal of devising therapeutic strategies to preserve or regenerate cartilage, bone, and intervertebral disc tissues. Moreover, his group investigates the effects of growth and systemic factors as well as gut microbiome on cell expansion, recruitment, and differentiation of progenitor populations into chondrocytes, osteoblasts, and osteoclasts in the context of aging.

# Symposium Papers

## Clinical Hour Abstracts

| | | |
|---|---|---|
| 1 | Urvi Patel | Intramedullary Nail Versus Plate Fixation for Diaphyseal Humerus Fractures: A Retrospective Comparative Analysis |
| 2 | James Brodell | Determining the Role of Posterior Pelvic Ring Fixation Density in Post-operative Pelvic Ring Displacement |
| 3 | Dominique Rinfret | Outcomes Following Cubital Tunnel Release With and Without Ulnar Nerve Transposition |
| 4 | Derek Schloemann | New York's opioid restriction law and disparities in opioid fills after total hip/knee arthroplasty |
| 5 | Mina Botros | Phenotyping 1-year Dissatisfaction and Poor Outcomes in Primary Total Knee Arthroplasty Patients with PAM, PROMIS, and OSPRO-YF: Baseline Data Results from 267 Consecutive TKA Patients |
| 6 | Elaine Xu | Concordance of patient-perceived sports bra size with objective measurement |

## Rosier Awards Post-Doctoral Trainee Presentations

| | | |
|---|---|---|
| 7 | Sarah Catheline | Mitochondrial genetics influences osteogenic potential of mesenchymal stem cells and bone phenotype in a sex-dependent manner |
| 8 | Haiyin Li | TriNetX Analytics Network analyses of the USA population reveals bidirectional associations between Achilles tendinopathy and hypertension mediated by voltage-gated Ca2+ channel CaV1.2 |
| 9 | Himanshu Meghwani | CCL20/CCR6 limits the disease severity in Staphylococcus aureus osteomyelitis by increasing Th17 and macrophage recruitment at the site of inflammation |
| 10 | Youliang Ren | Real-Time Fluorescent Microscopy Assessment of PAD4-Mediated NETosis and NET Degradation by S. aureus Nuclease During Nidus Formation on Metal Implants |

## Rosier Awards Pre-Doctoral Trainee Presentations

| | | |
|---|---|---|
| 11 | Emmanuella Adjei-Sowah | Tendon-Targeted delivery of drug-loaded nanoparticles to modulate healing |
| 12 | Justin Jablonski | Neurological Markers of Pain and Functional Disability during Romberg's Test in Patients with Lower Back Pain |
| 13 | Nick James | Localized Knee Irradiation Creates Persistent DNA Damage in Chondrocytes and Promotes Joint Hyperalgesia |
| 14 | Zachary Sechrist | Ablation of Tumor Derived IGFBP-3 Attenuates Cancer-Associated Skeletal Muscle Wasting via Downregulation of the Ubiquitin Proteasome Pathway |
| 15 | Eliya Tazreena Tashbib | The Role of PRDM16 in Craniofacial Development |
| 16 | Ming Yan | 3D printed PCL scaffolds containing amorphous calcium phosphate nanoparticles promote long bone regeneration through osteoimmunomodulation |

## Rosier Award Best Poster Finalists

| | | |
|---|---|---|
| 17 | Kiana Chen | Androgen Treatment Exhibits A Protective Role Against Focal Erosions in TNF-Induced Inflammatory Arthritis in Mice |
| 18 | Cih-Li Hong | The Role of Bone Remodeling in Regulating Hematopoietic Cell Expansion |
| 19 | Kyle Jerreld | Raman Spectroscopy and Reference Point Indentation: Investigating the Predictive Value for Fracture Risk in Femoral Necks |
| 20 | Mark Kenney | High-Throughput Micro-CT Analysis Identifies Sex-Dependent Biomarkers of Erosive Arthritis in TNF-Tg Mice and Differential Response to Anti-TNF Therapy |
| 21 | Gulzada Kulzhanova | Integrative scRNA-seq and spatial transcriptomics uncovers distinct macrophage-fibroblast cross-talk in human hip synovium between patients with FAI and hip OA |
| 22 | Sashank Lekkala | Semi-Automated Cell Tracking and Quantification of Neutrophil Swarming to MRSA on a Bone Implant in a Murine Femur Model |
| 23 | Tianfeng Miao | Tracing the Fate of the Subtypes of Endothelial Cells during Auto- and Allograft Repair and Reconstruction |
| 24 | Yue Peng | Distinct Mast Cell Subpopulations within and around Lymphatic Vessels Regulate Lymph Flow and Progression of Inflammatory-Erosive Arthritis in TNF-tg Mice |
| 25 | Emily Quarato | High levels of efferocytosis by mesenchymal stromal cells increases their senescence and decreases bone |
| 26 | Noah Salama | Aged Mesenchymal Stem Cells Exhibit Distinct Post-Efferocytic Polarization In Vivo by Single Cell RNA Sequencing |
| 27 | Azmeer Sharipol | Acute myeloid leukemia (AML)-on-a-chip recapitulates the leukemic cell-mediated dysregulation of the bone marrow microenvironment in vitro |
| 28 | Celia Soto | Effects of Elevated Lactate in Acute Myeloid Leukemia Bone Marrow Microenvironment Dysfunction, with a Dual Role of GPR81 Signaling in Macrophage Polarization and Leukemia Cell Growth |
| 29 | Chen Yu | Mitochondrial Metabolism Determines Mesenchymal Stem Cell Fate |
| 30 | Victor Zhang | The Role of Type III Collagen in TEndon Fibrosis: Insights from Hydrogel Models for Scarless Tendon Repair |

## Posters

| | | |
|---|---|---|
| 31 | Nikhil Ailaney | Physical and Cognitive Function during Post-Acute Care following Total Joint Arthroplasty among Medicare Beneficiaries: Trends from 2013-2018 |
| 32 | Nikhil Ailaney | Short Term Pain in Cemented versus Cementless Total Knee Arthroplasty: A Systematic Review and Meta-Analysis |
| 33 | Rahul Alenchery | Unraveling the Role of mTOR in Tendon Fibrosis: Implications for Targeted Therapies and Scar-Free Healing |
| 34 | Mina Botros | Cutibacterium acnes deforms and invades submicron osteocyte lacuno-canalicular networks (OLCN) following implant-associated osteomyelitis |
| 35 | James Brodell | Increased Pelvic Asymmetry following Pelvic Ring Fixation of Lateral Compression Injuries When Compared to Anterior-Posterior Compression Injuries |

| | | |
|---|---|---|
| 36 | James Brodell | Exploring Differences in Length of Stay and Discharge Patterns Among Pelvic Ring Injury Patterns |
| 37 | Joseph Bucukovski | Using Integrated Photonic Sensors in a Tendon-on-a-Chip Model |
| 38 | Philomena Burger | A Comparative Analysis of Outcomes Using PROMIS After Operative Versus Non-operative Treatment of Achilles Rupture |
| 39 | Philomena Burger | Assessing the Musculoskeletal Health Literacy and Social Network Distribution of Hip and Knee Osteoarthritis Patients at an Academic Medical Center |
| 40 | Thomas Carroll | Diagnosis of Ulnar Neuropathy at the Elbow Using Ultrasound – A Comparison to Electrophysiologic Studies |
| 41 | Thomas Carroll | Development of de Quervain's Tenosynovitis After Distal Radius Fracture |
| 42 | Thomas Carroll | Clinical and Radiographic Outcomes Following Volar Locked Plating Versus Dorsal Bridge Plating for Distal Radius Factures: A Propensity Score-Matched Analysis |
| 43 | Thomas Carroll | Predicting Acute Median Neuropathy in Perilunate Injuries |
| 44 | Alexander Chirokikh | Comparison of Patient-Reported Outcome Instruments in the Pre-Operative Evaluation of Cubital Tunnel Syndrome |
| 45 | Alexander Chirokikh | Where Does Ultrasound Fit in the Diagnostic Algorithm for Cubital Tunnel Syndrome? |
| 46 | Michael Christof | Effects of Sex and Derivation Location on Osteoclast Formation and Activity |
| 47 | Wimeth Dissanayake | Characterization of the bone marrow mesenchymal stromal cells in low dose irradiation model |
| 48 | Akhil Dondapati | Endoscopic Carpal Tunnel Release with MAC Versus Local Anesthesia - Analysis of Operative Times and Patient Reported Outcomes |
| 49 | Renae Duncan | Role of mitochondrial genetics in the response of osteogenic cells and bone tissue to mechanical stimulation |
| 50 | Jabea Ekabe | SLAMF7 engagement augments TNF-α secretion in activated monocytes |
| 51 | Eloise Fadial | PRDM16 positively regulates chondrogenesis and knee joint homeostasis |
| 52 | Hunter Gilbreath | A Novel Method for Evaluating Disability and Function in Patients with Injuries Sustained in Sports Medicine Utilizing Human Motion Lab |
| 53 | Rajkumar Govindan | GsMTx4 conjugate reduces chondrocyte vulnerability to mechanical injury ex vivo |
| 54 | Melissa Holloway | Functional Outcomes and Complications Following Anterolateral Versus Posterior Surgical Approaches for Open Reduction and Internal Fixation of Humeral Shaft Fractures: A Retrospective Review |
| 55 | Melissa Holloway | No Differences in Clinical, Functional, or Patient-Reported Outcomes Following Trial of Non-operative Management Prior to Open Reduction and Internal Fixation of Humeral Shaft Fractures |
| 56 | Chen Jiang | Autologous and Allogenic In vivo Engineered Extracellular Matrix as Tissue-Engineered Periosteum for Defect Repair |
| 57 | Xingyu Jing | Piezo2 Regulation in Chondrocytes Post-Exercise |
| 58 | Jane Jurayj | Patient Demographics Does Not Correlate with Patient Reported Quality of Knee and Hip Osteoarthritis Care |
| 59 | Christina Kaszuba | The Role of Taurine in Hematopoiesis |
| 60 | Amal Khan | Elucidating the Mechanism of CCL3-Driven Bone Marrow Dysfunction during Acute Myelogenous Leukemia |

| | | |
|---|---|---|
| 61 | Alanna Klose | Constructing a mixed Arrayed Imaging Reflectometry sensor for simultaneous quantification of antibodies and cytokines in human serum |
| 62 | Manohar Koduri Veera Venkata | Engineering microvasculature in periosteum biomimetic for bone defect repair and reconstruction |
| 63 | Mikkael Lamoca | Investigating the Effects of Stiffness and Topography on TRPV4 |
| 64 | Kevin Lee | An Intravital Imaging Protocol to Visualize and Phenotype the Associated Niche of Clonal Hematopoiesis |
| 65 | Melissa MacLiesh | Characterizing bone marrow interstitial pH by two-photon ratiometric imaging |
| 66 | Michaela Malin | Disparities in no-show rates in a sports medicine orthopedic clinic |
| 67 | Alyson March | In vitro surrogate for vascularization to predict hydrogel mediated allograft healing in tissue engineered periosteum |
| 68 | Katya McDonald | Identification of T cell exhaustion as a biomarker of Staphylococcus aureus chronic osteomyelitis in humanized mice |
| 69 | Hayley Miller | StretchToC: a tendon-on-a-chip platform for studying the impact of mechanical forces in fibrotic adhesions |
| 70 | Philip Milton | A novel adoptive dendritic cell targeting delivery of TNF combined with an IAP antagonist to treat breast cancer |
| 71 | Samantha Muscat | Characterizing the Achilles Tendon Mechanoresponse to Voluntary Wheel Running |
| 72 | Swachi Patel | High levels of MSC Efferocytosis Cause Myeloid Skewing |
| 73 | Urvi Patel | The Effect of Racial and Economic Inequity on Complication Rates and Patient-Reported Outcomes Following Open Reduction and Internal Fixation of Humeral Shaft Fractures |
| 74 | Melanie Perkins | Role of PD-1 in B cell dysregulation in autoimmunity |
| 75 | Tiffany-Rae Robinson | Leveraging a Poly(ethylene glycol) (PEG) Biomaterial to Guide Tenocyte Fate |
| 76 | Andrew Rodenhouse | Postoperative Complications of the Hand Following Shoulder Surgery |
| 77 | Derek Schloemann | Association of Medicare Merit-Based Incentive Payment System Quality Scores with Unplanned Hospital Visits after Outpatient Orthopedic Surgery |
| 78 | Derek Schloemann | Association of Patient, Surgeon, and Facility Factors with Unplanned Hospital Visits after Outpatient Orthopedic Surgery |
| 79 | Derek Schloemann | Association of New York's opioid prescribing restrictions with opioid fills following total hip and knee arthroplasty |
| 80 | Gilbert Smolyak | Pharmacological Modulation of Extrinsic Macrophage Recruitment to Facilitate Regenerative Tendon Healing |
| 81 | Levy Sominsky | Optimization of an In Vitro Model of Staphylococcal Abscess Communities to Study Bactericidal Mechanisms |
| 82 | Janet Tran | Impact of Social Deprivation on Cubital Tunnel Syndrome |
| 83 | Janitri Venkatachala Babu | Targeting TRPC6 for Discogenic Chronic Back Pain |
| 84 | Valerie Voytsekhovskaya | Bone increase in mice with global Axl loss of function is not due to changes in embryonic skeletal development |
| 85 | Brian Wise | Achilles Tendon Impingement Elicits Spatially-Dependent Change in Aggrecan Metabolism |
| 86 | Anthony Yosick | Longitudinal µCT Image Analysis for User-Defined Region of Interest in Critical-Sized Bone Defects |

| | | |
|---|---|---|
| 87 | Yaxin Zhang | Sex-dependent Piezo1 and Piezo2 Functional expression in articular cartilage |
| 88 | William Zhuang | Diversity among academic sports medicine surgeons in the United States |
| 89 | Wendy Zimmerman | The Effects of Slit3 on Angiogenesis and Osteogenesis of Bone Marrow Cells Isolated from AplinCreERT2 and BMXCreERT2 Mice |
| 90 | Jose Corredor | Disability and Function Outcome Measurements Reports for Patients with Musculoskeletal Disorders |
| 91 | Hansen Lu | An Objective Assessment of Low Back Disorder Patients' Disability and Function using a Wearable Inertial Measurement Unit |

# *Clinical Hour Abstracts*

## Disclaimer

**PAPER #1**

**TITLE:** Intramedullary Nail Versus Plate Fixation for Diaphyseal Humerus Fractures: A Retrospective Comparative Analysis

**PRESENTING AUTHOR:** Urvi J. Patel, MD, MS

**CO-AUTHOR(S):** Melissa R. Holloway, BS, Thomas J. Carroll, MD, Sandeep Soin, MD

**LAB PI/MENTOR:** John P. Ketz, MD

**ABSTRACT**

Purpose: The purpose of this study is to analyze the outcomes following intramedullary nail (IMN) fixation versus open reduction and internal fixation (ORIF) in patients with diaphyseal humeral shaft fractures. We specifically sought to compare time to radiographic union, complication rates, operative times, operative blood loss, and functional outcomes.

Methods: We retrospectively reviewed patients undergoing surgical intervention for diaphyseal humeral shaft fractures at a single, level-1 trauma center. Ultimately, 193 patients met our inclusion criteria. Patients under the age of 18, those with impending pathologic fracture, and those with intra-articular fracture extension were excluded. Demographic characteristics, AO/ OTA fracture classification, time to union, complications, operative details, and PROMIS outcomes were reviewed and analyzed. Statistical significance was set at $p<0.05$.

Results: In our cohort, 152 patients underwent ORIF and 41 patients underwent IMN fixation for their humeral shaft fracture. Time to surgery averaged 5.42±10.7 days and 7.52±7.16 days for the ORIF and IMN groups, respectively ($p=0.24$). Mean intraoperative blood loss was 333±315 cc for the ORIF cohort and 155±126 cc for the IMN cohort ($p<0.01$). Total operative time was 214±86 mins and 191±58 mins for the ORIF and IMN groups, respectively ($p=0.21$). Time to union was 17.8±9.3 weeks in the ORIF group and 19.1±10.6 weeks in the IMN group ($p=0.23$). Six patients in the ORIF group and 4 patients in the IMN group went on to non-union ($p=0.15$). We found 29 patients in the ORIF group and 2 patients in the IMN group to have iatrogenic radial nerve palsy post-operatively ($p=0.04$). Secondary radial nerve palsy was significantly predicted by increased time to surgery ($p=0.02$) and patients with type 12-A humeral shaft fractures ($p=0.01$). There was no significant difference in PROMIS Physical Function (PF) ($p=0.97$), Depression ($p=0.18$), and Pain Interference (PI) ($p=0.72$) scores across the two groups.

Conclusion: Our study demonstrates that IMN fixation for diaphyseal humerus fractures presents with lower rates of intraoperative blood loss and iatrogenic radial nerve injury. Factors which predicted radial nerve injuries were longer times to surgery and OTA classified type A fractures. Total operative time, time to union, PROMIS scores, and the incidence of nonunion and postoperative infections were equivocal between the two cohorts.

**PAPER #2**

**TITLE:** Determining the Role of Posterior Pelvic Ring Fixation Density in Post-operative Pelvic Ring Displacement

**PRESENTING AUTHOR:** James D. Brodell, Jr., M.D.

**CO-AUTHOR(S):** Hashim Shaikh, Urvi J. Patel, M.D., John P. Ketz, M.D., John T. Gorczyca, M.D.

**LAB PI/MENTOR:** Sandeep Soin, M.D.

**ABSTRACT**

Purpose

To determine if posterior pelvic ring fixation density affects post-operative pelvic ring displacement. We hypothesized that greater posterior pelvic ring fixation density leads to less post-operative pelvic ring displacement.

Methods

A retrospective chart review was performed for all patients who underwent surgical fixation of pelvic ring injuries. Patients were included if they had an anterior-posterior pre-operative, same day post-operative, and six month follow up plain films of the pelvis available. Measurements were made according to the methodology previously described by Keshishyan. We stratified our cohort into categories based on the presence of sacroiliac (SI) or trans-sacral trans-iliac (TS) screws: (0 SI: 0 TS, 1 SI: 0 TS, 1 SI: 1 TS, 0 SI: 1 TS, 0 SI: 2 TS, 2 SI: 0 TS, and finally 2 SI: 1 TS). Change in pelvic displacement was determined by subtracting the displacement at final follow up from the displacement measurement immediately following fixation. Significance was set at a p-value $< 0.05$.

Results

279 patients met our inclusion and exclusion criteria. Average age was 45±19 years. Average time of radiographic final follow up was 1.3±7 years. Average change in displacement was 1.0±6.5mm. The three most frequently observed constructs were: 1SI: 0 TS (32.6%), anterior only fixation (26.1%), and 2SI: 0 TS (18.9%). One-way ANOVA analysis demonstrated no significant difference in preoperative displacement between the 7 groups ($p=0.14$). Regression analysis found that patients who had (1SI: 0 TS) screw had significantly less change in displacement when referenced against patients with no posterior constructs (0SI: 0 TS). No significant difference was found between the remaining constructs and change in displacement when referenced against patients with 0 SI: 0 TS screws. Finally, it should be noted that the number of screws placed in the anterior pelvic ring was nonsignificant in predicting loss of reduction at final follow up.

Conclusion

We found that one SI screw leads to decreased displacement at final follow-up relative to no posterior fixation, though more dense posterior fixation constructs did not prevent displacement. Traditional fixation methods combined with restricted weight bearing provide adequate restriction to motion of the pelvis. Increased posterior fixation density does not result in decreased pelvic motion.

**PAPER #3**

**TITLE:** Outcomes Following Cubital Tunnel Release With and Without Transposition

**PRESENTING AUTHOR:** Dominique Rinfret

**CO-AUTHOR(S):** Dr. Thomas Carroll, Dominique Rinfret, Justin Wong, Dr. Akhil Dondapati, Dr. Constantinos Ketonis

**LAB PI/MENTOR:** Dr. Constantinos Ketonis

**ABSTRACT**

Introduction:
Cubital tunnel release (CuTR) for ulnar neuropathy at the elbow (UNE) is an increasingly common procedure. The decision to transpose the ulnar nerve is determined in large part by the subluxation status pre-operatively and intra-operatively. The purpose of this study was to evaluate the outcomes following CuTR with and without ulnar nerve transposition. We hypothesize that patients with subluxation who ultimately underwent transposition would have more severe pre-operative electrodiagnostic studies (EDX) and greater symptom improvement.

Methods:
This is an 8-year retrospective study of 94 patients who underwent isolated CuTR with or without transposition. Patients younger than 18 years old, older than 75 years old, those undergoing revision surgery, and those undergoing concomitant procedures were excluded. EDX measurements and severity scores were compared between the two groups.

Results:
In total, 34 patients underwent CuTR with transposition and 60 patients without transposition. The transposition group was significantly younger (45.0 +/- 14 vs 54.1 +/- 11.3; $p<0.05$). Sex, race, ethnicity, and laterality were similar between the two cohorts ($p>0.05$). Pre-operative EDX severity score was worse among the transposition group (Severe: 41.2% vs 18.3%; $p<0.05$). Pre-operative Tinel's sign was similar between the two groups (47.1% vs 58.3%; $p=0.35$). The proportion of patients with pre-operative nerve subluxation and intra-operative subluxation was higher among the transposition cohort (Pre-Op: 26.5% vs 0.0%; $p<0.05$) (Intra-Op: 67.6% vs 0.0%; $p<0.05$). Post-operative numbness and tingling as well as ulnar motor weakness was similar between groups (Numbness/Tingling 35.3% vs 41.7%; $p=0.36$) (Ulnar Motor Weakness 23.5% vs 11.7%; $p=0.33$).

Conclusions:
Compared to patients who ultimately did not undergo ulnar nerve transposition, those undergoing CuTR with transposition were significantly younger, had more severe EDX severity, and had a higher proportion of pre-operative and intra-operative subluxation. The proportion of patients reporting subjective symptoms as well as objective physical exam findings pre- and post-operatively was similar between groups. Revision surgery and complication rates between both groups were not significantly different.

**PAPER #4**

**TITLE:** New York's opioid restriction law and disparities in opioid fills after total hip/knee arthroplasty

**PRESENTING AUTHOR:** Derek Schloemann, MD, MPHS

**CO-AUTHOR(S):** Benjamin Ricciardi, MD; Meredith Rosenthal, PhD; Kevin Fiscella, MD, MPH; Jalpa Doshi, PhD; Caroline Thirukumaran, MBBS, MHA, PhD

**LAB PI/MENTOR:** Caroline Thirukumaran, MBBS, MHA, PhD

**ABSTRACT**

Introduction
New York (NY) implemented Section 3331 in July 2016 to limit the prescription of opioids for acute pain to 7 days. Our objective is to examine the association of Section 3331 with racial/ethnic differences in opioid fills following total hip/knee arthroplasty (THA/TKA) for Medicare beneficiaries.

Methods
We used 2014-2019 Medicare data to identify THA/TKA in NY (treatment group) and California ([CA]; the control group-CA did not have a similar opioid restriction). Outcomes were 1+ opioid fills in the 15 days before admission to 7 days after discharge ("7-day"), 8 to 30 days after discharge, and 31 to 90 days after discharge. Key independent variables were state (NY/CA), phase (before[2014-2015] or after[2017-2019] Section 3331 implementation), patient race/ethnicity (White, Black, Hispanic), and their interactions. We estimated multivariable hierarchical linear probability models with triple differences estimation (a method for policy evaluation). All models controlled for patient- and hospital-level covariates, and hospital random effects.

Results
For 71,565 encounters, the mean age (SD) was 73.77(5.56) years, 61.55% were female, and 94.50% were White. On multivariable analysis and before Section 3331, opioid fill rates in the 7 day period were 88.84%, 87.92%, and 74.93% for White, Black, and Hispanic patients in NY. With Section 3331 implementation, opioid fill rates in the 7 day period increased by 2.57% points for White (95% CI: 1.10 to 4.04, p<0.001) and 19.78% points for Hispanic patients (95% CI: 4.07 to 35.48, p=0.01) in NY. Hence, Section 3331-associated increase in opioid fills in NY was 9.24% points higher for White (95% CI: 7.49 to 10.99, p<0.001) and 25.79% points higher for Hispanic patients (95% CI: 9.14 to 42.44, p=0.002) compared to CA. However, these increases were not different between race/ethnicity groups.

Conclusion
Section 3331 was associated with a significant increase in opioid fills in the immediate post-TJA period for White and Hispanic patients. Because Section 3331 restricts opioids to 7 days, higher-than-average opioid prescriptions are filled during this period. However, these changes did not significantly differ between racial/ethnic groups, highlighting that the law did not differentially influence opioid access for Black/Hispanic compared to White patients.

**PAPER #5**

**TITLE:** Phenotyping 1-year Dissatisfaction and Poor Outcomes in Primary Total Knee Arthroplasty Patients with PAM, PROMIS, and OSPRO-YF: Baseline Data Results from 267 Consecutive TKA Patients

**PRESENTING AUTHOR:** Mina Botros

**CO-AUTHOR(S):** Hashim Shaikh, Kevin T. McCaffery, Ashley Owens, Courtney Jones, Edward M. Schwarz, Thomas G. Myers

**LAB PI/MENTOR:** Dr. Schwarz & Dr. Myers

**ABSTRACT**

INTRODUCTION: The ability to properly identify patients who are deemed high risk for dissatisfaction and poor outcomes is crucial to allow surgeons to target preoperative optimization to provide maximum value patients, payors, and health systems. To this end, the long-term objective of this study is to identify the proportion of patients undergoing total knee arthroplasty (TKA) who are at high risk for dissatisfaction or poor outcomes by the utilization of the Patient Activation Measure (PAM), Patient Reported Outcomes Measurement Information System (PROMIS), and Optimal Screening for Prediction of Referral and Outcomes-Yellow Flag (OSPRO-YF). Utilization of the PAM and PROMIS scores is limited in the TKA patient population. Use of the OSPRO-YF has not been reported in the TKA patient population to date.

METHODS: This is a single site, prospective, observational, IRB-approved study, where we enrolled 267 consecutive patients undergoing TKA within our institution. Subjects were asked to complete a PAM survey, PROMIS survey, and OSPRO-YF questionnaire. Patients also filled out questionnaires/surveys preoperatively, 6 weeks follow-up, 90-day follow-up, and at 1 year. The primary outcome is the mean pre-surgery PAM score among patients who are satisfied versus those that are dissatisfied. To calculate the study sample size assumptions were made based on previous studies in total joint arthroplasty populations. To show a mean difference of 15 points in the pre-surgery PAM scores in patients who are satisfied versus dissatisfied requires 23 subjects per group. Satisfaction is assessed at 1 year. Demographic variables were collected from individual patient information extracted from subject's chart. Included subjects are those older than 18 years of age undergoing primary TKA. Excluded subjects are patients with any previous knee surgery beyond a knee scope. A poor outcome is defined as a manipulation under anesthesia, emergency room visit within 90 days, readmission within 90 days, or reoperation within 1 year. For this preliminary analysis of the baseline data, we compared the hypothesized "high risk group" (PAM levels 1 or 2) versus "low risk group" (PAM levels 3 or 4) based on previous studies.

RESULTS: Among the 267 enrolled subjects, 244 (91%) were classified as low risk PAM 3 or 4. There was no difference in age sex, race, or laterality between groups. Of note, high-risk subjects had higher PROMIS Pain score (63.16 ± 4.35 vs, 59.58 ± 6.03; $p<0.01$) and higher PROMIS depression score (50.8 ± 8.5 vs. 46.02 ± 8.2; $p<0.01$), but there was no difference in preoperative PROMIS physical function score ($p=0.71$) and KOOS Jr scores ($p=0.34$). High-risk subjects tended to have a significantly higher mean number of "flags" on OSPRO-YF subscale measures PHQ9 (48% vs. 18%; $p<0.001$), STAI (39% vs. 14%; $p<0.01$), STAXI (26% vs. 6%; $p<0.001$), PSEQ (70% vs. 46%; $p=0.03$), SER (61% vs 37%; $p=0.03$). Additionally, high-risk patients have a significantly higher number of "flags" on the OSPRO-YF negative mood domain (65% vs. 27%; $p<0.0001$) and have a higher median OSPRO-YF yellow flag count (7 vs 4; $p<0.01$).

CONCLUSION: Preliminary analysis of this prospective dataset demonstrate that a large majority of elective TKA patients are at low risk of dissatisfaction. We also found a significant correlation among low patient activation (PAM 1 or 2) and nearly half of the yellow flags across the OSRPO-YF subscales as well as the PROMIS pain and PROMIS depression subscales. While the relationship between these preoperative measures and satisfaction at 1 year have yet to be determined, we hypothesize that at least some of these measures will identify domains for preoperative optimization and therapeutic intervention to significantly improve value. It is crucial that establishing PAM, PROMIS and OSPRO-YF thresholds for high-risk patients whose activation level could be modified prior to elective TKA is of great value to patients and healthcare systems.

**PAPER #6**

**TITLE:** Concordance of patient-perceived sports bra size with objective measurement

**PRESENTING AUTHOR:** Elaine Xu

**CO-AUTHOR(S):** Katherine Rizzone, Sarah Lander, Michael Maloney, Rebecca Grant, Sarah Lesko, Bianca Edison, Courtney Jones

**LAB PI/MENTOR:** Katherine Rizzone

## ABSTRACT

**Introduction**

Sports bras are an essential piece of sporting equipment for women to be able to participate comfortably in sports and physical activity. The breasts sit atop of the chest with minimal anatomical support and move with multidirectional forces. This motion can lead to breast pain during activity, which is a commonly reported obstacle to physical activity for women. Dampening of these motions with suitable support for the breasts can enable women to participate in sport. However, in the limited data that exists on sports bra fit, it has been found that women wear ill-fitting bras more often than well-fitting bras. Furthermore, bra fit appropriateness has not been previously studied in an American cohort or in an adolescent population. Our hypothesis was that most women are not wearing appropriately fitting bras while being active.

**Methods**

This was a cross-sectional study of girls and women participants who were seen in the University of Rochester Medical Center (URMC) Orthopaedics sports medicine clinics for a musculoskeletal complaint. Women and girls ages 11-64 years old were eligible for recruitment. All subjects gave informed consent for inclusion before their participation in the study. The study protocol was approved by the URMC Institutional Review Board. Participant demographics, sports bra characteristics, preferences, and history of sports bra usage were collected from each participant, in addition to their self-reported bra size. Bra size was objectively measured by study staff using a uniform method of measuring band and bust size. Cup size was calculated from these measurements. Statistical analyses were performed to assess for concordance using SAS, version 9.4 (Cary, NC).

**Results**

There were 69 women and girls in the cohort. Mean age was 22.5+/-12.4 years and 88.4% were white. The most commonly self-reported band size was 34 (n=21), cup size B (n=19) and the most commonly reported comprehensive bra size was 34A (n=8). The most commonly measured band size was 34 (n=26), cup size C (n=17), and the most commonly measured comprehensive bra size was 34B (n=12). Of the 58 reported band sizes, 56.9% did not match the objectively measured band size, with the vast majority of discordance being underestimations (87.9%). Of the 59 reported cup sizes, 44.1% did not match the objectively measured cup sizes, with the majority of the discordance being overestimations (61.5%). Examining both components (cup and band size), there was 58.1% discordance between self-reported and objectively determined measurements.

While the majority of participants (69.6%) were satisfied/very satisfied with the fit of their sports bra, only a third (34.8%) reported they had previously had a professional bra fitting and 39.1% reported that they felt their breast size had increased in the past year. The top feature for selecting a sports bra was the amount of support it provided (62.3%). More than half (69.6%) felt that a sports bra was important/very important to their ability to participate in activity and 11.6% had not practiced or worked out due to lack of a sports bra.

A third (33.3%) reported they had breast pain and 26.1% reported breast swelling during their menstrual cycle. 33.3% of women reported that breast swelling affects the fit of their sports bra and 27.3% felt asymmetry impacts the fit of their sports bra. A small segment reported they avoid working out because of how their breasts (7.3%) or nipples (10.1%) look.

**Conclusions**

Our results show that there is a large discordance between perceived and objectively measured sports bra size. Improper bra fit may be a contributor to women being inactive or prevent them from comfortably participating in sports. Important next steps from this pilot project are to purposefully recruit a more representative sample of subjects to better reflect the demographics of American women, in addition to looking at data in athletes versus non-athletes and obese and non-obese women.

# *Rosier Award Finalists Post-Doc Abstracts*

## Disclaimer

**PAPER #7**

**TITLE:** Mitochondrial genetics influences osteogenic potential of mesenchymal stem cells and bone phenotype in a sex-dependent manner

**PRESENTING AUTHOR:** Sarah Catheline

**CO-AUTHOR(S):** Renae Duncan, Roman Eliseev

**LAB PI/MENTOR:** Roman Eliseev

**ABSTRACT**

Introduction: Osteoporosis is the most common bone disease in the world with estimated 200 million cases globally. While aging and sex steroid levels are considered critical risk factors for osteoporosis, mitochondrial function and genetics are increasingly being recognized as determinants of bone health. Recent studies show that mitochondrial genome variants in different human populations have developed out of a need to modify mitochondrial coupling efficiency to create heat based on geographical location. In humans, bone phenotype correlates to mitochondrial haplogroup, with more efficient mitochondria resulting in stronger bones. Thus, we hypothesize that mitochondrial mtDNA haplogroup and oxidative phosphorylation efficiency are determinants of bone phenotype.

Methods: To test our hypothesis, we use C57BL/6 and C3H mice that have different mtDNA haplogroups and also different bone phenotype and aging-related bone loss. We also use mitochondrial nuclear exchange (MNX) mice that feature mtDNA from either C57BL/6 or C3H mice and the nuclei from the opposite strain (C3Hn;C57mt a.k.a. C3H MNX mice or C57n;C3Hmt a.k.a. C57 MNX). Using these strains, the effect of mtDNA transfer on bone phenotype can be studied. Serum, hindlimbs and vertebrae were harvested from 3-month (3M) and 13-month-old (13M) WT and MNX mice from both strains for micro-CT, histology, biomechanical testing, and serum CTX-1 and P1NP ELISA (systemic readouts of bone resorption and bone formation, respectively). Bone marrow stromal cells (BMSCs) were harvested from C57 WT and C57 MNX mice and osteogenic induction was measured using alkaline phosphatase staining and qPCR. Ongoing experiments are evaluating the in vitro osteogenic potential of C3H WT vs. MNX BMSCs and the in vivo osteoclast and mature osteoblast populations histologically, as measured by TRAP staining and osteocalcin immunofluorescence.

Results: Despite having more efficient C3H mitochondria, C57 MNX mice show no obvious improvement over C57 WT mice in bone phenotype as revealed with micro CT. Interestingly, consistent with our hypothesis, female C3H MNX mice that have less efficient C57 mitochondria, show a reduction in both trabecular BV/TV and cortical thickness relative to WT femurs at 13M. This accelerated bone loss in the 13M-old C3H MNX female femurs corresponded to a reduction in biomechanical strength. In addition, 13M-old female C3H MNX mice display significantly decreased P1NP and increased CTX-1 serum concentrations relative to WT controls. Since MNX is global, the effects may be due to systemic changes. Therefore, we are now focusing on in vitro studies specifically in osteogenic lineage. Our initial in vitro experiments indicate that BMSCs from male C57 MNX mice have increased osteogenic markers relative to WT cells, namely enhanced alkaline phosphatase staining and Sparc and Ibsp gene expression. Curiously, BMSCs from female C57 MNX mice show a reduction in these markers. BMSCs from C3H WT and MNX mice are currently being analyzed.

Discussion: Our in vivo data suggests that mtDNA exchange for the more efficient C3H haplotype in C57BL/6 mice is not sufficient to induce changes in bone phenotype in vivo even though it did induce osteogenic markers in males in vitro. In contrast, mtDNA exchange for the less efficient haplotypes C57 haplotype makes C3H MNX female mice more susceptible to bone loss in aging and showed enhanced bone resorption and reduced bone formation. The bone phenotype of male C3H MNX mice was relatively unchanged by mtDNA exchange. Collectively, both sets of data indicate sexual dimorphism in the effect of mitochondrial genetics on bone phenotype and influence.

**PAPER #8**

**TITLE:** TriNetX Analytics Network of the USA population reveals bidirectional association between Achilles tendinopathy and hypertension mediated by voltage-gated Ca2+ channel 1.2

**PRESENTING AUTHOR:** Haiyin Li

**CO-AUTHOR(S):** Christopher Mendias, David Ciufo, Chike Cao

**LAB PI/MENTOR:** Chike Cao

**ABSTRACT**

Achilles tendon is highly prone to acute- and overuse-induced injuries that lead to chronic tendon degeneration called tendinopathy. Achilles tendinopathy is often associated with pain and disability. The pathogenic mechanisms of Achilles tendinopathy are largely unknown. Current standard of care for Achilles tendinopathy does not result in effective long-term functional recover. Using novel transgenic CaV1.2 mouse models, we observed potent regulatory effects of increased CaV1.2 function on Achilles tendinopathy. Given the fact that dysregulation of CaV1.2 expression/activity has been implicated in hypertension (HT), we hypothesized that aberrant CaV1.2 function is a common pathogenesis underlying both diseases. We performed association studies between two diseases to test this hypothesis.

We used the TriNetX network that captures the electronic health records of over 111 million patients from 74 Healthcare Organizations. We first performed a cross-sectional study to investigate the prevalence of HT among Achilles tendinopathy patients and its potential association with Achilles tendinopathy. Odds ratio (OR) and 95% confidence interval (CI) were used to quantify the correlation with eliminated confounding factors by population stratification and matching. To determine the cause-and-effect relationship between these two diseases, two 7-year follow-up cohort studies were carried out, with Cohort Study 1 having HT as the exposure factor and Achilles tendinopathy as the outcome, while Cohort Study 2 having Achilles tendinopathy as the exposure and HT as the outcome. Confounding factors were further eliminated by population stratification. To elucidate the role of CaV1.2 in the association of Achilles tendinopathy and HT, we performed an additional 7-year follow-up cohort study on hypertensive patients with the exposure cohort taking Ca2+ channel blockers (CCB) and the control on medications other than CCBs. Relative risk (RR), hazard ration (HR), 95% CI were used to detect the association and the effect of CCBs on the reverse association between the two diseases.

In the cross-sectional study, we found that HT was more prevalent among Achilles tendinopathy patients than in patients without tendinopathy (50.44% vs 15.09%, $p<0.001$). Association analysis found that the incidence of Achilles tendinopathy was highly correlated with HT. Hypertensive subjects had ~four times the odds of having Achilles tendinopathy compared to controls (OR: 4.05, 95%CI: 4.01 to 4.08). After stratification of age, race, BMI, and gender to minimize confounding factors, these two diseases remained associated. In the retrospective cohort studies, we found that in patients over 30 years old without previous tendinopathy, a diagnosis of HT was associated with increased incidence of Achilles tendinopathy in the following 7 years. This association remained strong after population stratification and more prominent in aged subjects. Likewise, we found that in patients without previous HT, a diagnosis of Achilles tendinopathy was associated with increased incidence of HT in all age groups (over 18 years old) in the following 7 years. Furthermore, in the cohort study to evaluate the effect of CCB intervention, we found that hypertensive patients who were on CCBs to control their blood pressure had a 26% decreased risk of developing Achilles tendinopathy than hypertensive patients on other medications (HR:0.74, 95%CI: 0.62-0.88). In contrast, we didn't detect significant effect of ACEI.

In summary, we identified a bidirectional association between Achilles tendinopathy and HT by analyzing TriNetX database, suggesting there is no cause-and-effect relationship between two diseases, but a shared pathological mechanism may underlie both disease development. Furthermore, CCB intervention reduces the risk of Achilles tendinopathy in hypertensive patients, indicating that aberrant Cav1.2 function may be a predisposing factor for future Achilles tendinopathy.

**PAPER #9**

**TITLE:** CCL20/CCR6 limits the disease severity in Staphylococcus aureus osteomyelitis by increasing Th17 and macrophage recruitment at the site of inflammation

**PRESENTING AUTHOR:** Himanshu Meghwani

**CO-AUTHOR(S):** Sandercock KM, McDonald K, Saito M, Constantine R, Lenigk S, Rodriguez A, Owen JR, Kates SL, Schwarz EM and Muthukrishnan G

**LAB PI/MENTOR:** Gowrishankar Muthukrishnan

**ABSTRACT**

Implant-associated osteomyelitis remains a significant healthcare burden. Staphylococcus species are responsible for 75% of all osteomyelitis cases, with Staphylococcus aureus being the primary pathogen and methicillin-resistant S. aureus (MRSA) causing 50% of all implant-associated infections. The most devastating outcome of S. aureus osteomyelitis is multiple organ failure followed by death due to sepsis, and the underlying immune mechanisms are largely unknown. In a clinical pilot study, we found that serum cysteine–cysteine motif chemokine ligand 20 (CCL20) chemokine levels were significantly high (~5 fold) in patients with S. aureus osteomyelitis and even higher (~100 fold) in patients that died due to osteomyelitis-induced sepsis. CCL20 signals monogamously through its receptor CCR6, and the ligand-receptor pair is responsible for the chemotaxis of dendritic cells (DC), effector/memory T cells, and B cells. It is involved in recruiting both the proinflammatory IL-17-producing helper T cells (Th17) and immunosuppressive regulatory T cells (Treg) to sites of inflammation. The role of CCL20 in host immunity against S. aureus osteomyelitis is unknown and we hypothesize that CCL20/CCR6 axis is essential to limiting the S. aureus infection severity during this disease. We first wanted to identify the cellular source of CCL20 after S. aureus bone infection, so we used murine calvarial MC3T3-E1 cells, primary bone-marrow-derived osteoblasts, and macrophages harvested from bone marrow of C57BL6 mice were differentiated into osteoblasts and macrophage subsets (M0, M1 (IFN-γ (50ng/ml)), and M2 (IL-4 (20ng/ml)) and subjected to MRSA USA300 LAC infection (MOI 0, 1, 10, and 50) for 24 hours. CCL20 levels were measured in the culture supernatant via ELISA. We used WT C57BL6, CCL20-/- and CCR6-/- knockout mice of age 10-12 weeks for in vivo transtibial L-shaped pin model of implant-associated osteomyelitis using bioluminescent MRSA (USA300 LAC::lux) strain. We performed longitudinal assessments of disease severity as a measure of 1) body weight, 2) Bioluminescence assay (BLI), 3) ex vivo terminal assessment of CFUs of tibia and internal organs, and 4) histopathology (H& E and Brown-Brenn stain) and micro-CT (bone osteolysis and reactive bone formation). The immunofluorescence was performed to examine the influence of CCL20/CCR6 axis on immune cell (T-cell and macrophage) recruitment to the site of S. aureus infection.

In vitro studies confirmed osteoblasts and macrophages (M0 and M2 subtypes) secrete CCL20 following S. aureus infection. In vivo, we observed that CCL20-/- and CCR6-/- mice exhibited higher disease severity than WT C57BL6 mice. Longitudinal BLI measurement of bacteria confirmed increased early planktonic S. aureus load in CCL20-/- and CCR6-/- compared to WT mice. Terminal ex vivo CFU assessments (14 days post-op) revealed a significant increase in soft tissue CFU in CCL20-/- mice and bone CFU in CCR6-/- mice compared to WT mice. Micro-CT analyses revealed increased bone loss in CCR6-/- mice. Interestingly, we observed reduced staphylococcal abscess communities (SAC) formation in CCR6-/- mice compared to WT. Using IHC, we showed increased recruitment of CCR6+ T cells (Th17 subtype) and macrophages adjacent to the SACs only in the wildtype mice and not in the CCR6-/- mice. Collectively, our findings show that CCL20/CCR6 axis is essential for the recruitment of CCR6+ T-cells and macrophages, with CCR6 potentially contributing to increased CCL20 production in a feed-forward manner. Moreover, our findings suggest that the CCL20/CCR6 axis is indispensable for limiting S. aureus induced osteomyelitis.

**PAPER #10**

**TITLE:** Real-time Fluorescent Microscopy Assessment of PAD4-Mediated NETosis and NET Degradation by S. aureus Nuclease During Nidus Formation on Metal Implants

**PRESENTING AUTHOR:** Youliang Ren

**CO-AUTHOR(S):** Youliang Ren, Karen L. de Mesy Bentley, Jason Weeks, Thomas Xue, Ye Shu, Allie Jia Hui Tay, Sashank Lekkala, Shu-Chi A. Yeh, Edward M. Schwarz and Chao Xie

**LAB PI/MENTOR:** Chao Xie

**ABSTRACT**

INTRODUCTION: S. aureus is the most common pathogen in implant-associated osteomyelitis. Currently, there are no experimental systems that directly quantify neutrophil and bacteria behavior on the implant in real time. Recent literature on soft-tissue infections demonstrated crucial roles for protein arginine deiminase 4 (PAD4)-dependent neutrophil extracellular traps (NET) and S. aureus Nuc degradation of NETs as dominant determinates of immunity and infection respectively.1 In this study, we tested the hypotheses that: 1) neutrophils undergo both lytic and viable NET formation after phagocytosing bacteria on contaminated implants and PAD4 inhibition leads to exacerbated nidus formation and bacterial growth; and 2) Nuc deficient S. aureus fail to form nidi on implants and are rapidly cleared by phagocytic neutrophils.

METHODS: Under approval by the UCAR, bone marrow red-fluorescent neutrophils were collected from 12-week-old CatchupIVM-red mice and added to cell culture wells containing etched sterile and S. aureus (EGFP+USA 300) contaminated titanium pins. Longitudinal scanning confocal microscopy was performed for 6 hours, then SYTOX Blue was added to the co-culture to stain the nucleic acid of dead cells. Scanning electron microscopy (SEM) evaluated bacteria and biofilm formation and the morphological characteristics of neutrophils on the pin surface. GSK484 (PAD4 inhibitor) was added to the culture dish to assess the role of NETosis, and S. aureus strain ΔNuc AH1680 EGFP was used to assess the role of NET degradation. The volume of bacteria and neutrophils was calculated by Imaris to evaluate the swarming ability of neutrophils in different groups. Statistical difference was determined by 1-way ANOVA ($p<0.05$).

RESULTS: SEM demonstrated S. aureus growth within the grooves and confirmed NETosis following neutrophil addition to co-cultures. Real-time fluorescent microscopy confirmed neutrophil swarming towards S. aureus on the pin, phagocytosis of bacteria and NETosis. These results demonstrate that swarming neutrophils in the USA300 or ΔNuc AH1680 co-cultures show significantly higher traveling displacement and velocity than co-cultures treated with GSK484. PAD4 inhibition results in dramatically increased S. aureus proliferation and reduction of swarming of neutrophils leading to a nidus that is primarily comprised of bacteria in static biofilm. In contrast, ΔNuc S. aureus present within implant groove at 1hr were efficiently cleared by large numbers of swarming phagocytic neutrophils by 6hrs, suggesting that degradation of NETs into biofilm eDNA is required for nidus formation. SYTOX blue staining of these co-cultures confirmed the presence of NETs in and around the nidus, absence of NETs in GSK484 treated cultures, and robust NETs in and around the nidus formed by ΔNuc AH1680 EGFP. Quantitative analyses confirmed the increase in bacteria volume and lack of neutrophil swarming in GSK484 treated cultures.

DISCUSSION: This approach enables direct assessment of bacteria and host cell behaviors in real time. Our demonstration that surface etching guides nidus formation to the grooves allows for 100% success in the prospective ROI and overcomes this obstacle. We also confirm the critical roles of NETs and their remodeling by S. aureus Nuc in the prevention and exacerbation of nidus formation on the implant respectively.

SIGNIFICANCE: This is the first in vitro real time imaging model of S. aureus nidus formation in the presence of phagocytic neutrophils on metal implants with quantitative outcomes of bacteria and neutrophil behavior. It can be used to characterize antimicrobial surfaces and assess drug therapies.

REFERENCES: 1) Von Kockritz-Blickwede M,(2022).

ACKNOWLEDGEMENTS:This work was supported by the NIH awards R21AR081050, P30 AR069655 and P50 AR072000.

# *Rosier Award Finalists Pre-Doc Abstracts*

## Disclaimer

**PAPER #11**

**TITLE:** Tendon-Targeted delivery of drug-loaded nanoparticles to modulate healing

**PRESENTING AUTHOR:** Emmanuella Adjei-Sowah[1,2]

**CO-AUTHOR(S):** Baixue Xiao[1,2], Danielle S. W. Benoit[1,2], Alayna E. Loiselle[1,2]

**LAB PI/MENTOR:** Alayna Loiselle

**ABSTRACT**

**Introduction**: Satisfactory tendon healing following acute injury is marred by a fibrotic response that impairs complete functional recovery. Current approaches in treating tendon injuries involve surgical and physical therapy techniques, however, there is a need for biological augmentation of the healing process to promote regenerative healing. Moreover, tendon-specific targeting of systemic pharmacotherapies is limited. Using spatial transcriptomic profiling, we recently identified a spatiomolecular cluster enriched for inflammatory processes that is defined by Acp5, the gene that encodes for Tartrate resistant Acid Phosphatase (TRAP), and demonstrate robust TRAP activity in the healing tendon. As such, we hypothesize that employing a TRAP binding peptide nanoparticle (TBP- NP) delivery system will result in high affinity targeting of TRAP+ cells in the healing tendon. In addition, we will use this tendon-targeted drug delivery system to blunt S100a4 expression, via delivery of a small molecule transcriptional repressor, Niclosamide. Given the key role for S100a4 in promoting fibrotic tendon healing, we expect that tendon-targeted S100a4 inhibition will promote regenerative tendon healing.

**Results**: *TBPNPs effectively target sites of high TRAP activity in vivo and inhibit S100a4 gene expression*: Although untargeted SCP-NPs demonstrated some accumulation at the repair site, TBP-NPs resulted in significantly higher accumulation (~four-fold vs. SCP-NP, $p<0.05$), and prolonged retention (14 days), relative to SCP-NPs. About 50% of TBP-NPs present in the bridging scar tissue of the tendon were internalized by F4/80+ macrophages after NP administration, identifying them as the primary cells that internalize TBP-NPs. S100a4 is a calcium binding protein which has been implicated in tendon fibrosis. To knockdown S100a4 activity, TBP-NPs were efficiently loaded with a small molecule drug (~80% loading efficiency), Niclosamide (TBP-NPNiclosamide) and delivered to mice 7 days post-op. Significant inhibition of S100a4 gene expression was achieved with TBP-NPNiclosamide systemic delivery 72h after administration, establishing an opportunity to modulate tendon healing using this drug delivery system. Ongoing studies are investigating the morphological and biomechanical outcomes of the tendon after treatment with TBP-NP-NEN.

**Discussion**: Without targeting strategies, small molecules exhibit poor tendon targeting, hence, to enhance drug accumulation at tendon repair sites, a suitable and effective drug delivery system is required. The principal goals of this study were: i) establish that TBP-NPs enhance tendon-targeting of systemic treatment, ii) identify the primary cells that take up TBP-NPs within the tendon, and iii) establish knockdown of S100a4 gene expression during tendon healing using this DDS. While macrophages are primarily associated with phagocytic functions, our co-localization studies of TRAP and TBP-NPs suggest that macrophages exhibit an enhanced affinity for the targeted nanoparticles likely due to TRAP expression, leading to their preferential uptake during the late inflammatory period. S100a4, which is expressed by both macrophages and tenocytes has been implicated in tendon fibrosis. The targeted knockdown of S100a4, facilitated by macrophage targeting, establishes a direct link between cellularmanipulation and the subsequent effects on the healing response, which will be determined via functional biomechanical and histological studies. Moreover, the potential to replicate results showing improved tendon healing after 50% knockdown of S100a4 in previously established genetic mouse models using this translational mechanism is of considerable significance. Collectively, these data demonstrate that TBP-NPs substantially enhance targeting of systemic treatments to the healing tendon and establish that TBP-NPs can be used to deliver a drug to modulate tendon healing due to both high-efficiency targeting and sustained retention of NPs.

**PAPER #12**

**TITLE:** Neurological Markers of Pain and Functional Disability during Romberg's Test in Patients with Lower Back Pain

**PRESENTING AUTHOR:** Justin Jablonski

**CO-AUTHOR(S):** Lu H, Corredor J, Chang I, Tome J, Haddas R

**LAB PI/MENTOR:** Ram Haddas

**ABSTRACT**

**Introduction:**
Pain quantification is key in evaluating patients, and numerous researchers and clinicians have developed methods to do so. Patient-Reported Outcome Measurements (PROMs), such as the visual analog scale (VAS), are commonly used to assess pain and disability. These surveys are designed to encapsulate patient experience, putting quantitative measures on patient pain. However, the subjective nature of PROMs can impair pain quantification, as responses can be subjective and are influenced by external factors. Electroencephalograpy (EEG) is a noninvasive objective measure of brain activity, and so the use of EEG in quantifying pain has been researched repeatedly. Several papers have proposed EEG markers related to pain, which often revolve around measurements such as band powers and peak frequencies in frequency ranges related to relaxation (alpha, 7-13 Hz), conscious thought (beta, 13-30 Hz), and cognitive processes (theta, 4-7 Hz). Recording EEG during active trials measures a more natural pain response than previous static trials, to better identify neurological markers of lower back pain in patients. Balance is the ability of the body to maintain a stable center of mass, requiring musculoskeletal and sensorineural coordination that can be impaired by pain to increase sway. This study looks into correlating measures of pain, brain activity, and balance deficits in low back pain patients.
**Methods:**
Five subjects (4M, 1F, ages 19-40) wore a wireless EEG system while performing a five-minute Romberg's test. Trials were performed in a 'normal' eyes-open (EO) state, a 'normal' eyes-closed (EC) state, and a 'painful' eyes-open (EOP) state, with chronic back pain simulated through an electrostimulation device applying moderate current to the erector spinae in the lumbar region. EEG data was recorded (with artefact reduction), and pain level was recorded at 30-second intervals using a 0-10 VAS. Sway was recorded through a wearable sensor placed on C7. Alpha, beta, and theta relative bandpowers and peak frequencies were extracted from EEG, and these and average pain measures were compared with One-Way ANOVA to identify significant differences between conditions. Pearson's correlation was used to identify relationships between EEG markers and pain, to determine which markers could be used to predict patient pain.
**Results:**
Significant differences were found in brain activity, seen in relative bandpower and peak frequency differences across all frequency ranges in multiple electrodes (alpha EO=0.0216, EC=0.0798, EOP=0.0202, $p<0.05$; beta EO=0.0113, EC=0.0280, EOP=0.0107, $p<0.05$; theta EO=0.0566, EC=0.0424, EOP=0.0437, $p<0.05$). Pain level was also significantly different across all three conditions, but was much higher in the pain trial than the other two (EO=0.37, EC=0.10, EOP=2.8, $p<0.05$). Peak theta frequency was strongly correlated with pain level ($r2 = 0.68$), whereas bandpowers were weakly correlated with pain ($r2 < 0.33$).
**Discussion:**
This study was first in correlating measures of pain, brain activity, and balance deficits in low back pain patients. Significant differences were identified in bandpowers, pain levels, and peak frequencies for multiple electrodes across alpha, beta, and theta frequency ranges between conditions, with the pain conditions showing the highest VAS scores and more brain activity.
**Significance:**
Our method was able to successfully identify neurological marker indicating pain and disability in patients during a Romberg Test. Identification of EEG-based markers will allow for better evaluation of subject pain and disability during motion capture, helping to develop a new dimension in the analysis of patient pain and DFOMs.

**PAPER #13**

**TITLE:** Localized Knee Irradiation Creates Persistent DNA Damage in Chondrocytes and Promotes Joint Hyperalgesia

**PRESENTING AUTHOR:** M. Nick James

**CO-AUTHOR(S):** Danielle Benoit, Jennifer Jonason

**LAB PI/MENTOR:** Jennifer Jonason

**ABSTRACT**

INTRODUCTION: Osteoarthritis (OA) is a common and progressive condition characterized by loss of articular cartilage which causes chronic joint pain and loss of mobility. While aging is a significant risk factor for OA, aging is also thought to be a consequence of cumulative DNA damage. Recently it was shown that either aged or OA human knee cartilage contained more DNA-damaged chondrocytes relative to young or healthy cartilage. Furthermore, proinflammatory pathways are activated in response to DNA double-strand breaks (DSBs), notably stimulating the nuclear factor κB (NF-κB) pathway. We previously identified increased NF-κB activity in aged chondrocytes and demonstrated early OA onset in young mice using a model of chondrocyte-specific NF-κB induction. Whether DNA damage causes proinflammatory signaling in chondrocytes and other joint cell types has not been well-characterized. Here, we used highly localized X-rays to induce DNA damage in mouse knee joints to examine the hypothesis that DNA damage leads to chronic proinflammatory signaling in chondrocytes, pain-related behaviors, and ultimately OA onset.
METHODS: Male C57BL6/J mice, 4 months of age, were irradiated with either a single 8.2 Gy dose (n=3-6) or a more clinically relevant dose of 3, 8.2 Gy fractions separated by 48 hours each (n=3-8) using a 3x3mm collimator centered on the right hind knee joint for X-ray localization. Non-irradiated mice and/or non-irradiated contralateral limbs acted as controls. At 6 months after irradiation mouse mobility and pain-related behaviors were assessed by locomotor, gait, rotarod, and knee pressure application measurement (PAM). Mouse hind limbs were collected 2 hours, 48 hours, or 1 week, after irradiation for and processed for quantitative γH2AX immunohistology to evaluate the DNA DSB repair response in vivo. Significance was determined by Students t-test or 2-way ANOVA with post-hoc Tukey's multiple comparisons.
RESULTS: At 2 hours after a single dose, nearly 75% of articular chondrocytes were γH2AX+. Despite significant repair of DNA DSBs, about 15% chondrocytes contained persistent DNA DSBs 1 week after treatment. Notably, synoviocytes completely repaired from a single dose within 48 hours. After 3, 8.2 Gy fractions, DNA DSBs were significantly more abundant in chondrocytes one week after irradiation compared to contralateral controls. Mice that received 3 fractionated doses 6 months prior displayed only a slight decline in rearing behavior by locomotor test. However, gait analysis revealed significantly decreased front right limb stride time, front track width, and all step sequence counts. There was no significant decrease in fall times of irradiated mice by rotarod. PAM thresholds were significantly lower in only irradiated limbs, indicating knee hyperalgesia.
DISCUSSION: These results highlight the importance of the DNA damage response in our understanding of the pathogenesis of OA in aging. Surprisingly, DNA DSBs persisted at least a week after irradiation in chondrocytes compared to more rapid DNA repair in synoviocytes suggesting cell type-specific responses to DNA damage. Although we observed little effect on mouse mobility by locomotor and rotarod behavioral tests, we recorded a surprising compensation effect from the front right limbs of irradiated mice and consistently lower pain thresholds by PAM. This could indicate effects like inflammation in synovium before mobility is substantially affected by cartilage degeneration. We are currently assessing effects up to 9 months after knee joint irradiation on joint tissue structures by μCT and IHC methods to better understand the DNA damage response in joint cell types.
SIGNIFICANCE: Our findings demonstrate that knee joint irradiation induces hyperalgesia and gait abnormalities, laying the groundwork for a potential model for age-related OA development.

**PAPER #14**

**TITLE:** Ablation of Tumor Derived IGFBP-3 Attenuates Cancer-Associated Skeletal Muscle Wasting via Downregulation of the Ubiquitin Proteasome Pathway

**PRESENTING AUTHOR:** Zachary Sechrist

**CO-AUTHOR(S):** Edward Schwarz

**LAB PI/MENTOR:** Calvin Cole

**ABSTRACT**

INTRODUCTION: Pancreatic ductal adenocarcinoma (PDAC) is the fourth leading cause of cancer-related deaths, and its incidence is expected to rise. A notable detractor for patients with PDAC is skeletal muscle wasting (SMW), which leads to reduced physical function and response to treatment, and shorter life expectancy. Thus, SMW interventions may reduce disease and treatment-related complications to improve survival and quality of life. Our lab previously identified tumor secreted insulin-like growth factor binding protein 3 (IGFBP-3) as a potential driver of PDAC-induced SMW in a pre-clinical murine model. Furthermore, the roles of TGF-b signaling, and ubiquitin proteasome pathway (UPP) activation have been duly noted in SMW. However, their role in PDAC-related SMW has yet to be elucidated. Recent literature supports an interaction between IGFBP-3 and TGF-b signaling in muscle. Here we tested the hypothesis that genetic depletion of IGFBP-3 in the KCKO PDAC tumor cell line decreases its ability to induce SMW in mice via TGF-b signaling and results in decreased activation of the UPP in a model of PDAC-related SMW.
METHODS: C57BL/6J female mice (6-8 weeks old) were scanned using dual energy X-ray absorptiometry (DEXA) to acquire baseline lean mass measurements of the lower hindlimbs. Mice were randomized into two experimental tumor-bearing groups (n=14/ group): 1) parental KCKO-Luc (PDAC), or 2) KCKO-Luc IGFBP-3-/- (KO). PDAC and KO mice were compared to non-tumor control (NTC) (n=10) mice. Mice were injected orthotopically with 1x10^5 of either murine KCKO-Luc or IGFBP-3 KO tumor cells. Weekly DEXA monitored longitudinal changes in lean mass. Mice were sacrificed based on previously established failure to thrive criteria or at the predetermined 100-day endpoint. At sacrifice serum, and legs were harvested. Quadriceps and tibialis anterior (TA), muscles were preserved for transcriptional analysis. ELISA was performed on serum for the quantification of IGFBP-3. RNA was extracted from quadriceps muscles for transcriptional analysis of igfbp3, tgfbr1, and UPP associated genes: trim63 and fbxo32. Statistical analyses were performed using GraphPad Prism software. One-way ANOVA was used to analyze within group and between group changes in IGFBP-3 concentrations, lean mass, and transcriptional expression. Kaplan–Meier estimator of survival was used to quantify survival of experimental mice. $p<0.05$ was considered significant. RESULTS: PDAC mice experience significantly reduced survival compared to KO mice that maintained 100% survival at day 100 ($p<0.0001$). PDAC mice displayed increases in systemic IGFBP-3 compared to NTC ($p<0.01$) and KO mice ($p <0.001$) while no difference was observed between NTC and KO animals. Furthermore, PDAC mice lost significantly more lean mass as measured by DEXA compared to NTC mice ($p<0.0001$). KO mice experienced a significant loss of lean mass compared to NTC mice ($p<0.05$), however, they also experienced a significant attenuation when compared to PDAC mice ($p<0.0001$). RT-qPCR analysis on muscle indicated that PDAC mice display significantly increased expression of igfbp3 and UPP associated genes trim63 and fbxo32 compared to NTC and KO mice while no difference was seen between NTC and KO mice. Moreover, KO mice have reduced expression of tgfbr compared to NTC and PDAC mice, which suggests decreased TGF-b dependent catabolism in KO skeletal muscle.
DISCUSSION: In this study, we demonstrated a relationship among upregulation of IGFBP-3, TGF-b dependent UPP activation, and SMW. Tumor-specific ablation of IGFBP-3 significantly attenuates the loss of lean mass measured via DEXA and improves survival. Further work will validate IGFBP-3 dependent effects on SMW and investigate therapeutic neutralization of IGFBP-3 as a treatment for PDAC-induced SMW.
FUNDING: This research is supported by NIH grants (K01 CA240533 and P30 AR69655).

**PAPER #15**

**TITLE:** The Role of PRDM16 in Craniofacial Development

**PRESENTING AUTHOR:** Eliya Tazreena Tashbib

**CO-AUTHOR(S):** Victoria Hansen, Eloise Fadial, Alexis Klee, Gourango Pradhan, Chia-Lung Wu

**LAB PI/MENTOR:** Chia-Lung Wu

**ABSTRACT**

INTRODUCTION: Epigenetic alterations contributing to craniofacial anomalies constitute more than half of congenital deformities, affecting approximately 1% of live births. Previous studies have shown that mice with mutations in PRDM16, a zinc finger transcriptional factor and methyltransferase, exhibited mandibular hypoplasia due to shortened Meckel's cartilage, suggesting its potential role in chondrogenesis. However, mice with PRDM16 global knockout (KO) are neonatal lethal; thus, the molecular mechanism underlying how PRDM16 regulates craniofacial chondrogenesis and cartilage homeostasis postnatally remains largely unknown. Therefore, a comprehensive analysis of PRDM16 through conditionally cartilage-specific KO is required. We hypothesize that PRDM16 is a master regulator in chondrogenesis during craniofacial development.

METHODS: All animal procedures were approved by UR IACUC. Cartilage-specific, PRDM16 KO mice (Col2a1-Cre; Prdm16flox/flox) were generated. Cre-negative littermates were used as controls (WT). PRDM16 KO was confirmed through Western blot analysis of costal cartilage. To examine the craniofacial bone and cartilage development at the embryonic stage, E18.5 WT, and KO mice were stained with Alcian Blue and Alizarin Red (whole mount staining). Mouse skulls were harvested from 4 wk and 12 wk old WT and KO mice submitted for uCT and Safranin O/Fast green staining (n=5 for all groups). Data were analyzed with Student's t-test within the same sex and time point.

RESULTS & DISCUSSION: The whole mount staining revealed that PRDM16 KO mice had a trend toward decreasing nasal ($p=0.26$) and cranial lengths ($p=0.06$) vs. WT mice. Postnatally, we observed that at 4 wk, female KO mice exhibited decreased nasal length ($p<0.05$) and cranial length ($p<0.01$) vs. WT mice, with no remarkable changes in other craniofacial bones, including total mandible length, anterior to posterior mandible ratio, and condylar axis. Interestingly, the deletion of PRDM16 resulted in increased nasal bone mineral density (BMD) in female KO mice vs. WT. For male KO mice at 4 wks of age, a significant reduction in cranial length vs. WT was noted, but their nasal length remained largely unaffected despite an observed trend of increased nasal BMD. Next, we examined if the altered lengths between KO and WT mice persist through adulthood. Both female and male KO mice had significantly shorter nasal and cranial lengths than their WT counterparts at 12 wk of age. However, female KO exhibited lower nasal BMD than WT, opposite to the observation at 4 wk of age. In contrast, male KO mice remained having higher nasal BMD vs. WT at 12 wk of age. These results suggest that PRDM16 may have a sex-dependent effect on craniofacial development. Furthermore, histological analysis revealed that at 4 wk and 12 wk of age, male KO showed shorter length of anterior nasal septal cartilage (NSC) along with decreased columnar chondrocytes and Saf-O staining vs. WT. The changes in chondrocyte phenotype and decreased cartilage matrix production imply potentially altered cartilage homeostasis and endochondral ossification in the NSC of the male PRDM16 KO mice, providing a possible explanation for their increased nasal BMD compared to WT mice. Currently, we are conducting histological analysis of the NSC in the female WT and KO mice.

CONCLUSION: Our study indicates that mice with cartilage-specific PRDM16 KO exhibited a sex-dependent alteration in nasal length and BMD. These abnormalities appear to be related to the changes in chondrocyte phenotypes in the NSC. Our histological analysis suggests that loss of PRDM16 may promote chondrocyte hypertrophy while enhancing osteogenesis in male KO mice. The findings from this study will provide valuable insights into the functionality of PRDM16 in craniofacial development.

**PAPER #16**

**TITLE:** 3D printed PCL scaffolds containing amorphous calcium phosphate nanoparticles promote long bone regeneration through osteoimmunomodulation

**PRESENTING AUTHOR:** Ming Yan

**CO-AUTHOR(S):** Anthony Yosick, Bei Liu, Hani Awad

**LAB PI/MENTOR:** Hani Awad

**ABSTRACT**

3D-printed calcium phosphate scaffolds, commonly employed as substitutes for bone allografts, have deficiencies in biomechanical properties and osteoinductivity. Aiming to surmount these limitations, this study endeavors to optimize bioinks, composed of a polymer-ceramic blend, to facilitate extrusion-based 3D printing of scaffolds that exhibit superior mechanical attributes. Additionally, the study integrates carboxymethyl chitosan-amorphous calcium phosphate nanoparticles (CMC/ACP NPs) as the ceramic component in polycaprolactone (PCL)-based scaffolds, with the intent of enhancing osteoinductivity. Previous research has demonstrated the potential of high doses of CMC/ACP NPs to promote osteogenesis, modulate macrophage polarization, and inhibit osteoclasts. Therefore, I hypothesized that these nanoparticles, upon burst release from PCL scaffolds post-implantation in vivo, rapidly accumulate to orchestrate anti-inflammatory macrophage behavior and constrain osteoclast activity, while simultaneously stimulating osteoblast mineralization, culminating in robust bone restoration. To validate this hypothesis, NP-laden PCL scaffolds were implanted in critical defects of rat radii, and their regenerative potential was juxtaposed with that of PCL and Calcium Phosphate (CaP)-laden PCL scaffolds. The synthesis of CMC/ACP NPs, hereafter termed NPs, ensued by stirring CMC in a dibasic phosphate solution, followed by a gradual addition of a calcium chloride dihydrate solution, as elucidated in earlier studies. PCL was dissolved in an organic solvent mixture, and CaP microparticles, a fusion of tricalcium phosphate and hydroxyapatite, were blended with the PCL solution prior to 3D printing. Scaffolds were then implanted into critical rat radial defects (3 mm); one group (n=9 per scaffold type, 27 animals total) underwent longitudinal micro-CT scans at 2, 4, 6, 8, and 10 weeks, followed by biomechanical 4-point bending tests at 10 weeks post-implantation. Another group (n=2 per scaffold type per time point, 18 animals total) was harvested for histology and underwent tissue sectioning at 2, 4, and 10 weeks; quantitative analysis used TRAP staining at the scaffold-bone interface. All animal procedures adhered to approved protocols. Notably, the NP group exhibited accelerated bone formation within 2 to 4 weeks, sustaining this bone volume over a span of 10 weeks, unlike the PCL and CaP groups. Mechanical evaluations at the 10-week mark unveiled that the NP group showcased enhanced mechanical properties in contrast to both PCL and CaP counterparts. Quantitative analysis of TRAP staining indicated distinct trends, with the NP group showing reduced staining in the initial weeks, which intensified at 10 weeks. Immunofluorescence staining reflected dynamic macrophage behavior, with the NP group exhibiting consistent expression of CD206. Discussion revolves around the pivotal role of osteoclasts in bone repair, particularly in later stages, necessitating optimal implant strategies that curtail untimely osteoclast activity and sustain bone repair integrity. The findings underscore the efficacy of NP-laden scaffolds in promoting bone formation and hindering osteoclast activity early on, culminating in improved mechanical properties. This study further draws on the correlation between NP concentrations, macrophage polarization effects, and accelerated bone formation. The clinical relevance of this research lies in addressing the limitations of existing bone graft substitutes, offering a cost-effective solution that not only augments mechanical support but also orchestrates positive osteoimmunomodulatory effects, thereby contributing to orthopedic and reconstructive surgery.

# *Rosier Award Finalists 3MT Posters*

## Disclaimer

**PAPER #17**

**TITLE:** Androgen Treatment Exhibits A Protective Role Against Focal Erosions in TNF-Induced Inflammatory Arthritis in Mice

**PRESENTING AUTHOR:** Kiana L. Chen

**CO-AUTHOR(S):** Adelaide Weidner, Olga I. Astapova, Edward M. Schwarz, and Homaira Rahimi

**LAB PI/MENTOR:** Homaira Rahimi

**ABSTRACT**

Rheumatoid arthritis (RA) is characterized by chronic joint inflammation and bone erosion and is female predominant. The TNF-transgenic (TNF-Tg) murine model of RA develops inflammatory erosive arthritis and displays a sex difference in disease, with females having worse disease than males. Studies suggest androgens provide a protective effect against joint disease and TNF-mediated bone erosion. We have previously shown that the removal of endogenous sex hormones in TNF-Tg males significantly worsens their inflammatory erosive disease. Here, we investigated whether treatment of TNF-Tg mice with exogenous androgen ameliorates erosive disease.

TNF-Tg male mice were orchiectomized followed by subcutaneous implantation of either 5α-dihydrotestosterone (DHT) or placebo pellet at 1-month old (n = 3/group). Pellets released 1.5mg of DHT or placebo for 60 days (0.025mg/day). Micro-computed tomography (μCT) scans of hindpaws were taken at 3-months old and compared with μCT data of same age intact TNF-Tg males and orchiectomized wildtype (WT) males (n = 4-6 paws/group). The total bone volumes (mm3) of the cuboid, talus, and navicular and lateral intermediate cuneiform were compared between all groups. The volumes of the distal region of the metatarsals were compared between TNF-Tg groups. Paw deformation scores and weights were taken weekly from 1 to 3 months old. The weekly weights of same age sham TNF-Tg male mice were compared between orchiectomized TNF-Tg groups. Serum and paws were obtained for analysis and histology. Values are reported as the mean +/- standard deviation.

Placebo-treated orchiectomized TNF-Tg mice had significantly more bone volume loss than DHT-treated orchiectomized TNF-Tg mice and other cohorts in the cuboid (0.34 ± 0.03 Orchiectomized TNF-Tg + Placebo; 0.43 ± 0.02 Orchiectomized TNF-Tg + DHT; 0.43 ± 0.06 Intact TNF-Tg; 0.45 ± 0.05 Orchiectomized WT), talus (0.97 ± 0.09 Orchiectomized TNF-Tg + Placebo; 1.10 ±0.06 Orchiectomized TNF-Tg + DHT; 1.21 ± 0.07 Intact TNF-Tg; 1.12 ± 0.05 Orchiectomized WT), and navicular and lateral intermediate cuneiform (0.78 ± 0.04 Orchiectomized TNF-Tg + Placebo; 0.87 ± 0.03 Orchiectomized TNF-Tg + DHT; 0.94 ± 0.04 Intact TNF-Tg; 0.93 ± 0.04 Orchiectomized WT). Segmented hindpaw images of the TNF-Tg cohorts showed bone erosion in the periarticular regions of the metatarsals. Placebo treated orchiectomized mice had less bone volume in the distal metatarsals than DHT-treated orchiectomized TNF-Tg mice and intact TNF-Tg mice (0.23 ± 0.05 Orchiectomized TNF-Tg + Placebo; 0.28 ± 0.07 Orchiectomized TNF-Tg + DHT; 0.27 ±0.07 Intact TNF-Tg). Orchiectomized TNF-Tg mice with placebo had significantly higher mean paw deformation scores at 4 weeks post-surgery ($p = 0.03$). Orchiectomized TNF-Tg mice also gained significantly less weight than sham TNF-Tg mice by 6 weeks post-surgery ($p = 0.03$). DHT treatment of orchiectomized TNF-Tg mice resolves that weight loss over time.

Androgen treated orchiectomized arthritic mice had significantly improved bone volumes, limiting bone erosion even in the presence of ongoing inflammation. Clinical measures of weight loss and arthritis also improve with androgen treatment. These finding suggests sex hormones have a relationship with the immune system and cells in inflammatory-erosive disease that warrants further study. Histological analysis of the paws and osteoclastogenic cultures of bone marrow cells with androgen treatment are ongoing to delineate the mechanism of androgen effects on inflammation.

**PAPER #18**

**TITLE:** The Role of Bone Remodeling in Regulating Hematopoietic Cell Expansion

**PRESENTING AUTHOR:** Cih-Li Hong

**CO-AUTHOR(S):** Kevin Lee, Zi Yin, Haiyin Li, Melissa MacLiesh, Wimeth Dissanayake, Laura Calvi, Chike Cao, Shu-Chi A. Yeh

**LAB PI/MENTOR:** Shu-Chi A. Yeh

**ABSTRACT**

Abstract

Clonal expansion of hematopoietic stem cells (HSCs) carrying leukemia-associated mutations stands out as a pivotal factor governing the progression of myelodysplastic syndromes (MDS)1. As MDS is typically diagnosed at advanced age, patients who failed eligible therapies and progressed to leukemia have dismal prognosis2. Therefore, elucidating mechanisms underlying clonal expansion will help identify novel therapeutic candidates. Although various systemic factors, including acute inflammation3 and aging4, have been shown to provide selective pressure to promote proliferation of mutated stem cells, our prior findings showed that clonal expansion of hematopoietic cells occur almost exclusively at the bone remodeling sites 5. Given the intimate crosstalk of the skeletal and hematopoietic compartments 6, our findings raised a question whether the use of osteoporosis medications, such as the anti-resorptive bisphosphonates, will suppress HSC proliferation in response to inflammation and progression of clonal disorders. To test whether bone remodeling affects clonal expansion, we conducted experiments using adult HSC reporter mouse model (Mds1GFP) 5 challenged with sterile inflammation (Lipopolysaccharide, LPS, 35 µg per mouse administered one day before imaging) or in the disease model, where 2.5x 106 Tet2+/- bone marrow cells were transplanted into 0.5 Gy irradiated wild-type mice. Thereafter, these mice were treated with anti-resorptive zoledronic acid (ZOL, 1.2 µg over 3 doses for a week) or vehicle control (PBS) and imaged a day after the last treatment. Sequential bone front staining with a 2-day interval was performed before imaging to annotate the bone marrow predominated by bone formation, resorption of active remodeling, as described previously 5. Using intravital imaging, we showed that ZOL significantly reduced the frequency of dividing cells that formed cell doublets with intercellular distance of 5-10 microns ($p=0.0003$ when compared to the vehicle control, Kolmogorov-Smirnov test). In the disease model, ZOL led to a significant reduction of GFP+ voxels within a consistent volume of interest in the calvarial bone marrow ($p=0.0084$, unpaired t-test). Notably, the few expanded clones after ZOL treatment remained exclusively at the remodeling sites. In addition, analyses from TriNetX patient database further revealed that osteoporosis patients who were prescribed with bisphosphonates (BS) had reduced risk of developing MDS (Hazard ratio = 0.54, $p<0.001$). Taken together, these results suggested the involvement of the bone marrow microenvironment, mediated by bone remodeling, in modulating cell expansion. Future work will be focused on comparisons with anabolic treatment using intermittent PTH (1-34), functional in vivo imaging to track cell dynamics (e.g., division, migration) along with bone turnover, and spatial resolved transcriptomic analyses to decode the molecular pathways involved in the local bone remodeling activities to sustain clonal expansion of hematopoietic cells.

References

1. Bowman, R. L. et. al., Cell Stem Cell, 22 (2), 2018
2. Prébet, T. et. al., J. Clin. Oncol., 29(24), 2011
3. Cook, E. K. et. al., Exp. Hematol., 83, 2020
4. Jaiswal, S. & Ebert, B. L., Science, 366(6465), 2019
5. Christodoulou, C. et. al., Nat., 578(7794), 2020
6. Hoffman, C. M. et. al., Bone, 119, 2019

**PAPER #19**

**TITLE:** Raman Spectroscopy and Reference Point Indentation: Investigating the Predictive Value for Fracture Risk in Femoral Necks

**PRESENTING AUTHOR:** Kyle Jerreld

**CO-AUTHOR(S):** Sashank Lekkala, Christine Massie, Andrew Rodenhouse, Andrew Berger, Constantinos Ketonis, Hani Awad

**LAB PI/MENTOR:** Hani Awad

**ABSTRACT**

Bone mineral density (BMD), the basis for DXA diagnosis of OP, only explains 21% of all non-vertebral fractures in men and 44% in women. Raman spectroscopy, capable of molecular fingerprinting, has been used in identifying the quality of the mineral (hydroxyapatite) and matrix (collagen) components of bone. While fracture risk can be estimated based on DXA T-scores and fracture risk assessment tools such as FRAX, it remains to be established whether Raman compositional parameters correlate with fracture risk. We then used the FRAX tool to assess the individuals' fracture risk. We hypothesized that Raman spectroscopy and RPI mechanical outcomes can predict a patient's fracture risk.

Femoral necks were obtained from patients undergoing total hip arthroplasty. Each sample was divided into quadrants: Inferior, superior, anterior, and posterior. We used DXA to measure the BMD. To measure the Raman signal, the samples were excited using an 830nm, 150mW laser, and the scattered light was collected. Each spectrum was an average of 5 spectra with an integration time of 60 seconds. A custom code was used to calculate the Raman outcomes. For RPI, the samples were rehydrated in PBS for 2 hours before testing. Samples were tested with an indentation force of 10 N and a frequency of 2.0 Hz for a total of 10 cycles. The ten-year probability of a major osteoporotic and hip fractures were calculated using the FRAX tool. Principal component analysis was performed to reduce the dimensionality of the data. A one-way analysis of variance adjusted with Tukey HSD was performed to test quadrant differences. Multivariate regression models with the principal components were then used to test the statistical associations between the predictor variables (Raman and RPI) and the FRAX probabilities.

Femoral neck specimens were obtained from 32 male and 28 female THA patients. Since measurements in the inferior quadrants were the most reliable, all correlations described are based on measurements in that quadrant. The Mineral:Matrix ratio trended towards being lower, whereas the Carbonate:Phosphate ratio and pyridinoline increased with age, but not sex or BMI. None of the RPI outcomes correlated with age, sex or BMI. Multivariate regressions showed that Raman PC1 was a significant explanatory variable for several RPI outcomes. BMD did not correlate with FRAX outcomes, but predictably, we estimated higher FRAX probabilities in females, which also correlated with age but not BMI. Further, multivariate regressions of the 4 Raman principal components revealed significant correlations with FRAX ten-year probability of a major osteoporotic fracture ($R^2$=0.19). The regressions improved to $R^2$=0.245 for females and $R^2$=0.223 for males, respectively. However, in females, PC2 had the highest correlative weight ($p=0.06$), whereas PC1 had the highest correlative weight in males ($p<0.05$). Similar correlations could be observed for the FRAX ten-year probability of a hip fracture, although the model was not significant for females.

Our findings highlight the potential of Raman spectroscopy for assessing fracture risk in osteoporosis patients. BMD did not show a significant correlation with FRAX outcomes, suggesting the need for additional metrics in fracture risk assessment. Raman principal components, based on classic compositional parameters, displayed significant correlations with FRAX ten-year probabilities, particularly when stratified by sex, thereby supporting our initial hypothesis. This work shows promise in introducing new, more sensitive markers for osteoporosis risk stratification. The limited correlations between RPI mechanical outcomes and FRAX suggest that further research is needed to understand the role of mechanical properties in bone fracture risk. Overall, this study offers preliminary evidence towards the incorporation of Raman spectroscopy as a potentially more reliable metric for osteoporosis screening and management.

**PAPER #20**

**TITLE:** High-Throughput Micro-CT Analysis Identifies Sex-Dependent Biomarkers of Erosive Arthritis in TNF-Tg Mice and Differential Response to Anti-TNF Therapy

**PRESENTING AUTHOR:** H. Mark Kenney

**CO-AUTHOR(S):** H. Mark Kenney, Kiana L. Chen, Lindsay Schnur, Jeffrey I Fox, Ronald W Wood, Lianping Xing, Christopher T Ritchlin, Homaira Rahimi, Edward M. Schwarz, and Hani A. Awad

**LAB PI/MENTOR:** Edward Schwarz & Hani Awad

**ABSTRACT**

**Background**: Development of valid and reliable disease activity biomarkers is critical for diagnostics, prognostics, and novel drug development. Although computed tomography (CT) is the gold-standard for quantification of bone erosions, there are no consensus approaches or rationales for utilization of specific outcome measures of erosive arthritis in complex joints. In the case of preclinical models, such as sexually dimorphic tumor necrosis factor transgenic (TNF-Tg) mice, disease severity is routinely quantified in the ankle through manual segmentation of the talus or small regions of adjacent bones primarily due to the ease in measurement. Herein, we sought to determine the particular hindpaw bones that represent reliable biomarkers of sex-dependent disease progression to guide future investigation and analysis.
**Methods**: Hindpaw micro-CT was performed on wild-type (n=4 male, n=4 female) and TNF-Tg (n=4 male, n=7 female) mice at monthly intervals from 2-5 (females) and 2-8-months (males) of age, where female TNF-Tg mice exhibit early mortality from cardiopulmonary disease at approximately 5-6-months. Further, 8-month-old WT (n=4) and TNF-Tg males were treated with anti-TNF monoclonal antibodies (n=5) or IgG placebo isotype controls (n=6) for 6-weeks with micro-CT imaging every 3-weeks. For image analysis, we utilized our recently developed high-throughput and semi-automated segmentation strategy in Amira software. Synovial and osteoclast histology of ankle joints was quantified using Visiopharm.
**Results**: Our analysis method demonstrated comparable automated segmentation accuracy in wild- type and TNF-Tg hindpaws before correction (79.2±8.9% vs 80.1±5.1%, *p=0.52*), determined through analysis of ~9000 individual bones by a single user. Compared to other bone compartments, the tarsal region demonstrated a sudden, specific, and significant bone volume reduction in female TNF-Tg mice by 5-months (4-months 4.3± 0.22 vs 5-months 3.4± 0.62 $mm^3$, *p<0.05*). This sexual dimorphism was associated with unique bone-specific changes across time, as the cuboid showed significantly reduced bone volumes at early timepoints compared to other tarsals (i.e., 4-months: Cuboid -24.1±7.2% vs Talus -9.0±5.9% of 2-month baseline). Additional bones localized to the anterolateral region of the ankle were also responsible for the dramatic erosions in the tarsal region of females, coinciding with increased synovitis and osteoclast frequency. In TNF-Tg mice with severe arthritis, the talus ($\eta^2$ = 0.21) and calcaneus ($\eta^2$ = 0.22) exhibited the most sensitive response to anti-TNF therapy (large effect size >0.138).
**Conclusions**: Taken together, we demonstrated that sexual dimorphism of arthritis in TNF-Tg mice is bone-specific, where the cuboid serves as a reliable biomarker of erosive arthritis. Adoption of similar approaches in additional pre-clinical or clinical translational models holds potential to enhance quantitative biomarkers of monitoring bone erosions towards early intervention and evaluation of therapeutic efficacy.

**PAPER #21**

**TITLE:** Integrative scRNA-seq and spatial transcriptomics uncovers distinct macrophage-fibroblast cross-talk in human hip synovium between patients with FAI and hip OA

**PRESENTING AUTHOR:** Gulzada Kulzhanova

**CO-AUTHOR(S):** Mina Botros, John Reuter, Victoria Hansen, Eloise Fadial, Benjamin Ricciardi, Brian Giordano, Chia-Lung Wu

**LAB PI/MENTOR:** Chia-Lung Wu

**ABSTRACT**

Introduction: Hip osteoarthritis (OA) affects one in four people by the age of 85, and it is linked to abnormal hip morphology including Cam-type femoroacetabular impingement (FAI), a condition of osseous protrusion from femoral head-neck junction that impinges on the acetabulum. Thus, FAI patients may exhibit labral tears and cartilage delamination, gradually leading to the development of hip OA (secondary to FAI). Therefore, FAI has been considered as a unique early-phase hip OA model for studying regulators implicated in disease progression. Here, we hypothesize that FAI and hip OA synovial cells exhibit distinct transcriptomes and altered synovial cell-cell interactions. By using integrative single-cell RNA sequencing (scRNA-seq) and spatial transcriptomics (Spatial-seq) approaches, we aim to explore the disease markers and signaling pathways that will help us predict potential targets for early and late hip OA treatments.

Methods: Human hip synovium samples were harvested from patients with Cam FAI or hip OA according to approved UR IRB protocols. 5 FAI (3 males) and 3 male OA samples were submitted to UR GRC for scRNA-seq and Spatial-seq. Distinct cell populations were annotated based on unbiased clustering and differentially expressed genes. The cells were then mapped to Spatial-seq datasets to visualize their spatial locations and determine potential cell-cell interactions. Cell-cell crosstalk and downstream activated genes were identified by MultiNicheNet R package. Functional analysis of cell subsets was determined by Gene Ontology (GO) enrichment.

Results and Discussion: Myeloid, NK, non-hematopoietic, and endothelial cells were identified as major conserved cell groups between FAI and hip OA synovium. Sub-clustering of CD45+/CD14+ cells yielded 5 distinct cell types: pro-inflammatory macrophages (MΦ), anti-inflammatory MΦ, and fibrotic MΦ, monocytes, and dendritic cells. Re-clustering CD45- non-hematopoietic cells resulted in 4 different cell groups: lining and sublining fibroblast (FLS) as well as endothelial cells and pericytes. Compared to FAI synovium, OA synovium exhibited 1.4-, 1.75-, and 2.65-fold increase in CCL4+/CCL3+ MΦ, MFAP2+/MDK+ sublining FLS, and endothelial cells, respectively. The finding that endothelial cells were significantly increased in OA vs. FAI synovium is supported by the evidence of increased vasculature in OA. Increased vasculature in OA synovium may promote infiltration of inflammatory myeloid cells into the synovium, promoting joint inflammation and OA progression. Additionally, to visualize their spatial locations in the FAI and hip OA synovium, cell populations identified by scRNA-seq were mapped to Spatial-seq datasets. For example, we observed that CCL4+/CCL3+ pro-inflammatory MΦ and MFAP2+/MDK+ sublining FLS are spatially adjacent to each other, suggesting potential cell-cell interactions. Using MultiNicheNet, we identified that CCL4+/CCL3+ MΦ may modulate inflammation and cell survival of synovial MFAP2+/MDK+ FLS in hip OA synovium by activating CXCL8, IL17R, and BCL2A1 via CSF1-SIPRA signaling pathway. Interestingly, ANXA4, CMKLR1, and TNFSF10 were predicted as activated genes downstream of CSF1-SIRPA pathway between CCL4+/CCL3+ MΦ and MFAP2+/MDK+ FLS in the FAI synovium. Our GO analysis suggests that these three genes are involved in the negative regulation of NF-kB signaling, providing a possible explanation why FAI synovium is less inflamed versus OA synovium.

Conclusion: In summary, we identified dynamic changes in synovial cell populations and cell-cell crosstalk during disease progression (i.e., FAI vs. hip OA). Most importantly, our results suggest that targeting distinct signaling molecules at different disease stages may be required to prevent hip OA progression from FAI.

**PAPER #22**

**TITLE:** Semi-Automated Cell Tracking and Quantification of Neutrophil Swarming to MRSA on a Bone Implant in a Murine Femur Model

**PRESENTING AUTHOR:** Sashank Lekkala

**CO-AUTHOR(S):** Youliang Ren, Jason Weeks, Allie Jia Hui Tay, Kevin Lee, Bei Liu, Thomas Xue, Joshua Rainbolt, Ye Shu, Chao Xie, Edward M. Schwarz, Shu-Chi A. Yeh

**LAB PI/MENTOR:** Edward M. Schwarz, Chao Xie

**ABSTRACT**

Introduction: Implant-associated osteomyelitis remains a major orthopaedic problem. As neutrophil swarming to the surgical site is a critical host response to prevent infection, elucidation of this dynamic behavior in vivo is central to understanding the host response. To this end, we developed a longitudinal imaging of bone marrow (LIMB) system to visualize bacteria and host cell dynamics proximal to a transfemoral implant in a murine model. While descriptive data from this model provided insights on "the race for the surface", quantitative outcomes of neutrophil swarming are needed for hypothesis testing research and product development. Therefore, we aimed to develop a robust semi-automated protocol to analyze LIMB videos of fluorescent bacteria and leukocytes for the quantification of neutrophil swarming behaviors.

Methods: We modified the previously developed LIMB system [1] to image a fixed region of interest proximal to a transfemoral implant. Catchup mice with tdTomato expressing neutrophils received a transfemoral pin with or without EGFP-expressing USA300 methicillin-resistant Staphylococcus aureus (MRSA). At 2-, 4-, and 6-hours post-implantation, real-time videos (30 minutes long) were obtained using intravital two-photon laser scanning microscopy. The semi-automated cell tracking protocol was adapted from Trainable Weka Segmentation (TWS) [2] and TrackMate [3] (Fiji/Image J), and customized MATLAB code for data integration. In brief, image stacks were drift-corrected using the Image Stabilizer plugin. Minimum intensity projection was subtracted from the stack to remove stationary artifacts. To avoid inter-user variability primarily introduced by inaccurate cell identification, the neutrophils were first segmented using TWS, which uses a library of machine learning training features to generate a probability score of the foreground (cells). The probability maps generated were used as input for TrackMate to track moving cells based on cell diameter and total displacement. The tracks were manually verified and then quantitated using a custom MATLAB code. Mann-Whitney tests adjusted by the Holm-Šídák method were used to test for statistical significance.

Results: To determine if the protocol yields reproducible results, two users independently analyzed three LIMB time-lapses and compared the tracking metrics. Inter-reader reliability was excellent as ICC > 0.98 for all neutrophil swarming outcome measures ($p > 0.05$). Further, when Catchup mice were challenged with a MRSA-contaminated or sterile implant, we observed that the neutrophils proximal to infected pins traveled farther and faster. Specifically, the distance and displacement of the neutrophils were greater at 6 hours, while the speed and velocity were greater at all measured time points in infected animals compared to uninfected animals.

Discussion: The key innovation in our protocol is the use of TWS to segment the neutrophils, which eliminates the need for arbitrary user-defined thresholding. The protocol can be easily adapted to study the kinematics of different cells by changing the TWS classifier and the tracking parameters. An inherent limitation of all cell tracking protocols is that they perform less optimally when the density of cells is high. Future studies focusing on track connection rules and penalties will help address this issue.

Significance: Our reproducible cell tracking protocol allows quantitative investigation of immune mechanisms such as neutrophil swarming, pathogen evasion strategies, and the effects of different drugs on the kinematics of immune cells. Additionally, these metrics can serve as benchmarks for assessing the efficacy of antimicrobial implants.

References: [1] Reismann, D. et al. Nature Communications. 8, 2153 (2017). [2] Arganda-Carreras, I. et al. Bioinformatics. 33 (15), 2424–2426 (2017). [3] Tinevez, J.Y. et al. Methods. 115, 80–90 (2017).

**PAPER #23**

**TITLE:** Tracing the Fate of the Subtypes of Endothelial Cells during Auto- and Allograft Repair and Reconstruction

**PRESENTING AUTHOR:** Tianfeng Miao

**CO-AUTHOR(S):** Chen Jiang

**LAB PI/MENTOR:** Xinping Zhang

**ABSTRACT**

Autografts can be attributed to the robust osteogenic and angiogenic activities of periosteum –a highly cellularized and vascularized thin membrane covering the outer surface of bone. While the essential role of periosteum has been well recognized, the angiogenic role of periosteum and more importantly the blood vessel types coupling to periosteum-mediated repair remain superficially understood. The limited knowledge hinders further efforts aimed at engineering effective and functional vessel networks for enhanced bone defect repair and regeneration. The goal of our current study is to utilize two transgenic animal models that respectively labels sprouting (AplnCreERT2) and arterial (BmxCreERT2) endothelial cells (ECs) to trace the fate of subtypes of endothelial cells and delineate blood vessel network formation during periosteum-mediated healing of autograft and allograft. To understand the coupling of vessel subtypes with bone forming cells, we have generated Col1(2.3) GFP; AplnCreER; Ai14 (tdTomato) and Col1(2.3) GFP; BmxCreER; Ai14 reporter mice, which allow simultaneous imaging of osteoblasts with the respective ECs at the periosteal healing site during long bone defect repair. By tracing AplnCreER+ vessels during repair, we found that AplnCreER+ ECs gave rise to the majority of blood vessels at the injury site, including vessels in the soft tissue as well as in newly formed bone. At the early stage, AplnCreER+ vessels coupled with osteoblasts exhibited unique morphology distinct from vessels in soft tissues. These vessels have been described in the literature as CD31hi and EMCNhi type H vessels specialized in bone. These AplnCreER+ vessels were found to be remodeled to become CD31lo and EMCNlo type L vessels in remodeling bone marrow at the late stage of healing. In contrast to Apln, BmxCreER+ vessels were only found in smaller numbers scattered in soft tissue and within bone forming callus during early phase of repair, and some of the BmxCreER+ vessels directly connect to type H vessels in bone forming tissues. BmxCreER+ ECs were found to directly contribute to the formation of bone marrow vasculature at the stage of callus remodeling. However, unlike AplnCreER+ EC, the BmxCreER+ EC were rapidly remodeled and replaced within callus. By week 7, only a small number of BmxCreER+ EC were identified in the remodeling bone marrow, suggesting the dynamic changes of EC cell fate under the influence of injury milieu. To further characterize the vessel subtypes during healing, immunofluorescent staining was performed using Sca1 and EMCN antibodies. Sa1+ vessels showed no overlap with AplnCreER+ vessels, but exhibited similar distribution as BmxCreER+ vessels before injury and at the early stage of healing. Before injury, these vessels were absent amidst GFP+ osteoblasts beneath the growth plate, but mainly located in the diaphyseal region of long bone as large diameter arteries, overlapping with BMXCreER+ vessels. Following injury, Sca1 only labeled very few vessels in the early callus. In contrast, EMCN labeled the vessels beneath the growth plate which were also AplnCreER+. EMCN+ vessels expanded rapidly in the periosteal callus at the early stage of healing, overlapping with AplnCreER+ vessels. Taken together, our study demonstrates differential distribution and responses of the two subtypes of vessels during repair, suggesting the unique coupling of vessel types with osteoblasts and bone marrow. Our study also shown an unexpected differentiation of BmxCreER+ ECs to form bone marrow vasculature in periosteum callus at late stage of healing, suggesting that healing microenvironment could markedly impact the endothelial cell fate during repair and reconstruction. Further transcriptomic analyses delineating spatially controlled gene expression profiles associated with types of ECs are underway to understand the differential control of EC subtypes in response to healing microenvironment for effective regeneration.

**PAPER #24**

**TITLE:** Distinct Mast Cell Subpopulations within and around Lymphatic Vessels Regulate Lymph Flow and Progression of Inflammatory-Erosive Arthritis in TNF-tg Mice

**PRESENTING AUTHOR:** Yue Peng

**CO-AUTHOR(S):** H. Mark Kenney, Karen L. de Mesy Bentley, Lianping Xing, Christopher T. Ritchlin & Edward M. Schwarz

**LAB PI/MENTOR:** Edward M. Schwarz

**ABSTRACT**

Objective: Inflammatory-erosive arthritis is exacerbated by dysfunction of joint-draining popliteal lymphatic vessels (PLVs).(1) Synovial mast cells (MCs) are known to be pro-inflammatory in rheumatoid arthritis (RA).(2) However, in other settings they have anti-inflammatory and tissue reparative effects. Herein, we elucidate the role of MCs on PLV function and inflammatory-erosive arthritis in tumor necrosis factor transgenic (TNF-tg) mice that exhibit defects in PLVs commensurate with disease progression.

Methods: Whole mount immunofluorescent microscopy, toluidine blue stained histology, scanning electron microscopy, and in silico bioinformatics were performed to phenotype and quantify PLV MCs. Ankle bone volumes were assessed by µCT, while corresponding histology quantified synovitis and osteoclasts. Near-infrared indocyanine green (NIR-ICG) imaging measured lymphatic clearance as an outcome of PLV draining function. Effects of genetic MC depletion were assessed via comparison of 4.5-month-old WT, TNF-tg, MC deficient KitW-sh/W-sh (cKit-/-) (3), and TNF-tg x cKit-/- mice. Pharmacological inhibition of MCs was assessed by treating TNF-tg mice with placebo or cromolyn sodium (3.15mg/kg/day) for 3-weeks.

Results: PLVs are surrounded by MCT+/MCPT1+ MCs whose numbers are increased 2.8-fold in TNF-tg mice. The percentage of peri-vascular degranulating MCs was inversely correlated with ICG clearance. We also identified a novel population of MCT+/MCPT1- MCs that were embedded within the PLV structure. In silico single-cell RNA-seq (scRNAseq) analyses identified a population of PLV-associated MCs (marker genes: Mcpt4, Cma1, Cpa3, Tpsb2, Kit, Fcer1a & Gata2) with enhanced TGFbeta-related signaling that are phenotypically distinct from known MC subsets in the Mouse Cell Atlas.(4) Interestingly, the cKit-/- mice had greater lymphatic defects than TNF-tg mice, and TNF-tg x cKit-/- mice displayed an exacerbation of lymphatic dysfunction and inflammatory-erosive arthritis vs. TNF-Tg mice. Cromolyn sodium therapy stabilized PLV MCs, increased TNF-induced bone loss, synovitis, and osteoclasts, and decreased ICG clearance.

Conclusions: MCs are required for normal lymphatic function. Genetic ablation and pharmacological inhibition of MCs exacerbates TNF-induced inflammatory-erosive arthritis with decreased lymphatic clearance. Together, these findings support an inflammatory role of activated/degranulated peri-PLV MCs during arthritic progression, and a homeostatic role of intra-PLV MCs, in which loss of the latter dominantly exacerbates arthritis secondary to defects in joint-draining lymphatics, warranting investigation into specific cellular mechanisms.

Acknowledgments: This work was supported by NIH grants R01AG059775, R01AR069000, R01AR056702, & P30 AR069655.

References: 1) Bouta et al. Nat Rev Rheum. 14(2):94-106. 2018. 2) Pal et al. Front Immunol. 11:1234. 2020. 3) Grimbaldeston et al. Amer J Pathol. 167(3):835-48. 2005. 4) Kenney HM, et al. Arthritis Res Ther 24(1):64. 2022

**PAPER #25**

**TITLE:** High levels of efferocytosis by mesenchymal stromal cells increases their senescence and decreases bone

**PRESENTING AUTHOR:** Emily R. Quarato

**CO-AUTHOR(S):** Noah A. Salama, Yuko Kawano, Allison J. Li, Roman Eliseev, and Laura M. Calvi

**LAB PI/MENTOR:** Laura M. Calvi

**ABSTRACT**

Age-dependent bone loss is a manifestation of skeletal aging. Hallmarks of skeletal aging include mesenchymal stromal/stem cell (MSC) dysfunction and cellular senescence. However, the mechanisms inducing MSC senescence remain unclear. We found that MSCs contribute to the clearance of apoptotic cells in the bone marrow (efferocytosis). While rates of efferocytosis are low at homeostasis, in aging, MSCs increase their efferocytic activity. Thus we hypothesized that excess efferocytosis may contribute to MSC dysfunction and senescence, and represent a previously unknown mechanism of bone loss. In vitro, excess efferocytosis induced MSC dysfunction through increased mitochondrial fission and metabolic disruption. Additionally, MSCs with high efferocytic burden had transcriptional evidence of increased senescence, which we confirmed functionally. In a mouse model of enhanced efferocytosis by MSCs (PrxCrexBai1), we confirmed increased efferocytosis (70% to 85%) and efficiency by MSCs, and found that efferocytic MSCs had increased rates of senescence compared to controls (40% vs 20%). Consistent with a negative effect of excessive efferocytosis on bone homeostasis, Bai1 x PrxCre mice at 3 months had decreased cortical thickness, which significantly declined with age (12m) compared to controls. In this model, MSC dysfunction was also decreased as shown by CFU-F/OB counts. To confirm that the increase in MSC efferocytosis was a result of the actively working Bai1 receptor, we also created a subsequent model which introduced the Bai1 receptor with a mutation (Bai1AAA x PrxCre) that block its ability to initiate apoptotic cell engulfment. MSCs from the Bai1AAA x PrxCre model did not show an increase in MSC efferocytic activity or senescence compared to controls. We next profiled the efferocytic machinery in MSCs, and identified Axl, one of TAM receptors (Tyro3, Axl, MerTK) as the primary efferocytic receptor on MSCs. To confirm its role in MSC efferocytosis, we tested small molecule inhibitors of the TAM receptors on MSC in vitro and found that combined Axl and Tyro3 inhibition completely blocks MSC efferocytosis. In mice with global loss of Axl, MSCs had decreased efferocytic efficiency, and increased bone mineral density/content, trabecular number, and cortical thickness, in both young (3m) and aged (24m) mice. Additionally we confirmed in vitro that loss of Axl decreases MSC senescence at 24m. Collectively, our data support the idea that excess efferocytosis is a novel mechanism of bone loss. MSC efferocytosis is increased by defects in professional phagocytic cells, such as macrophages. Therefore, senescence induced by excessive MSC efferocytosis may be an underappreciated mechanism of bone loss in settings of defective macrophages, as in aging, obesity, autoimmunity, and diabetes-induced bone loss. Given the unique reliance of MSC efferocytosis on Axl, this novel mechanism may be pharmacologically targetable for the treatment of bone loss in aging and in other diseases caused, in part, by MSC efferocytic excess.

**PAPER #26**

**TITLE:** Aged Mesenchymal Stem Cells Exhibit Distinct Post-Efferocytic Polarization In Vivo by Single Cell RNA Sequencing

**PRESENTING AUTHOR:** Noah A. Salama

**CO-AUTHOR(S):** Emily R. Quarato, Yuko Kawano, Jane L. Liesveld, Laura M. Calvi

**LAB PI/MENTOR:** Laura Calvi

**ABSTRACT**

The bone marrow is a location for not only cellular production but also the elimination of naturally apoptotic cells. The clearance of these corpses in a safe non-inflammatory fashion is referred to as efferocytosis and is essential for not only hematopoietic function but also skeletal health. Our laboratory has recently shown that MSCs assist professional phagocytes such as macrophages with the clearance of apoptotic cells as non-professional phagocytes within the bone marrow microenvironment. Furthermore, we demonstrated that, while macrophages decrease efferocytic capacity with age, MSCs exhibit a concomitant increase in efferocytosis. Since it has been previously demonstrated that efferocytosis has substantial impact on polarization and metabolic activity in phagocytic cells, we examined the impact of efferocytosis on MSC differentiation and function using an MSC cell line (ST2 cells) and primary cells derived from young adult mice. These studies demonstrated that efferocytic activity by MSCs drives mitochondrial fission, decreasing their ability to perform osteoblastic differentiation. Efferocytic MSCs also demonstrated increased senescence and apoptosis in a dose dependent fashion.
Due to our data about the shift in efferocytic responsibility with age in vivo, we speculated that MSCs and macrophages may have distinct post efferocytic reprogramming or unique subsets with specialized efferocytic activity that change with age. To test this, we performed in vivo efferocytic challenges on young (4-6mo) and aged (20mo) WT mice using PKH labeled human derived neutrophils (10e6 cells/mouse). We then enriched for MSCs and macrophages and sorted cells that were positive or negative for the engulfed neutrophils for downstream single cell RNAseq. We have demonstrated as well as others in the efferocytic field that, although neutrophils rapidly degrade RNA during apoptosis, minor cargo transcripts can be detected in the phagocytic cells that engulf them. To reduce contaminant reads we utilized human derived neutrophils which will not align as readily with the mouse reference genome.

After subclustering on MSC lineage cells and macrophages separately we were able to identify efferocytically active cells across all clusters, but also identified clusters with higher efferocytic activity. Moreover, we were able to detect minor transcripts carried over from engulfed murine-derived targets in the highly efferocytic population that by QC cannot be excluded as contamination, doublets, or limited read depth. Our findings further confirm that MSCs do in fact perform efferocytosis at homeostasis across age groups and that we can detect post efferocytic differential expression on a single cell level. While we confirmed efferocytic potential in MSCs across age groups, we also noted a change in efferocytic processing by aged cells which appear to utilize distinct efferocytic receptors and internal

processing of engulfed targets compared to young. Furthermore, while young MSCs reconfirmed our prior bulk RNAseq and functional results that efferocytosis reduces osteogenic potential and drives apoptosis, aged MSCs demonstrated increased adipogenic potential and suggested a greater drive toward senescence over apoptosis. Interestingly, non-efferocytic aged MSCs demonstrated a similar baseline potential for adipogenic polarization to young. This could suggest that the well-known phenomenon of increased bone marrow adiposity in aging and osteoporosis could be partially explained by post efferocytic differences in aged MSCs. By better understanding efferocytic clearance at a single cell level, we may identify novel therapeutic targets that balance the clearance of apoptotic cells while mitigating potential detrimental impact on stromal progenitors. This strategy may be helpful in scenarios where apoptotic cells accumulate such as aging or in pathologic states such as fracture or cancer.

**PAPER #27**

**TITLE:** Acute myeloid leukemia (AML)-on-a-chip recapitulates the leukemic cell-mediated dysregulation of the bone marrow microenvironment in vitro.

**PRESENTING AUTHOR:** Azmeer Sharipol

**CO-AUTHOR(S):** Celia A. Soto, Amal Khan, Maggie L. Lesch

**LAB PI/MENTOR:** Danielle S.W. Benoit, Benjamin J. Frisch

**ABSTRACT**

Acute myeloid leukemia (AML) is an aggressive blood cancer characterized by the uncontrolled expansion of dysfunctional myeloid progenitor cells in the bone marrow (BM). AML-driven dysregulation of the BM microenvironment (BMME) leads to loss of normal hematopoiesis and BM failure. With the median diagnosis age of 68 and the growing aging population, AML cases are projected to climb substantially. The standard care for the majority of patients, introduced in the 1970s, results in an abysmal 5-year survival rate of ~30%. The lack of therapeutic advancement is partly due to the challenging task of recapitulating the signaling between AML cells and the BMME components in vitro such as the osteoblastic, mesenchymal stromal (MSC), and endothelial cells, and the matrix. To bridge this gap, our lab aims to develop AML-on-chip models (AML-chip) to study BMME dysregulation in vitro and as a tool to identify new therapeutic targets. Previously, we developed a murine BMME-chip model containing mineralized osteoblastic and flow-induced endothelial components using Emulate Chip-S1™ that can maintain the long-term function of hematopoietic stem and progenitor cells (HSPC) for at least 14 days in vitro (Sharipol et al., 2022). To develop the AML-chip, we cultured AML cells isolated from blast crisis chronic myelogenous leukemia (bcCML) mice in the marrow component of the BMME-chip with MSC, HSPC, and fibrin-hydrogel. At day 14, AML cells were maintained at 29.00±2.35% equivalent to disease burden at advanced stages of AML. Flow cytometry showed a 4-fold increase in HSPC in AML-chip, similar to in vivo, which may indicate loss of differentiation. Similar to in vivo experiments, we found that osteoblastic function is lost in AML-chip as shown by reduction of osteocalcin gene expression at day 7 and 14 (41.10±13.50% and 16.60±5.00% respectively compared to BMME-chip, $p=0.04$). This finding is reflected in the decrease of mineralization of the osteoblastic cells observed via histochemical imaging. We have previously reported that the chemokine CCL3 is elevated in AML patients as well as murine models, and that elevated CCL3 inhibits osteoblastic function. Strikingly, we found elevated levels of CCL3 in the effluent of AML-chip compared to BMME-chip (918.49±192.54 pg/mL and 498.73±79.05 pg/mL, $p=0.003$). Our results indicate that AML-chip can recapitulate the phenotypes reported in vivo, and supports the reliability of our system to recapitulate the human AML microenvironment in future experiments.

**PAPER #28**

**TITLE:** Effects of Elevated Lactate in Acute Myeloid Leukemia Bone Marrow Microenvironment Dysfunction, with a Dual Role of GPR81 Signaling in Macrophage Polarization and Leukemia Cell Growth

**PRESENTING AUTHOR:** Celia Soto

**CO-AUTHOR(S):** Maggie Lesch, Azmeer Sharipol, Amal Khan, Xenia Shafer, Michael Becker, Joshua Munger

**LAB PI/MENTOR:** Benjamin Frisch

**ABSTRACT**

Acute myeloid leukemia (AML) is within the top ten cancer subtypes with the most numerous deaths per year in the U.S. [SEER, NIH], with a ~90% mortality rate of the most-affected group, aged 65+, at five years past diagnosis. Morbidity is due to bone marrow microenvironment failure, loss of healthy blood cell production leading to infection, and common relapse from chemotherapy. Recent advances in the knowledge of the solid tumor microenvironment (TME) of multiple cancer types have revealed the complexities of cancer progression, including cancer cell secretion of metabolites and factors that lead to the polarization of immune cells to a cancer-permissive suppressive phenotype. To study the unique cancer microenvironment of the leukemic bone marrow, we performed metabolomics on AML bone marrow aspirate extracellular fluid. Higher metabolite levels were measured in the bone marrow of AML patients at diagnosis compared to healthy controls, including lactate (mmol/L = 3.62 vs 1.31, $p < 0.05$, $n = 5$), which has been implicated in the solid tumor microenvironment immune phenotypes and cancer cell growth and chemoresistance. We hypothesized that excess bone marrow lactate advances leukemia progression by similar mechanisms. However, as bone marrow is a unique tumor microenvironment, research is also needed on the contribution of lactate to diminished hematopoiesis and alterations at the stromal hematopoietic stem cell (HSC) niche. This study used: (i) a murine AML model of blast crisis chronic myelogenous leukemia (bcCML) that recapitulated the metabolomic analysis of human AML, and (ii) C57BL/6J wild type mice or a transgenic knockout of the extracellular lactate receptor GPR81 (GPR81-/-). Leukemia-associated macrophages (LAMs) were found to overexpress the mannose receptor CD206, a suppressive macrophage marker, and bulk RNA sequencing revealed a unique LAM phenotype with altered transcripts related to immune cell interactions. Then, LAMs in GPR81-/- bcCML mice had a reduced expression of CD206 (fold-change MFI = 4.98 vs 2.06, $p < 0.05$, $n = 11$) and reduced Arginase-1 expression compared to non-leukemic, suggesting that GPR81 signaling contributes to macrophage polarization. Next, hematopoietic potentiality was assayed by culturing murine hematopoietic stem and progenitor cells (HSPCs) then observing colony-forming ability (CFU-Cs) when plated in methylcellulose-containing media; exposure to physiologically-relevant elevated lactate levels (5-15 mmol/L) for 72 hours reduced CFU-Cs both when alone (fold-change = 0.43, $p < 0.01$, $n = 8$) and when cocultured with a stromal monolayer (fold-change = 0.41, $p < 0.001$, $n = 14$) consisting of bone marrow mesenchymal stem cells (MSCs), a key cell type of the HSC niche, and macrophages. This suggests that stromal bone support is not able to protect HSPCs from the effects of the lactate. Also, MSCs displayed reduced fibroblastic (fold change area 0.63, $p < 0.005$, $n = 17$) and osteoblastic colonies upon differentiation in the presence of elevated lactate. Knockout of GPR81 had little effect on these hematopoietic progenitor or supportive populations. Finally, leukemia progressed more slowly when bcCML was initiated using GPR81-/- leukemia cells compared to wild type (% leukemic bone marrow cells at day 13 = 11.75 vs 45.54, $p < 0.05$, $n = 5$). Notably, in serial passaging of leukemic colonies in vitro, leukemia stem cell repopulating ability of GPR81-/- bcCML cells was reduced compared to wild type (2.5 vs. > 7 passages, $n = 3$). These results suggest that lactate-GPR81 signaling contributes to AML LAM polarization, affects the hematopoietic potential of blood progenitor cells, and is critical to leukemia cell growth and repopulation. This research identifies lactate as a driver of AML progression, highlighting GPR81 as an exciting and novel therapeutic target for both leukemia cells and LAMs without major alterations to the bone marrow hematopoietic populations.

**PAPER #29**

**TITLE:** Mitochondrial Metabolism Determines Mesenchymal Stem Cell Fate

**PRESENTING AUTHOR:** Chen Yu

**CO-AUTHOR(S):** Yu, C, Sautchuk, R, Eliseev, RA

**LAB PI/MENTOR:** Eliseev, RA

## ABSTRACT

**Introduction:** Aging-related changes in bone marrow stromal (a.k.a. mesenchymal stem) cells (BMSCs) shift cell fate away from osteogenesis and towards adipogenesis. This leads to lower bone formation and higher bone marrow fat content. The mechanism(s) underlying such changes are not completely understood. Mitochondria are important cell organelles that not only produce energy but also determine cell behavior by regulating metabolism, signaling, calcium homeostasis, apoptosis, and other cellular processes. We have previously shown that mitochondrial activation is important during osteogenesis of BMSCs. Such activation is in large part due to a decrease in the activity of the mitochondrial permeability transition pore (mPTP) caused by downregulation of its positive regulator, cyclophilin D (CypD). We also found that in aged bone tissue, there is pathological opening of the mPTP which leads to mitochondrial dysfunction. Adipogenesis is an alternative fate for BMSCs, and the goal of our study was to determine how CypD and mPTP are regulated during this process and whether they play a role in BMSC fate shift.

**Methods:** RT-qPCR and western blot were performed to measure CypD expression in C3H10T1/2, a mouse embryonic mesenchymal cell line, and primary mouse BMSCs during adipogenesis. Live-cell mitochondria-specific fluorescent staining and Seahorse bioenergetic profiling were used to evaluate mitochondrial morphology and function, respectively. We used CypD gene, *Ppif,* promoter luciferase reporter assay and ChIP-PCR to study CypD transcriptional regulation during adipogenesis. To evaluate the effect of CypD deletion or overexpression in BMSCs on bone marrow fat, we used $Prx1^{Cre}$-mediated $Ppif^{f/f}$ or $caPpif^{TG}$ mouse models, respectively, and osmium tetroxide staining and histology analysis.

**Results:** We observed that during adipogenesis, BMSCs significantly upregulate glycolysis and increase CypD expression and mPTP activity. Confocal imaging shows that mitochondria are rounded and fragmented during this process, consistent with high mPTP activity. *Ppif* promoter analysis reveals multiple binding sites for adipo- genic C/EBP and inflammatory NF-κB transcription factors. Luciferase assay and ChIP-PCR analysis confirm C/EBPα as a transcriptional activator of CypD. NF-κB p65 translocates to the nucleus during adipogenesis and shows synergistic effect with C/EBPα in inducing *Ppif* expression, suggesting a potential link between 'inflammaging' and altered BMSC fate. *In vitro* CypD overexpression enhances, whereas CypD knockdown impairs adipogenesis. Pharmacological inhibition of CypD by NIM811 also impairs adipogenesis *in vitro*. Preliminary histology analysis shows that $Prx1^{Cre}$-mediated deletion of CypD in $Ppif^{f/f}$ mice decreases bone marrow fat in 12- month-old mice. Currently we are pursuing the effect of $Prx1^{Cre}$-mediated mouse models at 4 months or 12 months.

**Discussion:** BMSCs upregulate CypD expression during adipogenesis leading to increased mPTP activity, activated glycolysis and low mitochondrial function. It is consistent with the observation of fragmented and rounded mitochondria in mature adipocytes, thus establishing a metabolic profile that appears to be favorable for adipogenic lineage. Aging and age-related diseases are associated with chronic inflammation within tissues and increased intracellular inflammatory signaling. Transcriptional regulation of *Ppif* expression by C/EBPα and NF-κB p65 suggests a potential mechanism for age-related change of differentiation capacity in BMSCs.

**Significance:** Success of this project will provide better understanding of the regulatory role of mitochondria and CypD/mPTP during stem cell fate determination, especially adipogenesis of BMSCs. It will provide information about potential therapeutic targets to inhibit excessive adipogenesis in pathological conditions such as osteoporosis and age-related bone loss.

**PAPER #30**

**TITLE:** The Role of Type III Collagen in Tendon Fibrosis: Insights from Hydrogel Models for Scarless Tendon Repair

**PRESENTING AUTHOR:** Victor Zhang

**CO-AUTHOR(S):**

**LAB PI/MENTOR:** James McGrath, Hani Awad

**ABSTRACT**

Tendons have limited regenerative capacity resulting in the formation of fibrotic scars after injury. Of note, there is dysregulation of the normal extracellular matrix (ECM) environment and an influx of immune and vascular cells during healing. Healthy tendons are largely comprised of type I collagen. After injury, there is an increase in other collagen types such as type III collagen which can rise to account for 20% of all collagens. Our prior data has shown that altering the type I to type III collagen ratio leads to a dramatic change in the hydrogel ultrastructure for in vitro and microphysiological models. These changes inhibited the motility of immune cells migrating through hydrogels. In the current study, we investigate the effects of type III collagen on other relevant cells in tendon fibrosis. As type III collagen is expected to mimic scar tissue, we hypothesize that it will facilitate angiogenesis from endothelial cells akin to the neovascularization seen after injury. Additionally, we hypothesize that type III collagen hydrogels will promote the differentiation of tenocytes to myofibroblasts.

Commercially available collagen products were used to make 2 mg/mL hydrogels made of 95% type I and 5% type III collagen ("type I collagen") and 80% type I and 20% type III collagen ("type III collagen"). Human umbilical vein endothelial cells (HUVECs) were cultured as three-dimensional spheroids in collagen hydrogels with EGM-2 medium. After 24 hours of culture, sprout number and length were quantified. Human primary tenocytes were suspended in collagen hydrogels at 500,000 cells/mL and cultured in a custom-made microphysiological platform. Samples were cultured in a 10% FBS-supplemented medium for 5 days after which they were fixed and stained with an antibody targeting α-SMA and imaged using confocal microscopy. Contraction kinetics were compared by measuring the two-dimensional area of hydrogels in the device normalized to the starting area. Experimental results from type I and type III collagen groups were compared using Welch's t-test. For each condition, 19 spheroids were analyzed for angiogenesis experiments, and 5 hydrogels were analyzed for tenocyte experiments.

Spheroids cultured in type I collagen hydrogels had fewer (3.4 vs 7.4) and shorter (47 µm vs 55 µm) sprouts than their counterparts in type III collagen gels. Tenocytes had positive expression of α-SMA shown by immunofluorescence imaging regardless of collagen type. Cells in type I collagen hydrogels were aligned in the direction of strain provided by the device while those in type III collagen gels had more spread morphology with no alignment. Additionally, type I collagen gels contracted on average 29% of their area compared to only 10% contraction in type III collagen gels.

These results suggest that hydrogels with high type III collagen facilitate angiogenesis. This may be due to a direct response of endothelial cells to their biochemical environment or effects on cell migration during the phases of angiogenesis. The recapitulation of fibrotic neovascularization supports the use of type III collagen hydrogels in vitro for more accurate modeling of tendon fibrosis. The rapid contraction of type I collagen hydrogels and not type III gels was counter to our initial hypothesis. Cells in both hydrogels are positively expressing the α-SMA of contractile myofibroblasts despite differences in alignment and morphology. We hypothesize that the differences in the hydrogels alter the cells' ability to remodel the ECM. This may be relevant to scar resolution as fibrosis could prevent myofibroblasts from performing their normal function of closing wounds. Future work will use microrheology to characterize the viscoelastic properties of the hydrogels experienced by cells. We anticipate that these experiments will help to explain the differences seen in hydrogel remodeling and inform the design of culture protocols in our human Tendon-on-a-Chip studies.

# *Posters*

## Disclaimer

**PAPER #31**

**TITLE:** Physical and Cognitive Function during Post-Acute Care following Total Joint Arthroplasty among Medicare Beneficiaries: Trends from 2013-2018

**PRESENTING AUTHOR:** Nikhil Ailaney, MD

**CO-AUTHOR(S):** Meiling Ying, PhD; Benjamin Ricciardi, MD; Caroline Thirukumaran, MBBS, MHA, PhD

**LAB PI/MENTOR:** Caroline Thirukumaran, MBBS, MHA, PhD

**ABSTRACT**

Background
Although the use of skilled nursing facilities (SNF) and inpatient rehabilitation facilities (IRF) following total joint arthroplasty (TJA) have decreased, favoring discharge home under the care of home health agencies (HHA), physical and cognitive conditions of patients entering these settings has not been evaluated. This study aims to examine trends in the physical and cognitive function of Medicare beneficiaries discharged to SNFs, HHAs, and IRFs from 2013 to 2018 following TJAs.

Methods
We used the 2013-2018 Medicare enrollment, claims, and assessment data to examine the association between the endpoints of interest (discharge destination [SNF, HHA, or IRF], and the physical [measured using activities of daily living] and cognitive [measured using a range of setting-specific metrics] status of patients in each setting) and the year of TJA (2013-2018) by estimating multivariable multinomial, linear, and linear probability models that controlled for patient- and hospital-level covariates.

Results
On multivariable analysis of 1,278,939 TJAs, discharge to SNF decreased (44.15%[2013] to 21.57%[2018], $p<0.001$), HHA increased (46.72% to 72.47%, $p<0.001$), and IRF decreased (9.13% to 5.69%, $p<0.001$). For SNF, mean physical function scores (14.61[2013] to 14.23[2018], $p<0.001$) and patients with cognitive impairment (13.25% to 12.33%, $p=0.01$) decreased, indicating less dependence. Physical function scores (3.09 to 3.94, $p<0.001$) and cognitive impairment (13.95% to 16.52%, $p<0.001$) increased for HHA patients, indicating greater dependence. For IRF, the motor functional independence measure decreased (38.81 to 37.78, $p<0.001$), and cognitive dependence increased (39.08% to 46.36%, $p<0.001$), indicating greater dependence.

Conclusions
Over the study period, patients were increasingly discharged to HHA following TJAs. While SNF patients were less dependent over time, HHA and IRF patients were physically and cognitively more dependent. Each of these settings is likely to benefit from policy and fiscal support that helps them manage changes in the volume and clinical intensity of patients needing their services.

**PAPER #32**

**TITLE:** Short Term Pain in Cemented versus Cementless Total Knee Arthroplasty: A Systematic Review and Meta-Analysis

**PRESENTING AUTHOR:** Dr. Nikhil Ailaney

**CO-AUTHOR(S):** Dr. Matthew Barra, Dr. Derek Schloemann, Dr. Caroline Thirukumaran

**LAB PI/MENTOR:** Dr. Nathan B. Kaplan

**ABSTRACT**

Background
Cementless total knee arthroplasty (TKA) has increased in popularity to potentially improve long-term survivorship. Radiostereometric studies demonstrate increased component migration during the first 3-6 months in cementless constructs, generating concern for increased post-operative pain during early osseointegration. The purpose of this study was to evaluate short-term pain and function in cemented versus cementless TKA. We hypothesize that cementless TKA patients report increased pain during the short-term (<6 months) post-operative period.

Methods
MEDLINE, EMBASE, CINAHL, and Cochrane Library were searched for studies evaluating short-term outcomes of cemented versus cementless primary TKA. Studies involving hybrid fixation were excluded. Meta-analysis was performed using standardized mean difference (SMD) for primary outcomes (early post-operative pain) and weighted mean difference (WMD) for secondary outcomes (early post-operative function).

Results
Eleven studies were included. There was no significant difference in acute post-operative pain between cemented and cementless TKA within six months of index TKA (SMD 0.08 in favor of cemented TKA; p=0.10). Early post-operative Forgotten Joint Scores (WMD 0.81; p=0.81) and Knee Injury and Osteoarthritis Outcome Scores for Joint Replacement (WMD 0.80 in favor of cemented TKA; p=0.14) were also similar between groups.

Conclusion
There is no difference in short-term pain or early function between patients receiving cemented versus cementless TKA. This suggests that surgeons may utilize cementless TKA without fear of increased short-term pain due to micromotion. However, additional studies with uniform assessment methods are needed to further inform differences in short-term pain and early functional outcomes between cemented and cementless TKA.

**PAPER #33**

**TITLE:** Unraveling the Role of mTOR in Tendon Fibrosis: Implications for Targeted Therapies and Scar-Free Healing

**PRESENTING AUTHOR:** Rahul Alenchery

**CO-AUTHOR(S):** Hani Awad

**LAB PI/MENTOR:** Hani Awad

**ABSTRACT**

INTRODUCTION: The incomplete understanding of cellular and molecular processes in fibrotic tendon healing hinders regenerative therapies. A common fibrotic driver, Transforming Growth Factor-beta 1 (TGF-β1), affects matrix turnover, cell proliferation, α-SMA activation, and Plasminogen Activator Inhibitor 1 (PAI-1). RNA-Seq data identified PTEN, a master regulator of mTOR signaling, to be notably enriched in scarless healing of PAI-1 KO mice. Furthermore, our in vitro data has established how TGF-β1, PAI-1, and mTOR interact in tendon fibroblasts to regulate the fibrotic phenotype, α-SMA, Ki67, and γ-H2AX. With these findings in hand, our objective is to understand the role of mTOR in various cell types involved in tendon repair and evaluate mTOR inhibition as a disease-modifying therapy for injured flexor tendons.

METHODS: The murine injury model involves a partial laceration of the deep digital flexor tendon in the hind paw's middle digit of C57Bl6/J mice. Flow cytometry analyzed cells from D7 & D14 post-surgery (n=4/time point), probing for specific markers (Scleraxis, CD31, CD45), mTORC1 signaling proteins (SMAD2/3, PTEN, Akt, pS6, p4E-BP1), and fibrosis markers (α-SMA, Ki67, γ-H2AX). At D7 post-injury (n=2-3/group), we performed histology and Nanostring GeoMX spatial proteomic profiling. To assess mTOR inhibition effects, we administered 4 mg/kg Rapamycin or DMSO daily from D7-D16 post-injury (n=9-13/treatment). Uninjured tendons served as controls.

RESULTS: Using flow cytometry, we isolated cells from the tendon injury site and categorized them using markers (CD31 for endothelial cells, CD45 for leukocytes). At 7- and 14-days post-injury, CD45+ leukocytes increased significantly compared to uninjured tendons, while CD31−CD45− cells decreased. We further observed α-SMA and γ-H2AX to be upregulated with injury and associated with increased phosphorylated mTOR proteins (pS6 and p4E-BP1) in CD31−CD45− cells. CD31−CD45−SCX+ (tendon specific) cells showed sustained α-SMA activity up to 2 weeks post-injury. Using NanoString GeoMx, we investigated the peritendinous microenvironment at 7 days post-tendon injury, revealing an upregulation in mTOR-associated signaling proteins (phosphorylated S6, total S6, MET, and pan-AKT), downregulation of PRAS40, and increases in pro-inflammatory and macrophage markers (CD68, CD163, CD11b, Ly6C, CD14, CD45, CD11c). Injured tissue also exhibited enrichment in apoptotic markers (BIM, BCLXL, Caspase 3, BAD, Perforin, PARP) and reduced DNA damage response (γ-H2AX and P53). Given the observed association between the mTOR activation and tendon injury, we postulated that rapamycin might improve the tendon healing response. Rapamycin treatment in vitro suppressed αSMA activity, pS6, and p4E-BP1 activity in tenocytes. In vivo, Rapamycin-treated injured tendons showed accelerated increases in tensile stiffness and strength compared to DMSO-treated controls.

DISCUSSION: In summary, our study underscores mTOR signaling's key role in myofibroblast differentiation in injured tendon fibroblasts. This corroborates similar observations in other fibrotic conditions in major organs. The identification of mTOR activation, which seems associated with inflammation, is significant because it is a druggable target. Our results indicate that rapamycin treatment accelerates tendon strength and stiffness by suppressing immune response and α-SMA activity. These findings not only underscore the pivotal role of mTOR signaling in tendon repair but also highlight the potential of mTOR inhibitors like Rapamycin as a disease-modifying therapeutic strategy for tendon injuries. Since mTOR inhibitors are in clinical trials for pulmonary fibrosis, the association between mTOR signaling and poor outcomes of tendon injury makes mTOR a novel and promising therapeutic target for fibrotic peritendinous adhesions. Future research should optimize mTOR inhibitor dosage and timing for complete restoration of injured tendon biomechanics.

**PAPER #34**

**TITLE:** Cutibacterium acnes deforms and invades submicron osteocyte lacuno-canalicular networks (OLCN) following implant-associated osteomyelitis

**PRESENTING AUTHOR:** Mina Botros

**CO-AUTHOR(S):** Karen L. de Mesy Bentley, Derek Schloemann, Motoo Saito, Edward Schwarz, Benjamin F. Ricciardi, Gowrishankar Muthukrishnan

**LAB PI/MENTOR:** Gowrishankar Muthukrishnan

**ABSTRACT**

INTRODUCTION: There is a paucity of literature examining the pathogenesis of Cutibacterium acnes (formally known as Propionibacterium acnes) associated prosthetic joint infections (PJI). Total joint arthroplasty (TJA) is one of North America's most performed orthopedic elective procedures. The volume of primary and revision hip and knee replacement is reported to continue to increase dramatically over the next few decades. A major complication associated with TJA is PJI, one of the major reasons patients with total hip and knee replacements undergo revision surgery. Recently, there has been a rise in the number of reported C. acnes in the PJI associated with total hip and knee arthroplasty. The impact of C. acnes on an infected prosthesis can be underestimated due to the following reasons: 1) it is a common skin commensal organism; 2) C. acnes is challenging to culture; 3) it requires an increasing number of tissue samples and extended incubation time (usually up to 2 weeks). This study aims to develop a trans-tibial implant-associated osteomyelitis murine C. acnes model to examine its pathogenesis and ability to invade the bone niche.

METHODS: An in vivo murine C. acnes implant-associated osteomyelitis was developed, which included 20-week-old C57BL6 mice receiving trans-tibial titanium or stainless-steel pins inoculated with C. acnes. Infected mice were sacrificed on day-14 & -28, and the infected tibia, transtibial implant, soft tissue, and internal organs (heart, spleen, kidney, and liver) were harvested and processed for colony-forming unit (CFU) quantification, µCT, histology, and transmission electron microscopy (TEM) examination of the tibiae.

RESULTS: Scanning Electron Microscopy (SEM) demonstrated no difference between the attachment and biofilm formation of C. acnes onto titanium implant compared to stainless steel. SEM and CFU analysis of infected pins removed from the tibia showed no C. acnes on implants. Terminal CFU assessments showed extensive C. acnes dissemination to internal organs from the infected site. Histological comparison of infected C. acnes tibiae compared to S. aureus-infected ones showed dramatic differences in the extent of abscess formation. Moreover, µCT revealed significantly lower bone osteolysis in the C. acnes-infected tibia compared to S. aureus-infected animals. Most notably, TEM studies on C. acnes-infected tibia revealed evidence of osteocyte lacuno-canalicular network (OLCN) invasion by C. acnes.

CONCLUSION: C. acnes is capable of colonizing and invading the OLCN. This result defines a new mechanism of C. acnes persistence within the bone niche and a potential reservoir for this pathogen during chronic osteomyelitis.

**PAPER #35**

**TITLE:** Increased Pelvic Asymmetry following Pelvic Ring Fixation of Lateral Compression Injuries When Compared to Anterior-Posterior Compression Injuries

**PRESENTING AUTHOR:** James D. Brodell, Jr., M.D.

**CO-AUTHOR(S):** Hashim Shaikh, Urvi J. Patel, M.D., John P. Ketz, M.D. , John T. Gorczyca, M.D.

**LAB PI/MENTOR:** Sandeep Soin, M.D.

**ABSTRACT**

Purpose: The purpose of our study is to determine if there exists any difference in the quality of fracture reduction when comparing severity of initial injury patterns in pelvic ring injuries. We hypothesized that lateral compression (LC) type injuries would be more prone to malreduction relative to anterior-posterior compression (APC) type injuries.

Methods: We performed a retrospective chart review for all patients who presented with surgical pelvic ring injuries. Inclusion criteria consisted of patients greater than 18 years of age, those who underwent surgical treatment for traumatic pelvic ring disruption between 2011 and 2021, and those with available pre-operative and post-operative plain films. Demographic characteristics, mechanism of injury, and the Young-Burgess classification of injury were recorded. Pelvic ring displacement was measured at the time of injury and was compared with the immediate post-operative period. Measurements were made on AP pelvis X-rays according to the Keshishyan method. Pre-operative and post-operative pelvic ring displacement was then analyzed using bivariate independent t-test analysis. Statistical significance was set at $p<0.05$.

Results: 284 patients met the inclusion and exclusion criteria. The average age was 45.4 ± 19.0 years. 31.1% (88) of patients were obese, 66.2% (188) of patients were males, 21.4% (61) of patients were active smokers, and 31.3% (89) were former smokers at time of injury. LC type injuries were significantly more displaced than APC type injuries on initial presentation (16.3±13 mm vs. 13.2±11 mm respectively, p=0.02). LC injuries had significantly more post-operative asymmetry than APC injuries (8.3±9 mm vs 5.2±5 mm respectively, p=0.001). Interestingly, there was no difference in the amount of reduction (postoperative – preoperative displacement) between patients with APC and LC injuries (-9.6±12.2 mm vs -8.2±14.0, p=0.53).

Conclusion: We found significantly greater residual pelvic asymmetry post-operatively in LC-type pelvic ring injuries compared to APC-type pelvic ring injuries. We also found significantly greater residual pelvic asymmetry amongst all LC subtype injuries relative to APC subtype injuries. Current fixation methods may be less able to address pelvic asymmetry in LC-type injuries. These results may be useful in surgical planning as well as patient outcomes counseling.

**PAPER #36**

**TITLE:** Exploring Differences in Length of Stay and Discharge Patterns Among Pelvic Ring Injury Patterns

**PRESENTING AUTHOR:** James D. Brodell, Jr., M.D.

**CO-AUTHOR(S):** Hashim JF Shaikh, BS, Melissa Holloway, BS, Urvi J Patel, MD, MS, John P Ketz, MD, Sandeep P Soin, MD

**LAB PI/MENTOR:** Sandeep Soin, M.D.

**ABSTRACT**

Purpose

While descriptive studies regarding pelvic ring injury treatment and fixation strategies have been performed, little work has been done examining pelvic ring injury fixation outcomes. No studies have examined the length of stay and discharge disposition of these patients. We sought to better define the length of stay and discharge disposition for patients who sustain pelvic ring injuries.

Methods

This study was approved by the Institutional Review Board at the University of Rochester Medical Center. Patients undergoing pelvic ring fixation were identified using Current Procedure Codes (CPT): 27216, 27217, and 27218. Inclusion criteria were patients aged ≥18 years who survived their acute care stay, while exclusion criteria of in-hospital mortality or a history of prior pelvic ring injury/fixation. Primary outcomes were the Length of Stay (LOS) and discharge location. Demographic characteristics were also collected.

Results

284 individuals met the criteria for inclusion and exclusion. A significant difference was identified in LOS, with patients having an LC III injury exhibiting the longest average LOS (27.1 ± SD 25), followed by APC III (19.4 ± SD 15), LC II (18.2 ± SD 15), APC II (15.9 ± SD 14), VS (15.8 ± SD 12), LC I (14.6 ± SD 17), and finally APC I (11.5± SD 10) p=0.03 [Figure 1]. Overall, there was no significant difference observed among injury patterns concerning discharge disposition to SNF, with percentages of 80.0% for LC III, 72.4% for APC III, 71.4% for VS, 67.4% for LC II, 64.4% for LC I, 61.9% for APC II and 61.5% for APC II p=0.72

Regression analysis demonstrated that patients with an LC III injury (95% CI 4.32-23.3; p = 0.005) had a significantly longer LOS when compared to the other Young Burgess Injury patterns (Table 2). There was a significant association between patients who were active smokers (95% CI: 0.04-9.73; p = 0.04) or higher ISS scores (95% CI 0.32-0.58, p = 0.001) and a longer LOS.

The Young Burgess injury pattern was found not to significantly impact the odds of being discharged to a SNF (Table 3). Patients who were older (OR: 1.03, 95% CI 1.01-1.06, p = 0.001), had higher ISS scores (OR: 1.08, 95% CI 1.05-1.17, p = 0.001), or had a CCI of 3 or more (OR: 2.92, 95% CI 1.09-8.62, p = 0.001) had a significantly increased odds of being discharged to a SNF

Conclusions

While increasing severity of pelvic ring injury was found to be associated with longer in-hospital length of stay after fixation, this was not associated with an increased risk of discharge to skilled nursing facilities. This can help provide information for counseling pelvic ring injury patients.

**PAPER #37**

**TITLE:** Using Integrated Photonic Sensors in a Tendon-on-a-Chip Model

**PRESENTING AUTHOR:** Joseph Bucukovski, MS

**CO-AUTHOR(S):** Benjamin L. Miller, PhD; Hani Awad, PhD; James L. McGrath, PhD; John S. Cognetti, PhD; Raquel E. Ajalik, PhD, Hossein Abolhassani

**LAB PI/MENTOR:** Benjamin L. Miller, PhD

**ABSTRACT**

Tendinopathies, such as flexor tendon adhesions, contribute a large economic burden on the healthcare system and adversely affect quality of life. Although biomarkers have been examined in clinical contexts, there has yet to be a fully validated model system that can recapitulate the cellular and inflammatory environment of a single individual. Senescence-associated secreted proteins (SASP) are factors released during the pathological wound healing of tendon. In short, resident myofibroblasts in tendon tissue are activated by infiltrating macrophages during the inflammatory phase and are converted into senescent fibroblasts. These cells secrete SASP, which can then trigger a positive feedback loop whereby inflammation is prolonged, and a higher proportion of tissue resident fibroblasts become senescent. This overactivation is implicated in soft tissue fibrosis, or scarring, which is remarkably common among musculoskeletal injuries such as tendinopathy.

Through work published in the Awad Lab, a proposed mechanism of tendon fibrosis has been elucidated in mouse models. More recently, the Awad, McGrath, and Miller labs have formed a consortium to develop a human tendon-on-a-chip (hToC) or microphysiological system (MPS) to circumvent the challenges associated with animal model pathobiology, such as translatability to human clinical trials. As a member of this collaboration, I have been focusing on integrating on-board biosensors.

The current hToC device requires immunofluorescence microscopy and media sampling to assess the tendon microenvironment; however, these processes effectively end the experiment. Neither of these modalities are useful for continuous, and real-time monitoring of SASP quantification, which is why photonic biosensors will be crucial for the hToC. Most of my recent work has been geared towards redesigning the hToC such that the photonic sensor chips can be integrated seamlessly without interference or loss of physiological integrity in the tendon MPS.

To accomplish this goal, I am using photonic ring resonators (PhRR) as the biosensing modality of choice due to their high sensitivity, multiplex capability, and low cost of fabrication. The initial phase of sensor validation demonstrated dose-dependent titration of binding response from interrogating five purified SASP antigens simultaneously (5-plex). Thorough validation of the sensor binding response is crucial for having statistical confidence in real-time detection of cell culture secretions in situ.

Recent experiments have tracked the time-course behavior of SASP release from the tenocytes encapsulated in the collagen hydrogel (tendon tissue) and the HUVEC monolayer after co-culturing for several days. CCL2 (MCP-1) was detected in the microenvironment both at days 3 and 5 after seeding the devices, along with CCL3 (MIP-1α). This is consistent with Luminex endpoint assay data obtained from Raquel Ajalik in similar devices. Additionally, I observed that IL-17A levels increased on day 3, while IL-6 were similarly increased on day 5. The release of these interleukins may be associated with the devices being removed from the incubator. Therefore, I am prototyping an incubator for the optical stage that will contain 5% CO2, humidity, and physiological temperature control.

In future assays, transforming growth factor beta, or TGFβ stimulation, will serve as a proxy for macrophage-induced activation of resident myofibroblast cells and push these towards a senescent state. After several days of stimulation, I hypothesize that the shift from inflammation towards fibrosis will be apparent by observing contraction of the tendon tissue as well as a shift in the SASP release profile. The ability to monitor and detect SASP concentrations with the high time resolution offered by these integrated photonic sensors will be critical in determining the interplay between inflammation, senescence, and fibrosis and the progression of desired wound healing.

**PAPER #38**

**TITLE:** A Comparative Analysis of Outcomes Using PROMIS After Operative Versus Non-operative Treatment of Achilles Rupture

**PRESENTING AUTHOR:** Philomena Burger, BA

**CO-AUTHOR(S):** Mina Botros, MD, Zein El-Zein, MD, David Ciufo, MD

**LAB PI/MENTOR:** David Ciufo, MD

**ABSTRACT**

Background:
Achilles tendon rupture is a common injury in the adult population. The role of operative and non-operative management remains controversial with the development of functional rehabilitation programs. The purpose of this study is to evaluate and compare the patient-reported outcomes using Patient-Reported Outcomes Measurement Information System (PROMIS) after operative and non-operative treatment of acute Achilles rupture. PROMIS is a valid, reliable, and effective tool to evaluate patient outcomes after treatment for Achilles ruptures. Our hypothesis is that there is no significant difference in PROMIS scores between patients undergoing operative compared to non-operative treatment of Achilles rupture.

Methods:
Under an IRB-approved protocol, Achilles rupture was identified using ICD 9 and ICD10 codes of 727.67 and S86.0. Patients who underwent Achilles tendon primary repair were identified using CPT code 27650 (Repair, primary open or percutaneous, ruptured Achilles tendon). Revision Achilles repair and chronic Achilles ruptures were excluded. All patients treated non-operative underwent a strict functional rehabilitation protocol. We included patients treated between 1/1/2015 and 11/30/2022. PROMIS physical function (PF), pain interference (PI), and depression scores were routinely collected prospectively during the initial office visit and follow-up appointments. A distribution-based method used to determine the minimal clinically important difference (MCID), which was 1/2 standard deviation of each PROMIS domain. A medical records review was performed to collect patient demographic data. Statistical analysis was used to compare preoperative and postoperative scores and significance was indicated when $P<0.05$.

Results:
216 patients with Achilles tendon ruptured were included (115 Nonoperative versus 101 Operative). Patients treated non-operatively (age: 45.1 ± 15) were significantly older than those treated surgically (age: 35.6 ± 12.3; $p<0.001$). Sex distribution among the non-operative and operative groups were similar (18.3% vs 17.8% Female, $p=0.933$). The Operative group had a lower BMI compared to non-operative group (27.8 ± 4.3 vs. 29.5 ± 5.3; $p=0.004$). There is no statistical difference in the Achilles tendon re-rupture rate between both treatment groups (operative: 2% vs. 4.3%; $p=0.344$). Both treatment groups are effective in improving PROMIS PF, PI, and depression scores ($p<0.001$). The mean PROMIS PF change (pre- to post-treatment) is significantly greater in the operative, compared to the non-operative group (13.2 ± 13.9 vs. 9.5 ± 12.5; $p=0.042$). There was no difference pre- vs. post-treatment in mean PROMIS PI change (operative: -12.5 ± 11.5 vs. -10.8 ± 11.1; $p=0.134$) and PROMIS depression (operative: -3.9 ± 7.7 vs. -5.2 ± 9.3; $p=0.201$). MCID thresholds for the nonoperative vs. operative group were calculated as 5.7 vs. 6.3 in PROMIS PF, 4.3 vs. 4.2 in PROMIS PI, and a 4.15 vs. 4.9 in PROMIS depression, respectively. There is no difference in the number of patients that achieve MCID for PF, PI, and depression among both treatment groups at the 6-months follow-up period.

Conclusion:
In patients with Achilles tendon rupture, operative management may lead to statistically significant improvements in patient-reported physical function. However, nonoperative management was associated with similar overall rates of rerupture, PROMIS PI and depression outcomes, and chances of meeting MCID as those who underwent operative intervention. Nonoperative management of Achilles tendon rupture, similar to operative treatment, is a successful treatment option and leads to significant improvement in physical function, pain interference, and depression PROMIS scores.

**PAPER #39**

**TITLE:** Assessing the Musculoskeletal Health Literacy and Social Network Distribution of Hip and Knee Osteoarthritis Patients at an Academic Medical Center

**PRESENTING AUTHOR:** Philomena Burger, BA

**CO-AUTHOR(S):** Kevin McCaffery, BA, Gabriel Ramirez, MS, Rishi Balkissoon, MD, John Ginnetti, MD

**LAB PI/MENTOR:** John Ginnetti, MD

**ABSTRACT**

Background:
In the United States, osteoarthritis (OA) care expenditure – inclusive of total joint arthroplasty (TJA) – surpasses $300 billion annually with further escalation of spending anticipated. As a result, the U.S. has begun a transition to value-based TJA healthcare, rewarding quality of professional services and patient-care experience over traditional fee-for-service transactions. Health literacy (HL), defined as the ability to obtain, process, and understand health information in order to make appropriate health care decisions, has been identified as a social determinant of healthcare, potentially impacting patient-care experiences. Limited HL contributes to health disparities and ineffective care, and negatively affects healthcare outcomes in TJA as well as non-Orthopedic medical disciplines. HL is predominantly distributed in social networks, where patients draw upon the knowledge of others to make healthcare decisions. Patients may rely on physicians, family, friends, and acquaintances, as well as the internet and social media to shape their healthcare knowledge. The aim of our study is to explore the association of individual musculoskeletal HL on preferred lower-extremity osteoarthritis information sources. Our hypothesis is that patients with low musculoskeletal health literacy (LiMP score < 6) will preferentially utilize human informational sources.

Methods:
Patients presenting to the University of Rochester Department of Orthopaedics Ambulatory Care clinic with a primary diagnosis of severe hip and/or knee osteoarthritis were recruited. Patients with prior TJA were excluded. Participants completed a one-time 3-part survey which assessed patient desire for total hip/knee surgery, Literacy in Musculoskeletal Problems (LiMP) score, and patient healthcare informational sources. Mean LiMP scores were calculated for each information source and p-values were generated by comparing LiMP scores among participants who reported an information source, and participants who did not report that information source.

Results:
39 patients (39%) generated a LiMP score below 6. Participants identified their joint surgeon and staff (82%), friends/extended family with TJA (69%), friends/extended family without TJA (9%), primary care physician (42%), internet/media (33%), and coworkers/acquaintances with TJA (25%) as information sources. Out of the participants who reported internet/media sources, 29 (87.9%) used multiple websites through the use of search engines (Google, Yahoo, Bing), 13 (39.4%) used social media (YouTube, Facebook, Twitter, etc.), and 12 (36.4%) utilized University of Rochester websites. The mean LiMP scores were: 6.06 (±1.56, p=0.03) for the selection of total joint surgeon and staff and 5.90 (±1.81, p=0.98) for the selection of primary care doctor. The mean LiMP scores were 5.62 (±1.94, p=0.50) for the selection of spouse/partner, 6.00 (±1.41, p=0.90) for selection of children, 6.52 (±1.42, p=0.03) for selection of coworkers/acquaintances, and 6.36 (±1.43, p=0.05) for the selection of internet/media.

Conclusion:
A LiMP score of <6 indicates a limited musculoskeletal health literacy. All information-source groups, except for spouse/partner and primary care doctor, had an average LiMP score above six. Participants who chose spouse/partner as a source of information and participants who chose primary care doctor as a source of information had an average score below 6. Although not statistically significant, our findings suggest TJA health literacy interventions should target both individual patients and patients' social networks. Additionally, increasing the incidence of quality TJA experiences in undeserved social networks will help promote TJA in underserved populations.

**PAPER #40**

**TITLE:** Diagnosis of Ulnar Neuropathy at the Elbow Using Ultrasound – A Comparison to Electrophysiologic Studies

**PRESENTING AUTHOR:** Thomas John Carroll MD

**CO-AUTHOR(S):** Alexander Chirokikh BS, Julie Thon R EMG T, Courtney Marie Cora Jones PhD, Eric Logigian MD, Constantinos Ketonis MD PhD

**LAB PI/MENTOR:** Constantinos Ketonis MD PhD

**ABSTRACT**

Purpose: Given the relatively high false negative rate of electrodiagnostic studies (EDX) in patients with clinically diagnosed ulnar neuropathy at the elbow (UNE), we sought to determine if an alternative objective test could more reliably detect UNE. Additionally, we proposed to determine the relationship between cross-sectional area of the ulnar nerve ,EDX and clinical symptoms.

Methods: This was a retrospective study of patients presenting with symptomatic UNE. The performance calculations of EDX versus US were calculated using the clinical diagnosis of UNE as the reference standard. Standard EDX studies as well as US of the ulnar nerve were analyzed. Maximal cross-sectional area (CSA) of the ulnar nerve and EDX severity were analyzed for patients with each combination of US positive/negative, and EDX positive/ negative findings.

Results: Analysis was performed on 89 patients and 115 nerves with signs and symptoms of cubital tunnel syndrome. In total, 56 (49%) nerves were diagnosed as mild UNE by EDX, 32 (28%) nerves were diagnosed as moderate, 17 (15%) nerves were diagnosed as severe, and 10 (8%) nerves were negative for UNE. Maximal CSA was highly correlated with disease severity as determined by NCS/EMG. Compared to EDX+/US+, patients with EDX-/US+ showed higher rates of ulnar sensory loss and elbow tenderness with similar rates of positive Tinel and intrinsic muscle atrophy. In this sample of patients with clinically diagnosed UNE, 91.3% of patients demonstrated positive EDX studies while 94.8 had positive US.

Conclusion: Ultrasound is an alternative diagnostic modality to EDX that could be incorporated clinically in the diagnosis and management of UNE. US was able to consistently detect clinically positive CuTS demonstrating its utility as a confirmatory or supplemental test to the clinical assessment if one is required. US additionally may be able to better identify patients with early stages of UNE with negative EDX findings.

**PAPER #41**

**TITLE:** Development of de Quervain's Tenosynovitis After Distal Radius Fracture

**PRESENTING AUTHOR:** Thomas John Carroll MD

**CO-AUTHOR(S):** Brianna Caraet MD, Norman Madsen, MD, Danielle Wilbur MD

**LAB PI/MENTOR:** Danielle Wilbur MD

**ABSTRACT**

Background: We sought to determine the risk factors for the development of de Quervain's tenosynovitis after distal radius fractures. Our hypothesis is that longer periods of immobilization and higher energy fracture patterns, will correlate with the development of de Quervain's.

Methods: This is a 10-year retrospective study of 1451 consecutive patients with distal radius fractures presenting to a large academic institution. The incidence and relative risk of de Quervain's tenosynovitis within one year of sustaining a distal radius fracture was analyzed.

Results: In total, 41 patients developed post-traumatic de Quervain's Tenosynovitis at an average of 6.5 months. Among the operative cohort, the incidence was 2.2%, and that of the non-operative group was 3.8%. Among all affected patients, 78% admitted to strenuous, overuse activities or careers. Compared to the unaffected cohort, the de Quervain's group was more likely to be female and black with similar age and BMI. The traumatic cohort was less likely to respond to corticosteroid injections. A separate EPB sheath was noted in all patients requiring surgical release.

Conclusions: Non-operative distal radius fracture patients were 4.2 times more likely to develop de Quervain's than the general population, and 2.4 times more likely for those treated operatively. These patients were more likely to be female, black, and engaging in strenuous overuse activities or careers. They demonstrated higher energy fracture patterns and worse response to corticosteroid injections, more frequently requiring surgical decompression. Among those requiring surgery, patients were 2.5 times more likely to have a separate EPB sheath compared to those with atraumatic Quervain's.

**PAPER #42**

**TITLE:** Clinical and Radiographic Outcomes Following Volar Locked Plating Versus Dorsal Bridge Plating for Distal Radius Factures: A Propensity Score-Matched Analysis

**PRESENTING AUTHOR:** Thomas John Carroll MD

**CO-AUTHOR(S):** Akhil Dondapati MD, Michaela Malin BS, Constantinos Ketonis MD PhD, Warren Hammert MD, Ronald Gonzalez DO

**LAB PI/MENTOR:** Ronald Gonzalez, DO

**ABSTRACT**

Background: Distal radius fractures indicated for operative intervention are most commonly treated with volar locked plating (VLP) or dorsal bridge plating (DBP). The purpose of this study was to utilize a propensity score to match and compare the radiographic and clinical outcomes of patients undergoing VLP or DBP for distal radius fractures.

Methods: We performed a retrospective, propensity score-matched analysis of patients undergoing VLP or DBP treatment for isolated distal radius fractures from 2015 to 2022. Patients were propensity score matched by a total of 8 demographic and comorbidity factors, AO Foundation/Orthopaedic Trauma Association (AO/OTA) classification, and preoperative Patient-Reported Outcomes Measurement Information System (PROMIS) scores. Our primary outcomes included postoperative complications, wrist and forearm range of motion, grip strength, and radiographic measurements, including radial height, radial inclination, volar tilt, and articular step-off.

Results: Overall, 415 DBP and 2075 VLP were successfully propensity score matched and included in this study. Grip strength and range of motion measurements at 6-month follow-up, including wrist flexion, wrist extension, forearm pronation, forearm supination, radial deviation, and ulnar deviation, were increased in the VLP compared to DBP ($p<0.05$). Complication rates among both groups were relatively low, however, the rate of malunion and nonunion was significantly higher among the DBP group ($p<0.05$). Radial height, radial inclination, and articular step-off were improved in the VLP group compared to the DBP group ($p<0.05$), however, volar tilt was similar between groups. PROMIS Upper Extremity (UE) and Physical Function (PF) were significantly higher among the VLP group ($p<0.05$). There was no significant difference in PROMIS PI between groups.

Conclusions: When compared to DBP, patients undergoing VLP are more likely to have improved clinical and radiographic outcomes. While improvement in wrist and forearm range of motion and radiographic parameters is statistically significant, it may not be clinically relevant.

**PAPER #43**

**TITLE:** Predicting Acute Median Neuropathy in Perilunate Injuries

**PRESENTING AUTHOR:** Thomas John Carroll, MD

**CO-AUTHOR(S):** Mina Botros MD, Richard Lander MD, Sophia Moody BS, Megan L. Reitenbach MD, Danielle Wilbur MD

**LAB PI/MENTOR:** Danielle Wilbur, MD

**ABSTRACT**

Purpose: Perilunate fracture dislocation (PLFD) injuries are associated with the development of acute carpal tunnel syndrome (CTS). The purpose of our study identify factors that increase the likelihood of developing CTS in patients with PLFD. Additionally, we attempted to classify patients who did not initially undergo carpal tunnel release (CTR) at time of injury who eventually underwent CTR within the follow up period.

Methods: Patients presenting to a level-1 trauma center with isolated PLFDs (Mayfield III-IV) were retrospectively identified utilizing CPT and ICD-10 codes. Polytraumatized patients, those with a history of prior wrist trauma, or prior carpal tunnel symptoms or surgery were excluded. Outcomes of interest included the development of acute CTS, pre- and post- reduction changes in CTS symptoms, and associated hand and wrist fractures. Chi-square tests, Kruskal-Wallis tests, and multivariate logistic regression were used to examine the Predictors of developing CTS following PLFD.

Results: 43 patients were included in the final cohort, with a mean age of 44 years old, of which 77% were male. The most common fracture of the carpus included scaphoid fractures (9/43, 21%). The average time from presentation to reduction was 636 minutes. Acute CTS symptoms prior to reduction were present in 26% of patients and increased post reduction to 28%. There was no difference between the time to sedation and the presence of acute carpal tunnel symptoms ($p>0.05$). During initial surgical intervention, 79% underwent carpal tunnel release (27/34). Of the 7 patients who did not initially have a carpal tunnel release, 57% (4/7) required release within the follow up period.

Conclusion: Reduction of PLFDs did not significantly improve the number of patients with acute CTS. Over 50% of patients who did not undergo a CTR at the initial surgery required CTR within the follow up period.

**PAPER #44**

**TITLE:** Comparison of Patient-Reported Outcome Instruments in the Pre-Operative Evaluation of Cubital Tunnel Syndrome

**PRESENTING AUTHOR:** Alexander Alexei Chirokikh

**CO-AUTHOR(S):** Thomas John Carroll, Samantha Hoffman, David Speach, Courtney Marie Cora Jones, Constantinos Ketonis

**LAB PI/MENTOR:** Dr. Constantinos Ketonis

**ABSTRACT**

Background: Patient-reported outcomes are routinely used to assess disease severity in patients with cubital tunnel syndrome (CuTS). This study aimed to compare the relationships of patient-reported outcomes with clinical exam, electrodiagnostic (EDX), and ultrasound (US) measures.

Methods: Twenty-one patients presenting to an academic center with symptoms consistent with isolated CuTS were prospectively enrolled. Clinical exam measures were collected, including grip strength, key pinch, two-point discrimination, presence of Tinel's sign, and elbow flexion test result. Patients underwent EDX evaluation, and US was used to measure the cross-sectional area of the ulnar nerve around the elbow. Patients completed three questionnaires: Patient-Rated Ulnar Nerve Evaluation (PRUNE), Patient-Reported Outcomes Measurement Information System (PROMIS), and Disabilities of the Arm, Shoulder, and Hand (DASH). Questionnaire scores and clinical exam measurements were stratified based on EDX and US status. Pearson's correlations were used to assess the associations of questionnaire scores with objective measures.

Results: Significant differences in PRUNE, PROMIS-Physical Function (PROMIS-PF), PROMIS-Depression (PROMIS-D), PROMIS-Upper Extremity (PROMIS-UE), and DASH scores were observed between EDX groups, while no significant differences were seen between US groups. Scales that significantly correlated with both sensory latency and amplitude included: PROMIS-PF, PROMIS-PI, PROMIS-UE, and DASH. All questionnaires demonstrated significant correlations with sensory amplitude, while correlations with motor EDX or US outcomes were not observed.

Conclusions:
Patient-reported symptom severity is more closely associated with EDX diagnosis than US status. PROMIS-PF displayed stronger correlations to objective measures than other questionnaires. Sensory amplitude was the strongest predictor of subjective symptom severity relative to other measures.

**PAPER #45**

**TITLE:** Where Does Ultrasound Fit in the Diagnostic Algorithm for Cubital Tunnel Syndrome?

**PRESENTING AUTHOR:** Alexander Alexei Chirokikh

**CO-AUTHOR(S):** Thomas John Carroll, Samantha Hoffman, David Speach, Courtney Marie Cora Jones, Constantinos Ketonis

**LAB PI/MENTOR:** Dr. Constantinos Ketonis

**ABSTRACT**

Background: Ultrasound (US) has emerged as a promising supplement to electrodiagnostic studies (EDX) in the diagnosis of cubital tunnel syndrome (CuTS) and has potential to be performed by novice operators. Our objective is to understand the discrepancies in assessment between the two modalities and to assess the utility of US in CuTS diagnosis by a novice operator.

Methods: Patients who presented to a single tertiary academic medical center and clinically diagnosed with CuTS were prospectively enrolled. EDX studies were performed along with US measurements of the cross-sectional area (CSA) of the ulnar nerve by both a board-certified physiatrist and novice operator. EDX and US outcomes were compared among four diagnostic impression groups: EDX-/US-, EDX+/US-, EDX-/US+ and EDX+/US+.

Results: Sixteen patients were classified as abnormal by both EDX and US, 14 were classified abnormal by US only, 3 were classified abnormal by EDX only, and 6 were classified normal by both EDX and US ($p=0.008$, $K = 0.14$). The EDX+/US+ group had a significantly reduced sensory amplitude compared to the EDX-/US+ ($p=0.04$) group. Diagnostic classifications between a board-certified physiatrist and novice operator were in moderate agreement ($K=0.58$, $p=0.08$).

Conclusions: US detected a greater proportion of patients as abnormal compared to EDX. A subset of patients with clinical diagnoses of CuTS had normal sensory amplitudes but increased maximum nerve CSAs. Competency in US may be easily acquired with minimal training suggesting its potential to be extended for use by other members of the healthcare team.

**PAPER #46**

**TITLE:** Effects of Sex and Derivation Location on Osteoclast Formation and Activity

**PRESENTING AUTHOR:** Michael Christof

**CO-AUTHOR(S):** Kiana Chen, Xi Lin, Lianping Xing, Homaira Rahimi

**LAB PI/MENTOR:** Homaira Rahimi

**ABSTRACT**

Rheumatoid arthritis (RA) is a chronic inflammatory autoimmune disorder characterized by synovial inflammation and bone erosions. We study inflammatory erosive arthritis using the TNF-transgenic (TNF-Tg) murine model of RA. TNF-Tg mice have sexual dimorphism in their disease, with female mice having worse disease than males. We aimed to determine how sex and location of osteoclast precursors (OCPs) affect osteoclast (OC) growth and quantity, and if sex also affects osteoclast bone resorptive activity. We hypothesize that more osteoclasts will differentiate from bone marrow than peripheral blood and from female than male TNF-Tg mice, as well as greater bone resorption from female-derived, TNF-Tg OCs.

Bone marrow (BM) and peripheral blood mononuclear cells (PBMC) were harvested from 3-month-old female and male TNF-Tg mice (n=3 mice/group). Cells were cultured in OC differentiation media with 30ng/mL of Macrophage Colony-Stimulating Factor (M-CSF) and 30 ng/mL Receptor Activator of Nuclear Factor Kappa-B Ligand (RANK-L). After OC formation, cells were fixed and stained for tartrate-resistant acid phosphatase (TRAP). OCs were defined as cells with >3 nuclei and TRAP+. BM cells were also harvested from 3-month-old TNF-Tg and WT male and female mice and grown on bovine bone slices with 100ng/mL of M-CSF and 100ng/mL RANK-L. Bone slices were fixed and stained with TRAP and toluidine blue after 10 days of culture. ImageJ was used to analyze the bone pit area. Unpaired t-test, two-way ANOVA, and one-way ANOVA with Tukey's post-test for multiple comparisons were used for analysis. Values are reported as mean +/- standard deviation.

BM cells formed significantly more OCs than PBMC cells (392.6 +/- 83.65 vs 200.5 +/-87.28) from the same TNF-Tg mice. OCs formed from PBMCs were larger than those derived from BMs, evidenced by significantly increased percentage of OCs with >10 nuclei compared with BM OCs (35.85 +/-10.73% in PBMC-OCs vs 22.5 +/- 7.83% in BM OCs). No significant difference between sex in BM-derived OCs and PBMC-derived OCs was observed. There were more male-derived and female-derived BM OCs than female-derived PBMC OCs (399.9 +/- 47.24 and 385.3 +/- 122.9 vs 147.2 +/- 49.39). There were also more male-derived PBMC-OCs than female-derived BM-OCs for the percentage of OCs with >10 nuclei (42.17 +/- 11.24% vs 17.27 +/- 7.48%). There was no significant difference in bone pit sizes between TNF and WT male and female mice.

BM-derived OCPs produce more OCs than PBMCs yet PBMC-derived OCs have more >10 nucleated OCs, suggesting the origin of OCPs may affect OC activity. Bone pit sizes did not differ between sexes regardless of inflammatory environment, indicating OC activity is not affected. This finding suggests that once cells are committed to the bone resorption process, origin and sex have less effect early in the osteoclastogenesis pathway. Further studies are needed to determine whether specific sex hormones alter OC growth and activity.

**PAPER #47**

**TITLE:** Characterization of the bone marrow mesenchymal stromal cells in low dose irradiation model

**PRESENTING AUTHOR:** Wimeth Dissanayake

**CO-AUTHOR(S):** Melissa MacLiesh, Kevin Lee, Cih-Li Hong, Yuko Kawano, Hiroshi Kawano, Laura Calvi

**LAB PI/MENTOR:** Shu-Chi A. Yeh

**ABSTRACT**

Introduction: Clonal Hematopoiesis of Indeterminate Potential (CHIP) is a preleukemic condition originating from the clonal expansion of hematopoietic stem progenitor cells (HSPCs) carrying leukemia associated mutations. Though primarily manifesting in the elderly, the leukemogenic mutations underlying CHIP occur early in life, indicating that the disorder may be controlled by cell-extrinsic factors. Cross-regulations between the bone marrow microenvironment and HSPCs have been reported to govern heterogenous behavior of HSPCs; however, how the cell spatial organization with the niche governs functional heterogeneity has not been elucidated in CHIP. Although transplantation of congenic/reporter cells has been a standard approach to model CHIP, this approach requires genotoxic conditioning for the non-malignant cells to engraft, which compromises host hematopoiesis and the microenvironment. Therefore, we propose to leverage high-resolution live-animal microscopy and ultralow dose (0.5Gy) total body irradiation to study early expansion of benign clones in the minimally perturbed microenvironment. Characterization of the peri-vascular niche, a key HSC regulator, will better understand the impact of low-dose irradiation on the hematopoietic microenvironment. Here, we focused on vascular integrity and functional assessment of the mesenchymal stromal cells (MSCs). Vascular integrity reflects the level of inflammation. MSCs are critical components in the bone marrow niche of HSPCs. Osteo-primed or adipo-primed MSCs have demonstrated unique support for lympho- and myelopoiesis, respectively; thus, the preservation of their multipotency is important to fairly assess the cell-extrinsic factors in CHIP.

Methods: To examine vascular integrity, we quantified vessel diameters and used video-rate tracking of Rhodamine dextran (70kDa) leakage into the extravascular space (5-35 seconds following dye injection). To assess the impact of low-dose irradiation on MSC multipotency, non-irradiated and 0.5 Gy irradiated MSCs were exposed to osteogenic, adipogenic, or chondrogenic differentiation media, and were assessed by Alizarin Red, Oil Red O, and Alcian Blue staining respectively.

Results: Our results showed no increase in permeability or signs of vessel dilation at one week after transplantation, suggesting minimal inflammation after the radiation insult. We also showed that the 0.5 Gy model did not significantly alter the differentiation potential of MSCs. The finding is consistent with literature reports, where irradiation ranging from 0.1 Gy to 1 Gy preserved the trilineage differentiation and potency of MSCs. Adipogenesis is either unaffected or negatively affected by low levels of irradiation.

Conclusion: In conclusion, we showed that 0.5Gy irradiation preserved vascular integrity and likely preserved the muti-potency of MSCs as early as one week after exposure to 0.5 Gy conditioning. In the future, to further examine their hematopoietic support, MSCs and HSPCs will be co-cultured, followed by evaluations of HSPC function assessed with in vitro colony-forming unit cell (CFU-C) assays and the competitive transplantation assays in vivo. We will also perform local irradiation on the unilateral side of the calvaria and compare expression of key pro-inflammatory genes between the irradiated and non-irradiated side.

**PAPER #48**

**TITLE:** Endoscopic Carpal Tunnel Release with MAC Versus Local Anesthesia - Analysis of Operative Times and Patient Reported Outcomes

**PRESENTING AUTHOR:** Akhil Dondapati, MD

**CO-AUTHOR(S):** Thomas Carroll, MD, Constantinos Ketonis, MD, PhD

**LAB PI/MENTOR:** Constantinos Ketonis, MD, PhD

**ABSTRACT**

Purpose:
Carpal tunnel syndrome is the most common peripheral nerve compressive neuropathy seen in clinical practice. Patients who fail non-operative management are indicated for carpal tunnel release (CTR) surgery, which can be performed open or endoscopically. Efforts have been made to utilize local anesthesia instead of monitored anesthesia care (MAC) for endoscopic release. This study seeks to compare perioperative surgical times and post-operative outcomes in patients undergoing endoscopic CTR with local anesthesia versus MAC.

Methods:
This is a 6-year retrospective study of 1036 patients undergoing isolated endoscopic carpal tunnel release with MAC (n=607) versus local (n=429) anesthesia within an outpatient surgical center. A combination of Chi-Square and T-tests were used to compare the patient characteristics, operative details, and outcomes between the groups.

Results:
The local cohort demonstrated shorter total operating room time (26.7 +/- 4.3 vs 29.0 +/- 4.1 minutes; $p<0.05$), tourniquet time (12.4 +/- 2.5 vs 13.1 +/- 2.1 minutes; $p<0.05$), post-operative time to discharge (15.9 +/- 9.8 vs 53.8 +/- 11.0 minutes; $p<0.05$) and total time spent in surgical center (83.2 +/- 18.7 vs 129.3 +/- 20.7; minutes $p<0.05$). Pre- and post-operative PROMIS scores were similar between the two cohorts ($p>0.05$), however, PROMIS PI improved to a higher degree between pre- and post-op in the local group (-1.5 vs -0.8; $p=0.02$). Early and late surgical complications were similar between groups ($p>0.05$).

Conclusions:
Patients within the MAC cohort demonstrated longer total operating room time, tourniquet time, post-operative time to discharge, and total time spent in the surgical center. Early and late surgical complications, as well as pre- and post-operative PROMIS scores were similar between the two groups. Our findings suggest that local anesthesia is a safe and effective option for endoscopic CTR, and may offer advantages in terms of cost and convenience for patients.

**PAPER #49**

**TITLE:** Role of mitochondrial genetics in the response of osteogenic cells and bone tissue to mechanical stimulation

**PRESENTING AUTHOR:** Renae Duncan

**CO-AUTHOR(S):** Sarah Elizabeth Catheline, Chen Yu, Sandra Castillo Aguirre

**LAB PI/MENTOR:** Roman Eliseev

## ABSTRACT

INTRODUCTION:
Recent research has shown a pivotal role of mitochondria in osteoblast differentiation. Active mitochondria stimulate osteogenic processes while mitochondrial dysfunction contributes to bone aging. Reversing mitochondrial pathologies counteracts age-related bone loss. Mitochondrial genome SNPs forming mtDNA haplogroups, influence respiratory complexes efficiency. Interestingly, more efficient mtDNA haplogroups correlate with stronger bones, as seen in African haplogroup L when compared to Eurasian haplogroups. Mouse strains with different mitochondrial haplotypes, such as C3H/HeJ (C3H) and C57BL/6 (C57), also show variations in bone phenotype and aging. C3H mice have more efficient mitochondria and more robust bones than C57 mice. The goal of this study was to elucidate the role of mtDNA haplotype in the response of bone marrow stromal cells (BMSCs) to mechanical stimulation due to forced exercise.

METHODS:
Mice: We used 3-month-old C3H and C57 wild-type (WT) and mitochondrio-nuclear exchange (MNX) mice that have mtDNA from the opposing strain, i.e. C3H nucleus and C57 mitochondria (C3H MNX) and C57 nucleus and C3H mitochondria (C57 MNX).
Mouse Treadmill: Exercise regimen involving daily running sessions of 30 min over two weeks at 10 m/min with a 10-degree incline.
Bone micro-CT: Involves dissecting tibia, removal of soft tissue, fixation in 10% neutral buffered formalin for 72 hrs., and scanning using VivaCT 40.
Colony-forming units assay: A total of 0.5 million bone marrow cells were seeded into each well of a 6-well plate. Unattached cells were removed after 24 hrs. Cells were incubated for two weeks, facilitating the formation of colony-forming units (CFUs, colonies of >50 cells).
Osteoblast Isolation: Bone marrow from femurs is flushed, and endosteal cells are isolated via centrifugation of bone shafts. Hematopoietic and endothelial cells are immunodepleted using magnet. Real-time RT-PCR is used to analyze the expression of Alpl and Bglap genes.

RESULTS:
In the treadmill experiment, we observed that C57 MNX mice took more rests compared to their C57 WT counterparts with no significant difference in total distance covered. Osteoblasts from these mice showed a slight increase in the expression of Alpl and Bglap genes in untrained mice, consistent with more efficient C3H mtDNA haplotype. However, no significant alterations were observed between trained and untrained groups for both C57 MNX and WT mice. C3H MNX mice exhibited more rests and notably shorter distance covered when compared to C3H WT mice. This indicates that having less efficient C57 mtDNA haplotype leads to lower endurance. This also led to lower Alpl and Bglap expression in osteoblasts from untrained mice. Exercise stimulated CFUs, a trend consistently noted in both C57 and C3H mice. However, C3H mice exhibited a more robust CFU count overall. Micro-CT data analysis showed that exercise increased connectivity density and trabecular number in both C57 MNX and C57 WT mice. Micro-CT analysis of C3H strain is ongoing.

DISCUSSION:
Our results indicate that: 1) consistent with more robust bone phenotype, C3H mouse BMSCs are more efficient in colony-forming ability when compared to C57 strain; 2) mechanical stimulation induces colony formation by BMSCs and stimulates bone anabolism; and 3) replacing original mitochondria with less efficient C57 mitochondria reduces endurance in C3H mice. Overall, we have received significant evidence of the role of mitochondrial genetics and function in the response of osteogenic cells and bone tissue in general to mechanical stimulation. These data pave the way for studies of the role of mitochondrio-nuclear communication in skeletal tissues and suggest that mtDNA haplotype should be considered as an important determinant of bone health.

**PAPER #50**

**TITLE:** SLAMF7 engagement augments TNF-α secretion in activated monocytes

**PRESENTING AUTHOR:** Jabea Cyril Ekabe

**CO-AUTHOR(S):** Nida Meednu, Jennifer Anolik

**LAB PI/MENTOR:** Dr. Jennifer Anolik

**ABSTRACT**

**Background**

Rheumatoid arthritis (RA) is a chronic autoimmune inflammatory diseases affecting about 1% of the population. Management of RA is challenging due to the heterogenicity of disease, and disease progression in many patients despite current treatment strategies. Hence, there is a need to explore novel molecular mechanisms for the development of new therapeutic strategies. Monocytes and B cells play key roles in the pathogenesis of RA. Nevertheless, there is paucity of data exploring the cross- talk between monocytes and B cells in the context of RA. SLAMF7 is one of the membrane proteins that is expressed both in B cells and activated monocytes and have been shown to interact via homotypic interactions. Nonetheless, data on the effects of SLAMF7 interactions in B cells and monocytes via homotypic interactions is still at infancy.

**Objective**

The main objective of our study is to evaluate phenotypic and functional changes in monocytes and B cells in a B cell -monocyte co-culture system. Our first specific objective was to evaluate factors that increase SLAMF7 expression in monocytes, and how SLAMF7 affects cytokine secretion in monocytes.

**Methods**

To evaluate the conditions that upregulate SLAMF7, monocytes were purified from fresh human PBMCs and cultured overnight in M-CSF. The monocytes were then exposed to IFN-γ, TNF-α, CPG, and LPS for 24 hours. SLAMF7 expression in monocytes was measured via flow cytometry analysis. To evaluate the effect of SLAMF7 engagement on cytokine secretion by monocytes. Activated monocytes expressing SLAMF7 were stimulated with recombinant SLAMF7 and PBS(Control) for 8 hours and TNF-α secretion was measured using ELISA.

**Results**

Our study elucidated that IFN-γ and LPS are the main drivers of SLAMF7 upregulation in monocytes, increasing SLAMF7 expression by sevenfold compared to unstimulated monocytes. Furthermore, we also reported a threefold increase in TNF-α secretion in monocytes stimulated by recombinant SLAMF7 compared to the controls.

**Conclusion**

SLAMF7 upregulation is mediated by IFN-γ. Engagement of this receptor via homotypic interactions increases TNF-α secretion in activated monocytes.

**Key words**: Rheumatoid arthritis, SLAMF7, TNF-α, activated monocytes.

**PAPER #51**

**TITLE:** PRDM16 positively regulates chondrogenesis and knee joint homeostasis

**PRESENTING AUTHOR:** Eloise Fadial

**CO-AUTHOR(S):** Victoria Hansen, Eliya Tazreena Tashbib, Gulzada Kulzhanova, Alexis Klee, Helen Shammas, Gourango Pradhan, Jennifer Jonason, Chia-Lung Wu

**LAB PI/MENTOR:** Chia-Lung Wu

**ABSTRACT**

INTRODUCTION: Cartilage development is regulated by tightly coordinated genetic and epigenetic networks. We previously showed that PRDM16 is upregulated in the chondrogenesis of human induced pluripotent stem cells (hiPSCs). PRDM16 possesses PR domains with capacity for histone modification and zinc finger domains to enable protein-DNA or protein-protein interactions. Microdeletion of the 1p36 locus which includes the PRDM16 region is associated with severe limb defects in humans. PRDM16 is also a top down-regulated gene in subchondral bone of patients with osteoarthritis (OA). Mice with global knockout of Prdm16 results in abnormal osteogenic and chondrogenic differentiation. However, the detailed molecular mechanisms by which PRDM16 regulates chondrogenesis and joint homeostasis remain unknown. Here, we hypothesize that PRDM16 is a positive regulator in chondrocyte specification and knee cartilage homeostasis. We aim to elucidate the regulatory mechanisms of PRDM16 using a cartilage-specific, conditional knockout (KO) mouse strain and hiPSCs models.
METHODS: Animal procedures were compliant with UR IACUC. Prdm16 KO mice (Col2a1-Cre;Prdm16flox/flox) received surgery to destabilize the medial meniscus (DMM) on left knees at 16 wks old. Right knees were used as non-surgery control. Littermates without KO were used as WT. Both hind limbs were harvested 12-wk-post surgery for µCT (n = 5) and Safranin O (Saf-O)/Fast green staining (n = 3). Female and male mice were investigated independently. hiPSCs with inducible knockdown (KD) or overexpression (OE) of PRDM16 were differentiated into chondrocytes and harvested at day 28 (n = 4). Data were analyzed with one-way or two-way ANOVA with Fisher's LSD post-hoc, accordingly.
RESULTS & DISCUSSION: In both WT female and male mice, DMM joints exhibited decreasing bone mineralization density (BMD) in the medial meniscus (MM) vs. non-surgery joints (Female, $p < 0.01$; Male, $p = 0.07$). However, BMD of the MM was comparable between DMM and non-surgery joints in both male and female KO mice. These results suggest that investigation into the role of PRDM16 in osteogenesis or chondrocytes transitioning into osteoblasts is warranted. In the WT male mice, a trend of increased OA severity (i.e., osteophyte formation and loss of cartilage Saf-O staining) was observed in the DMM joints vs. the non-surgery joints ($p = 0.06$). Surprisingly, DMM did not lead to higher OA severity in the male KO mice; however, we are increasing our sample size in order to make a definitive conclusion (females with DMM also currently being analyzed). Most interestingly, non-surgery joints in the KO mice demonstrated more severe OA versus those in the WT mice ($p < 0.05$), suggesting PRDM16 is necessary for cartilage homeostasis. PRDM16 KD chondrocytes also exhibited severe loss of Saf-O staining, while OE of PRDM16 maintained high staining intensity. Furthermore, decreased DNA concentration was observed in the pellets of both edited lines vs. control, implying a link between PRDM16 and cell viability. Indeed, this result is consistent with previous findings showing that methyltransferase activity of PRDM16 is required for heterochromatin integrity and cell survival. Nevertheless, OE of PRDM16 results in significantly higher GAG production (comparable to non-edited control pellet) than KD line ($p < 0.01$) but with fewer cells (lower DNA content), suggesting that these OE cells are highly chondrogenic.
CONCLUSION: We show that PRDM16 positively regulates chondrogenesis and cartilage homeostasis, while loss of PRDM16 may alter cartilage response to injury. Currently, we are performing single-cell RNA- and CUT&RUN-seq of PRDM16 KD and OE hiPSCs at different stages of chondrogenesis. The findings from this study coupled with multimoics will further elucidate the genetic and epigenetic networks of PRDM16 governing cartilage development and homeostasis and may be used to enhance cartilage tissue engineering for clinical applications.

**PAPER #52**

**TITLE:** A Novel Method for Evaluating Disability and Function in Patients with Injuries Sustained in Sports Medicine Utilizing Human Motion Lab

**PRESENTING AUTHOR:** Hunter Gilbreath

**CO-AUTHOR(S):** Schillinger E, Corredor J, Lu H, Wong D, Jablonski J, Tome J, Haddas R

**LAB PI/MENTOR:** Haddas R

**ABSTRACT**

**Introduction:**
Due to lack of consensus on return to sport protocol, time of recovery, rate of reinjury, time of season, and athlete status, it can be hard for a clinician to determine when an athlete should be cleared to return to sport after injury to a lower extremity. Various objective criteria are used for determining return to sport such as Patient Reported Outcome Measurements (PROMs), radiographic measurements, strength tests, hop testing, and balance control but these measures can be objective and may not directly measure functionality and disability. Due to systemic involvement in sport, athletes can develop movement compensations that allow for successful sport participation and can be hard to detect by clinicians. Therefore, the purpose of this study was to develop objective tools to measure disability and functional outcome measurements (DFOMs) and to assess return to sport time using a motion capture system.
**Method:**
Patients underwent a battery of tests, such as Y-balance, drop-vertical jump, free squat, single-leg squat, cutting, and stair climbing. Utilizing technological advancements such as motion capture technology, force platforms and EMG used in a clinical setting allow for analysis of functional movement during these tests to obtain kinematics and kinetic data that can be used to make informed decisions about patient care and athletes return to sport. A clinical DFOMs report was generated for each patient.
**Results:**
Three healthy controls underwent the aforementioned battery of tests. We were able to quantify ranges of joint motion, peak joint angles at key activity timepoints, sway, adjunct joint compensation, time of activity completion, and joint reaction forces. Visualization of key DFOMs was achieved through graphics and videos included within the report, designed to compare conditions before and after medical intervention.
**Discussion:**
Our proposed DFOMs tool allow clinicians to better determine compensations that athletes may have developed and adapt rehabilitation to influence proper form during sports related movements. University of Rochester Medicine Motion Laboratories are utilizing these technologies for musculoskeletal patients to create evaluations and clinical reports that showcase kinematics and kinetic information such that it can be readily and easily used by doctors, athletic trainers and physical therapists to provide valuable insights into patient progress and recovery. These reports may increase patient's ability to become an active participant in their recovery as patients can visualize compensations, adjustments to form, and their own progress over the course of their recovery. The clinicians and patients will have the opportunity to compare the progress of their patients to a matched control group of healthy athletes of similar age, BMI, and gender.
**Significant/Clinical Relevance:**
The proposed reports use tests deemed relevant by surgeons and physical therapists, depending on injury type and using common tests for determining progress with patients who have undergone musculoskeletal sports injuries. Qualitative measures of functional movement allow clinicians to base return to play decisions and rehabilitation plans on measures compared to symmetrical analysis as well as healthy controls instead of expected recovery time. The implementation of the reports allows for individualized care plans and can increase the quality of care and ensure a safe return to sport.
**Key Words**: Disability and Functions Outcome Measurements (DFOMs), Clinical Reports, Motion Labs, Musculoskeletal Patients, Sports Medicine, Return to Sport

**PAPER #53**

**TITLE:** GsMTx4 conjugate reduces chondrocyte vulnerability to mechanical injury ex vivo

**PRESENTING AUTHOR:** Rajkumar Govindan

**CO-AUTHOR(S):** Dr. Thomas Suchyna, Dr. Whasil Lee

**LAB PI/MENTOR:** Dr. Whasil Lee

**ABSTRACT**

Introduction: Osteoarthritis (OA) is a prevalent progressive cartilage degeneration in load-bearing joints, and disease-modifying OA drugs (DMOADs) are urgently needed. Chondrocytes are cartilage resident cells that synthesize and remodel the cartilage extracellular matrix (ECM) and enhanced catabolic activities of chondrocyte and chondrocyte death lead directly to cartilage degeneration in OA [1][2]. We and others reported that Piezo1 and Piezo2 channels in chondrocytes play major roles sensing injurious loading and mediating inflammation-induced hyper-mechanosensation [2][4], thus Piezo channels are potential therapeutic targets for OA. Pre-treatment of GsMTx4D, a 34 aa peptide inhibiting pan Piezo channels [6][7] reduced chondrocyte death caused by mechanical injury in vitro [2], yet GsMTx4D treatment may be stymied by off-target effects or inefficient delivery over the ECM as other candidate DMOADs. We hypothesize that post-treatment of the cartilage targeting GsMTx4 reduces chondrocyte death caused by mechanical injury. Here, we conjugate Col2-binding sequence to GsMTx4D (GsM-Col) to enhance cartilage delivery, and we tested the drug efficacy by quantifying the mechano-vulnerability, defined as the susceptibility of articular chondrocytes to withstand injurious mechanical loading [3], using porcine cartilage explant and custom-designed impact device.

Methods: Cartilage explants were harvested from femoral condyles of porcine knees using a 4-mm biopsy punch. The explants were treated with GsMTx4D/GsM-Col (10 µM) for 40 min before the injury (pre-treatment) or for 40min after injury (post-treatment). Cartilage plugs were loaded with Calcein/PI dyes (Invitrogen) to visualize chondrocyte viability caused by the impact loading device with 1-mm biopsy punch, then imaged at 3 minutes and 20 minutes post-injury by a confocal microscope. The wound thickness of the hollow ring-shaped injury area of each sample was measured using ImageJ. The pre-treatment results were analyzed using one-way ANOVA with multiple comparisons and post-injury treatment was analyzed using unpaired t-test.

Results and Discussion: Cartilage explants with pre-treatment, both GsMTx4D and GsM-Col, showed reduced mechano-vulnerability (reduced thickness of injured area), yet GsMTx4D pre-treated groups exhibit statistically significant chondroprotective effect (69.5±11.7 µm) as compared to untreated controls (107±25.9 µm) ($p<0.005$) at both 3- and 20-min post-injury. Interestingly, post-treatment groups show that GsM-col group (86.43±24.13 µm) exhibit statistically significant chondroprotective effect compared to the control (110.8±17.04 µm). These data suggest that GsM-Col has more efficient cartilage delivery and may protect chondrocytes from mechanical and arthritic stimuli post-joint injury. The reduced chondrocyte death in post-treatment of GsMTx4/GsM-Col may resulted by inhibiting Piezo1 channels and Calcineurin1/ NFAT1 pathway [5]. These data suggest that GsM-Col can be DMOADs post-joint injury. Our future studies include quantifying chondro- and ECM-protective efficacy of GsMTx4 and conjugates in arthritic cartilage induced by inflammation and injury model ex vivo for longer period, as well as evaluate the drug efficacy using mouse OA models.

Significance/clinical relevance: Therapeutic options for OA are limited to addressing its symptoms and more efficacious treatments are currently explored for alleviating OA. GsMTx4 could be a potential drug that addresses not only the symptoms but also the underlying pathophysiology of the disease. Further in vivo and clinical studies might help elucidate the mechanism of action of GsMTx4.

Acknowledgements: NIH R35GM147054, R01AR082349 and P30AR069655.

References: [1] Hodgkinson, T., et.al (2022). [2] Lee, W., et.al. (2014). [3] Kotelsky, A., et.al. (2021). [4] Lee, W., et al (2021). [5] Ren, X., (2023). [6] Bae, C., et.al. (2011). [7] Radhakrishnan, G., et.al. (2017).

**PAPER #54**

**TITLE:** Functional Outcomes and Complications Following Anterolateral Versus Posterior Surgical Approaches for Open Reduction and Internal Fixation of Humeral Shaft Fractures: A Retrospective Review.

**PRESENTING AUTHOR:** Melissa R. Holloway, BS

**CO-AUTHOR(S):** Urvi J. Patel, MD, MS, BS, Thomas J. Carroll, MD, Sandeep Soin, MD

**LAB PI/MENTOR:** John P. Ketz

**ABSTRACT**

Purpose: The purpose of this study is to retrospectively assess and compare the complications, functional outcomes, and radiographic union rates following anterolateral versus posterior approach to open reduction and internal fixation in the treatment of humeral shaft fractures. We hypothesize comparable outcomes between the two groups with regards to post-operative patient reported outcomes, complication rates, and radiographic union rates.

Methods: We retrospectively reviewed patients undergoing surgical intervention with diaphyseal humeral shaft fractures at our institution. In total, 195 patients met our inclusion criteria. Patients under the age of 18 and those with intra-articular fracture extension were excluded. Demographic characteristics, OTA fracture classification, operative approach, time to union, complications, and PROMIS outcomes were reviewed and analyzed. Statistical significance was determined at $p<0.05$.

Results: The posterior approach was performed in 41 patients with type A fractures (n=28), type B fractures (n=6), and type C fractures (n=7), The anterolateral approach was performed in 154 patients with type A fractures (n=99), type B fractures (n=32), and type C fractures (n=23). There were no differences between the anterolateral and posterior approach cohorts with regards to time to surgery (29.7±62 vs. 18.6±32; p=0.27), mean intraoperative blood loss (352±319 vs. 266±198 cc; p=0.11), total operative time (206±80 vs.218±71 mins; p=0.46), or time to union (18±8 vs. 16±8 weeks; p=0.15). There were no differences between the groups for non-union, secondary radial nerve injuries, or severe post-operative pain or stiffness (p=0.69, p=0.99, p=0.19, respectively). Both cohorts showed similar PROMIS scores at the 6 month follow up for Physical Function (p=0.69), Pain Interference (p=0.38), and Depression (p=0.31).

Conclusion: While the posterior approach has been the traditional choice for fixation given the biomechanical advantage of plate application on the tension side of humeral shaft fractures, the anterolateral approach provides a safe alternative for open reduction and internal fixation. The anterolateral approach allows for supine positioning of the patient and yields comparable complication rates, union rates, and post-operative functional outcomes to those of a posterior approach.

**PAPER #55**

**TITLE:** No Differences in Clinical, Functional, or Patient-Reported Outcomes Following Trial of Non-operative Management Prior to ORIF of Humeral Shaft Fractures

**PRESENTING AUTHOR:** Melissa R. Holloway, BS

**CO-AUTHOR(S):** Urvi J. Patel, MD, MS, BS, Thomas J. Carroll, MD, Sandeep Soin, MD

**LAB PI/MENTOR:** John P. Ketz

**ABSTRACT**

Purpose: Treatment for humeral shaft fractures remains controversial as many patients are faced with the choice of operative versus nonoperative management. Recent studies have shown primary osteosynthesis of humeral shaft fractures to be safe and superior to nonoperative treatment. While many studies have reviewed the clinical and functional outcomes of operative versus nonoperative management for humeral shaft fractures, none to our knowledge have evaluated outcomes following trial of nonoperative treatment for humeral shaft fractures. We hypothesize that patients who trial nonoperative management prior to surgical intervention will experience similar functional recovery, but poorer patient reported outcomes.

Methods: We retrospectively reviewed patients who presented with humeral shaft fractures at our Level-I trauma center. Patients who trialed nonoperative management were separately reviewed from patients who underwent open reduction and internal fixation as primary treatment for their humeral shaft fracture. Post-operative complications, elbow arc of motion, time to radiographic union, and patient reported outcomes were investigated. Statistical significance was set at a p-value of $< 0.05$.

Results: Of the 138 included patients, 92 underwent primary osteosynthesis and 46 trialed initial nonoperative treatment. No differences were found in the patient age or BMI between the two cohorts (P=0.20 and P=0.99, respectively). The average time to operative intervention in the primary osteosynthesis group was 7 days (0-31 days), and 99 days (19-332 days) in the trial of non-operative treatment group ($p<0.01$). No differences were found with regards to intra-operative blood loss, total operative time, or time to radiographic union. No difference was found in the overall complication rates, including primary and secondary radial nerve injuries (P=0.28 and 0.84, respectively). Patients reported similar PROMIS Pain Interference (PI) (59.18±10.30 vs. 59.73±8.82; P=0.83), Depression (D) (51.57±13.15 vs. 51.34±10.70; P=0.94), and Physical Function (PF) (38.82±9.89 vs. 39.29±7.20; P=0.84) scores at their 6-month post-surgical follow up visits.

Conclusion: Patients who attempted a trial of non-operative management for humeral shaft fractures prior to open reduction and internal fixation had similar clinical, functional, and patient reported outcomes as those who underwent primary osteosynthesis. Patients who trialed non-operative therapy had similar union rates, complication rates, post-operative arc of motion and patient reported outcomes. Given our findings, surgeons can educate patients with humeral shaft fractures on the minimal risk associated with a trial of non-operative management, and similar clinical outcomes should they need or pursue surgical intervention at a later time.

**PAPER #56**

**TITLE:** Autologous and Allogenic In vivo Engineered Extracellular Matrix as Tissue-Engineered Periosteum for Defect Repair

**PRESENTING AUTHOR:** Chen Jiang

**CO-AUTHOR(S):** Tianfeng Miao, Nicholas Lenhard

**LAB PI/MENTOR:** Xinping Zhang

**ABSTRACT**

While periosteum tissue engineering has become a mainstay in repair and reconstruction, an emerging surgical technique named Masquelet technique that combines a foreign body reaction-induced vascularized tissue membrane with bone matrix for repair and reconstruction of large bone defect has gained wide attention in regenerative medicine. Combining bone tissue engineering technologies with induced membrane technique provides an exciting new arena for management of bone defect repair. Inspired by Masquelet techniques, we previously reported an approach utilizing foreign body reaction-induced, in vivo engineered decellularized extracellular matrix (dECM) as a periosteum mimetic for repair and reconstruction of segmental bone defects. The approach involves 3D printing, in vivo implantation of polylactic acid (PLA) templates, followed by depolymerization and decellularization to create a dECM matrix with desired pattern and architecture. The goal of our current study is to compare the reparative outcome using allogenic and autologous dECM as tissue-engineered periosteum for allograft bone-mediated large bone defect repair. To enhance the osteo-inductive activity of the engineered matrix, we examined the capacity of the dECM to bind and deliver BMP2 (100 ng/dECM) to bone healing site. Micro-CT scanning showed that treatment of allogenic, autologous and BMP2 loaded dECM matrix all achieved enhanced callus formation. Compared with allograft control, volumetric analysis demonstrated that allogenic dECM, autologous dECM, and BMP2-dECM had 1.36, 1.73, and 2.14-fold larger total new bone callus, respectively ($n=5-11$, $p<0.05$). Histologic analyses showed that compared with allograft and allogenic dECM, autologous dECM and BMP2-dECM induced significantly more periosteal bone callus formation across the surface of allograft, leading to better osseointegration between host and donor. Fluorescence images further showed newly formed bone tissues with Col1(2.3) GFP+ osteoblasts on allograft surface in each group. Histomorphometric analysis showed that fibrotic tissue formation in autologous dECM and BMP2-dECM treated samples was reduced to 55% and 36% of that of the control allograft. Consequently, bone formation was increased by 2.10 and 2.48-fold, respectively ($n=5-11$, $p<0.05$). Finally, the autologous dECM-wrapped allograft significantly improved biomechanics of bone allograft healing, restoring the torsional rigidity and maximum torque to 91% and 55% of those of intact femurs, while allograft alone only had 6% and 13% of those of the intact bone ($n=8-16$, $p<0.05$). Our data showed that autologous matrix induced more periosteal bone callus formation and recruited more osteoblasts to allograft surface than allogenic dECM. This could be attributed to the fact that allogenic scaffolds could generate a stronger immune response than autologous dECM during repair. Utilizing dECM, we showed that loading ~100ng BMP2 per dECM achieved markedly induction of periosteum callus formation, reduction of fibrotic tissue and further improvement of osseointegration. This result provides the potential to address the increased risk of adverse effects of delivering excessive amounts of BMP2 (often as high as 12 mg per treatment) to healing sites. Taken together, our results support that engineered autologous dECM could be directly used in bone regeneration applications or as a vehicle to deliver bioactive molecules to bone healing sites. The success of our current study could establish a new line of versatile, patient-specific, and periosteum-like autologous dECM matrices for bone tissue engineering, potentially offering personalized therapeutics to patients with impaired healing for one-stage repair and reconstruction of large weight-bearing defects. More analyses are currently underway to determine the immune cells including macrophage infiltration in allogenic and autologous dECM and examine the degradation of the allogenic and autologous dECM in vivo.

**PAPER #57**

**TITLE:** Piezo2 Regulation in Chondrocytes Post-Exercise

**PRESENTING AUTHOR:** Xingyu Jing

**CO-AUTHOR(S):** Alexander Kotelsky, Whasil Lee

**LAB PI/MENTOR:** Whasil Lee

**ABSTRACT**

INTRODUCTION: Mechanical loading from an active lifestyle is essential for chondrocyte metabolism and cartilage homeostasis. We previously reported the essential roles of Piezo1 mechanosensitive ion channels in osteoarthritis (OA) progression and mechanical injury-induced chondrocyte death (Lee et al., 2014, 2021). However, a significant knowledge gap exists concerning the roles of Piezo1 and Piezo2 mechanosensitive channels on cartilage maintenance post-exercise. Especially, Piezo2-mediated mechanotransduction has not been explored in articular chondrocytes in vivo. Our ultimate objective is to elucidate Piezo2-mediated chondrocyte mechanotransduction in response to exercise-driven physiologic loading. This report presents the gene regulations of Piezo1 and Piezo2 in articular cartilage using an exercised mouse model, as well as the mechanical susceptibility of chondrocytes post-exercise. We hypothesize that exercise-driven augmentation of Piezo2 channels in articular chondrocytes contributes to cartilage anabolism.

METHODS: Ethical approval was obtained by the UCAR committee (Protocol#: 2019-008). Eight-week old female C57BL6/J mice were subjected to Voluntary Wheel Running (VWR) system either with locked wheels (sedentary group) or unlocked wheels (exercise groups) for 1 or 2 weeks. Knee joints were harvested and fixed. Sagittal sections of medial side (thickness = 7µm) were labeled with anti-Piezo1 or anti-Piezo2 (ProteinTech, Inc.), and imaged by slide scanner (VS120) or Keyence. The fluorescent intensity was quantified by ImageJ and QuPath. All data was presented as Mean±SEM. One-way ANOVA and paired t-test were used for statistics. Mechanical death assay was conducted on the other knee joint from the same mouse. Femoral condyles were imaged by confocal microscopy before and after the impact (1mJ).

RESULTS: First, we observed differential expressions of PIEZO1 and PIEZO2 channels in chondrocytes of femoral and tibial cartilage. Cartilage thickness and anti-Piezo1 intensity were statistically insignificant between femoral and tibial chondrocytes. However, the PIEZO2 expression level is significantly higher in tibial cartilage than femoral. Second, PIEZO2 channels are augmented in exercised cartilage versus sedentary group. Interestingly, the number of PIEZO2-null chondrocytes decreased post-exercise (~12% to 4%) and highly-PIEZO2-expressed cells were increased post-exercise (18% to 37% in femoral cartilage; 33% to 52% in tibial cartilage). In addition, we also found chondrocyte vulnerability towards external impact decreased after exercise by having less cell death after applying the force.

CONCLUSIONS: We observed heterogeneous Piezo2 expression in articular chondrocytes, from Piezo2-null to highly-expressed cells. We further observed the augmented Piezo2 channels in exercised chondrocytes in medial femoral and tibial cartilage, yet less significant in lateral sides. It has been known that the medial cartilage bears higher weight while standing and walking than lateral sides (Liu et al., 2010), our results suggest that physiologic joint loading may differentiate Piezo2 expression in chondrocytes. In addition to our previous finding that Piezo 1 was upregulated in osteoarthritis (OA) but not Piezo2 as well as decreased cell vulnerability after exercise, Piezo2 may play a chondro-protective role compensating Piezo1 upregulation. With figuring out the role of Piezo2 in cartilage health, potential agonists can be investigated to facilitate rehabilitation process and applied to clinical. Considering the necessity of pericellular matrix (PCM) in maintaining cartilage homeostasis (Wilusz et al., 2014), we will further investigate how exercise regulates PCM and its association with Piezo2 regulation.

ACKNOWLEDGEMENTS: NIH R35GM147054, R01AR082349 and P30AR069655.

**PAPER #58**

**TITLE:** Patient Demographics Does Not Correlate with Patient Reported Quality of Knee and Hip Osteoarthritis Care

**PRESENTING AUTHOR:** Jane Jurayj, BA

**CO-AUTHOR(S):** Benjamin F. Ricciardi, MD, Caroline P. Thirukumaran, MBBS, MHA, PhD, Kathryn A. Miller, MD, Courtney Jones PhD, MPH, Katherine H. Rizzone, MD, MPH

**LAB PI/MENTOR:** Katherine H. Rizzone, MD, MPH

**ABSTRACT**

INTRODUCTION: Osteoarthritis (OA) is a degenerative joint disease responsible for significant pain and disability worldwide. International guidelines exist for the treatment of knee and hip OA, yet discrepancies exist in adherence to these guidelines. There are significant gender and racial disparities in OA care with females, Black Americans, and patients residing in areas with greater socioeconomic disadvantage have higher rates of OA, yet receiving reduced quality of care. The purpose of this study was to assess patient-reported quality of OA care using the OsteoArthritis Quality Indicator (OA-QI) and to explore clinical and demographic variables associated with greater reported quality of care. We hypothesize that disparities exist in patient-reported quality of OA care, with female and BIPOC patients achieving lower QI pass rates compared to white males. METHODS: This was a cross-sectional study conducted in an academic orthopaedic clinic setting. Eligible participants were adults >22 years with hip or knee arthritis who had not received joint replacement. Participants completed the OA-QI in clinic. The OA-QI is a validated 17-item survey that assesses patient-reported quality of OA care on factors such as: recommendations for education, weight loss, physical activity counseling, nutrition counseling, and medication counseling (score range of 0-100, 100 = top score), Chart extraction included demographic information, number of visits in the last 12 months,and co-morbidities. . State and national ADI were calculated. The primary outcome was total OA-QI score, which was calculated as the percent of QI measures achieved based on the total eligible QI measures for an individual. At the group level, an item pass rate was determined by the number of participants that achieved that QI measure (checked 'yes') divided by the total number of eligible participants (checked 'yes' or 'no'). Analyses was conducted using SAS and differences in means and frequencies were calculated using t-tests, chi-square, ANOVA and linear regression. RESULTS: The study cohort consisted of 107 participants. , the majority of whom were female (65.4%), white (88.8%) and visit was in regards to their knee OA (85%). The mean OA-QI scores for new patients (M =60.6, SD=22.1) were significantly lower than OA-QI scores for returning patients (M =74.0,SD =14.6)(p=0.03). OA-QI scores were significantly lower in participants that were referred to surgery (M=68.0, SD=17.93) than participants who were not (M=75.2,SD=13.9)(p=0.05). Two sample t-tests comparing mean OA-QI scores showed no significant differences when examined by gender, race, or ethnicity. OA-QI scores did not vary by the ADI. Referral for help with weight loss had the lowest pass rate (12.2%). BMI and new patient status were independent predictors of OA-QI score after adjustment for age and CCI. For every one-point increase in BMI, the OA-QI score increased by 0.42(p=0.04), and being a new patient was associated with a 13.2 decrease in OA-QI score compared to being a return patient (p=0.02). DISCUSSION: We did not find a relationship between OA-QI score and biological sex, race, age, or ADI score, suggesting that patient reported quality of information delivered was similar across a wide cross-section of OA patients in a tertiary referral setting. Consistent with prior work, the lowest pass rate for any of the QI items was referral for help with weight loss. Given the prevalence of obesity, and the link between excess body weight and OA symptoms, support with weight loss should remain a priority. The link between elevated BMI and higher pass rate may reflect increased education and guidance of obese patients around weight loss, physical activity, and lifestyle changes. While the lower pass rates in new patients may be explained by fewer opportunities to receive OA education, they point to a need to cover basic principles of OA progression and care at new patient visits.

**PAPER #59**

**TITLE:** The Role of Taurine in Hematopoiesis

**PRESENTING AUTHOR:** Christina M. Kaszuba

**CO-AUTHOR(S):** Benjamin J. Rodems, Sonali Sharma and Edgardo I. Franco

**LAB PI/MENTOR:** Jeevisha Bajaj

**ABSTRACT**

The bone marrow microenvironment consists of hematopoietic cells, non-hematopoietic stromal cells, and the extracellular matrix. This microenvironment can promote hematopoietic stem cell self-renewal, regulate lineage differentiation, and provide structural and mechanical support to the bone tissue. Recent work has shown that taurine supplements can mitigate the effects of aging and improve bone and muscle health. However, the effect of taurine on the hematopoietic system is not described. Taurine, a non-essential amino-acid, is transported into cells through a high-affinity taurine transporter (TauT), encoded by the SLC6A6 gene. We used a combination of taurine supplements as well as genetic TauT null mice to determine the role of this pathway in hematopoiesis. Our experiments show that taurine supplements significantly increase the in vitro colony forming ability of hematopoietic stem cells (HSC) as compared to controls, indicating a functional role of taurine in HSC maintenance/support. Several studies have identified a key role of bone marrow mesenchymal stromal cells (MSC) in providing support for HSCs. Our gene expression analysis of the bone marrow microenvironment indicates that in addition to HSCs, MSCs also express the taurine transporter SLC6A6. Our experiments with in vitro co-cultures show that this TauT expression is rapidly downregulated with osteogenic differentiation, indicating that more differentiated cells transport less taurine leaving excess taurine in the bone marrow microenvironment. Co-cultures of TauT+/+ and TauT-/- MSCs with normal, freshly isolated HSCs suggest that TauT-/- MSCs lead to an enrichment in HSC frequency compared to TauT+/+. Consistent with these observations we see an increase in HSC colony forming units. This data is consistent with our in vivo experiments where whole bone marrow was transplanted into TauT+/+ and TauT-/- mice and there was an increase in engraftment in TauT-/- mice likely because of excess taurine available in the bone marrow microenvironment. Collectively, our results identify TauT as a key regulator of hematopoiesis. This is significant as taurine could be used to expand HSCs in vitro for use in bone marrow transplants for patients suffering from diseases of the bone marrow or immune system.

**PAPER #60**

**TITLE:** Elucidating the Mechanism of CCL3-Driven Bone Marrow Dysfunction during Acute Myelogenous Leukemia

**PRESENTING AUTHOR:** Amal A. Khan

**CO-AUTHOR(S):** Maggie Lesch, Celia Soto, Azmeer Sharipol, Benjamin J. Frisch

**LAB PI/MENTOR:** Benjamin J. Frisch

**ABSTRACT**

Acute Myeloid Leukemia (AML) is an aggressive and common acute leukemia in adults. It is characterized by an increase in proliferation and blocked differentiation leading to an accumulation of immature cells. This leads to a loss in normal hematopoiesis and the overall disruption of the bone marrow micro-environment (BMME).

Studies show that C-C Motif Chemokine Ligand 3 (CCL3), which signals through two G- Protein coupled receptors, CCR1 and CCR5, has been associated with hematopoietic malignancies and BMME dysfunction [*Staversky et al., 2018*]. Furthermore, our initial research shows that CCL3 released by leukemic cells promotes leukemic progression [*Ackun-Farmmer et al., 2021*]. Our research in blocking CCL3 signaling using inhibitors delivered via bone-targeted nanoparticles showed a partial reduction in leukemic burden in blast-crisis Chronic Myelogenous Leukemia (bcCML) murine models, a clinically relevant model of AML [*Ackun-Farmmer et al., 2021*].

To understand the mechanism of CCL3-driven dysfunction in the BMME, we use CCR1 ($CCR1^{-/-}$), CCR5 ($CCR5^{-/-}$), and $CCR1^{-/-}$ and $CCR5^{-/-}$ (dKO) global knockout mice. As phenotypes in these mice have not been fully described, we are longitudinally characterizing the hematopoietic populations of healthy and leukemic dKO mice in comparison to wild type (WT) at regular intervals in addition to comparing dKO and WT recipients of leukemic transplants. Our initial analysis of the peripheral blood showed no significant phenotypic differences between the non-leukemic dKO and WT mice. However, initial complete blood count of the peripheral blood of leukemic dKO mice showed significantly higher levels of erythroid populations, namely the RBC (P value=0.019), hemoglobin (P value=0.018), and hematocrit count (P value=0.02), as compared to the WT leukemic mice where these populations were reduced. This may be due to lack of CCR1/5 receptors in the dKO mouse model which do not respond to leukemic CCL3 signaling. Furthermore, initial analysis of the myeloid and lymphoid precursor populations of healthy dKO vs. WT did not show any significant differences in the progression of the hematopoietic components. Therefore, CCR1 and CCR5 receptors may not be involved in regulating the hematopoietic balance, which suggests that they may be ideal targets for AML- specific therapy.

Further experiments aim to continue to decipher the phenotypic and functional capacity of the BMME components which include the hematopoietic stem and progenitors' cells (HSPC), mesenchymal stromal cells (MSC), the osteoblasts, and the macrophages in healthy and leukemic WT vs. dKO mice. We also aim to generate CCR1/5 knockout leukemic cell line and test its leukemic potential.

**PAPER #61**

**TITLE:** Constructing a mixed Arrayed Imaging Reflectometry sensor for simultaneous quantification of antibodies and cytokines in human serum

**PRESENTING AUTHOR:** Alanna Klose

**CO-AUTHOR(S):**

**LAB PI/MENTOR:** Dr. Benjamin Miller

**ABSTRACT**

Each year in the U.S.A. there are approximately 70,000 new Staphylococcus aureus infections following routine orthopedic surgery, costing $22 million to treat. Diagnosis currently requires an invasive and time-consuming culture of a sample from the infected tissue because a blood-based diagnostic test is not available. Significant progress has been made towards the development of such a tool, but the discriminatory ability as determined by Receiver Operating Characteristic (ROC) analysis has been unable to achieve the 0.95 Area Under the Curve (AUC) threshold comparable to FDA approved diagnostics. The AUC can be improved by including clinical laboratory data such as serum albumin levels into the analysis, but an ideal diagnostic tool should function independently. Given that the B-cells of the adaptive immune system secrete billions of antibodies into the bloodstream in response to infection, multiplex immunoproteomic tools should be able to detect inflammatory cytokines and S. aureus antigen-specific antibodies as surrogate markers of infection.

Established immunological assay techniques (ELISA, Luminex) rely on enzymatic or fluorescent labels conjugated to secondary or sandwich antibodies for antibody or cytokine detection. As such, these techniques cannot be used to simultaneously measure cytokines and antibodies because of fundamental cross-binding of secondary antibodies to sandwich antibodies. Arrayed Imaging Reflectometry (AIR) is an optical sensing technique that is theoretically capable of simultaneous detection of antibodies and cytokines because it doesn't require a label for detection. Instead, AIR measures the change from dark to bright as 633 nm light reflects off the sensor chip and into a CCD camera. The increase in intensity from dark to bright of each probe spot is mathematically related to the amount of target protein bound, or the change in thickness as target protein binds to capture protein. The capture proteins are arrayed in a grid pattern onto the sensor surface as aqueous droplets from a piezoelectric dispenser, and are then referred to as probe spots. The deposition parameters that achieve the anti-reflective condition are identified for each probe spot and applied to create a multiplexed sensor chip capable of simultaneously capturing 10s to 100s of different target proteins.

Simultaneous detection of antibodies and cytokines is challenging due to the wide range of concentration at which these proteins are present in serum, where specific IgG antibodies circulate at µg/mL to mg/mL, and cytokines are typically found at 1-500 pg/mL. This requires a sensor with a dynamic range that spans 9 orders of magnitude. AIR partially fulfills this requirement by collecting short, medium, and long CCD exposure times for each sensor chip thereby extracting quantitative information for low and high concentration targets from a single assay. It is straightforward to measure binding of antibodies to capture probes without using a label. However, the low pg/mL targets are difficult to quantify without using highly specific mass-building techniques to amplify the change in reflectivity due to the target binding to probe. The focus of this ongoing work is how to employ sandwich antibodies and enzymatic polymerization of 3,3'-Diaminobenzidine to build mass to amplify detection of six cytokines on a 27-plex mixed StaphAIR sensor chip while avoiding off-target and non-specific interactions with antibody capture probes and reference probes. This work requires careful consideration of how the sensor chip is constructed, how all probes on the sensor chip are formulated to achieve baseline anti-reflective conditions, and how the mass amplification protocol is designed. The result will be an assay that can simultaneously detect antibodies against Staphylococcus aureus and quantify cytokines secreted during bacterial infection. Such an assay could be useful as a diagnostic and prognostic tool for musculoskeletal infections.

**PAPER #62**

**TITLE:** Engineering microvasculature in periosteum biomimetic for bone defect repair and reconstruction

**PRESENTING AUTHOR:** Manohar Koduri

**CO-AUTHOR(S):** Chen Jiang, Tian Feng Miao, Samantha Mill, Xinping Zhang

**LAB PI/MENTOR:** Xinping Zhang

**ABSTRACT**

Introduction:
Periosteum is a multilayered dense connective tissue membrane that covers the outer surface of bones. The outer fibrous layer of periosteum consists of small collagen bundles with interspersed elongated fibroblasts. The inner cambium layer is highly cellularized and contains mesenchymal stem cells, osteoblasts, and chondroprogenitor cells that endow osteogenic potential of the periosteum. Periosteum is highly vascularized. Blood vessels in periosteum not only supply nutrients, oxygen and growth factors, but also contribute osteogenic and angiogenic cells to control the growth, repair and regeneration of bone tissue. Previous work from our lab have established a nanofiber-enabled layer-by-layer assembly approach to creation of a multilayered tissue engineered periosteum (TEP) for bone tissue repair and regeneration. To enhance the performance of the TEP construct, we propose to increase the thickness and perfusion efficiency of the construct by developing an implantable in-vitro perfusable microfluidic assembly that can be used to simulate the vascularization and bone specialized vessel formation during periosteum-mediated repair and regeneration. The project will leverage our established capacity for real-time monitoring of bone healing tissue as well as the growth and physiology of blood vessels via multiphoton microscopy and light sheet microscopy. A series of bio-fabrication techniques namely soft lithography, additive manufacturing, lab on a chip device, electrospinning, and layer-by-layer assembly will be used to generate geometrical features with high spatial and temporal arrangement of cells to mimic the cellular, molecular and architectural complexity of periosteum for in-vitro and in-vivo studies. The success of our project will create an improved, thicker TEP construct that can sustain cell survival and nutrient exchanges, further permitting a better understanding of the molecular and cellular interplay between osteogenic and angiogenic cell populations for controlled bone tissue regeneration.

Methodology:
The single layer of micro-vessel networks (~50 µm) will be fabricated using soft lithography patterning of collagen housed in plexiglass chamber which will be sealed by optical glass on top. The channels in collagen will be designed using PDMS as a mold and SU-8 as a photoresist. The integrated nano fabrication facilities of the University of Rochester will assist with manufacturing the perfusable microfluidic assembly. The device consists of two injection ports on the plexiglass; one for injecting the collagen gel and the other for air to evacuate from the closed mold during the injection. Two stainless steel dowel pins will be inserted into the other two holes in the top plexiglass to define the inlet and outlet of the microvessel networks. In validating micro-channels in the collagen scaffold, fluorescent beads will be perfused through the channels. The intact microchannels will further be seeded with endothelial cells and incubated at standard cell culture conditions to establish in-vitro vascularization. The endothelialized channels will be embedded in collagen containing mesenchymal stem cells and osteoblasts. The multilayered TEP construct will be made by layer-by-layer assembly of the vascularized collagen layers together with nanofibers seeded with bone marrow stromal cells and implanted in defective bone allograft model and in cranial window for examination of bone regeneration capacity and microenvironmental factors. The study will utilize phosphorescence life time imaging (PLIM) for measurements of oxygen distribution in the vascularized graft, NAD(P)H Autofluorescence Lifetime Imaging (FLIM) for cellular metabolism, and second harmonic generation for collagen degradation and bone regeneration. A multilayer (2mm) construct is expected to be developed to achieve more robust and uniform bone regeneration.

**PAPER #63**

**TITLE:** Investigating the Effects of Stiffness and Topography on TRPV4 Activation in AF Mechanotransduction

**PRESENTING AUTHOR:** Mikkael Lamoca

**CO-AUTHOR(S):** Gabbie Wagner and Johannes Hasler

**LAB PI/MENTOR:** Karin Wuertz-Kozak

**ABSTRACT**

Low back pain is closely associated with intervertebral disc (IVD) degeneration. This process is characterized by extracellular matrix (ECM) degradation in the annulus fibrosus (AF), leading to substrate stiffening and disorganization of the collagen architecture. These changes can affect cell behavior through mechanoreceptors like transient receptor potential (TRP) channels, particularly TRPV4, which is highly expressed in the AF and is linked to pain and inflammation. However, AF cell-substrate interaction with TRPV4 remains unexplored. We hypothesize that TRPV4 activation are influenced by substrate stiffness and topography, altering calcium (Ca2+) flux and modulating inflammation, and degeneration-related targets. The goal of this study is to fabricate substrates of different stiffness and topography and test the effects on TRPV4.

Chambers with various substrate stiffness were fabricated by adjusting the mixture of polydimethylsiloxane (PDMS) Sylgard 184 and 527 (0, 14, and 24 wt%) and cured at 65°C for 24 hours. The PDMS stiffnesses (Young's Modulus) were determined through uniaxial tensile testing at a 10 mm/s strain rate until rupture (n=5). Substrate biocompatibility was assessed using an alamarBlue assay with bovine AF cells (n=5). The effects of substrate stiffness on total and maximal Ca2+ influx in AF cells were explored following TRPV4 pharmacological activation (0.5 µM GSK101790A) with a Fura-2 QBT assay (n=5). To simulate the loss of collagen alignment, PDMS chambers were fabricated with aligned and random topographies via coaxial electrospinning. PDMS core fibers were obtained after dissolving the polyvinylpyrrolidone (PVP) sheath with 100% ethanol (EtOH) for 20 minutes. PVP removal was validated with nuclear magnetic resonance. Moreover, fiber diameter and alignment within 15 degrees was measured using scanning electron microscopy and FIJI imaging software. Statistical analysis included Kruskal-Wallis and Shapiro-Wilk tests for normality and one-way ANOVA using GraphPad Prism.

PDMS chambers were successfully fabricated with 9, 63, and 240 kPa stiffness and AF cell viability was greater than 80%. In addition, chambers of varying stiffness portrayed differing surface strains mimicking anatomical conditions. Upon TRPV4 activation, AF cells cultured on higher PDMS stiffness displayed increased total (1.23 fold change) and maximal Ca2+ flux levels (1.26 fold change) from 9 to 240 kPa substrates, highlighting TRPV4's mechanosensitive nature in AF cells and its potential influence on downstream targets. PDMS fibers were also successfully fabricated, closely matching collagen fiber diameters (2.97±0.49 µm).

Our biocompatible cell-substrate interaction model successfully mimics the different stages of degeneration. Increasing in vitro stiffness, as observed in vivo during degeneration, led to increased TRPV4 activation, as evidenced by enhanced Ca2+ flux; however, additional trials must be conducted for validation. Due to the stiffness-dependent TRPV4 activation and changes in intracellular Ca2+ concentration modulates cell behavior with ECM synthesis and promoting catabolism, TRPV4 activation represents an interesting pathway to study AF ECM synthesis and remodeling, thus creating a crucial feedback loop. To further improve the cell-substrate interaction model to study IVD degeneration, incorporating topography to mimic healthy (aligned) and degenerated (random) AFs is also highly significant. Ongoing experiments are working to identify relevant ECM, inflammatory, and degeneration-associated downstream targets and improve the fabrication of aligned PDMS fibers. In the future, experiments will also investigate stiffness and topography in combination with the mechanical activation of TRPV4 through cyclic stretching. Overall, a better understanding of AF cell-substrate interaction and the mechanotransduction process may contribute to developing new tissue engineering models and novel TRP-based therapeutics.

**PAPER #64**

**TITLE:** An Intravital Imaging Protocol to Visualize and Phenotype the Associated Niche of Clonal Hematopoiesis

**PRESENTING AUTHOR:** Kevin Lee

**CO-AUTHOR(S):** Cih-Li A. Hong, Zi Yin, Melissa MacLiesh, Wimeth Dissanayake, Yuko Kawano, Hiroki Kawano, Christina Kaszuba, Benjamin Rodems, Judith Runnels, Michael W. Becker

**LAB PI/MENTOR:** Shu-Chi A. Yeh

**ABSTRACT**

Clonal Hematopoiesis of indeterminate potential (CHIP) is a condition where blood cells are produced from a few clones of hematopoietic stem cells (HSCs) carrying leukemia-associated driver mutations[1]. Although selective pressures from low-grade inflammation of the bone marrow microenvironment have been shown to promote mutant cell expansion[2–7], clonal expansion of leukemia and activated HSCs[8,9] was not uniform. Therefore, we focus on disease-initiating niche, which is defined as a highly spatially restricted marrow cells surrounding rare HSCs. The goal is to identify the novel niche factors for therapeutic targeting.

Specifically, we leveraged high-resolution, video-rate in-vivo imaging for rapid surveillance through calvarial bone marrow. This enabled us to identify and capture dynamics of the transplanted rare cells in a minimally perturbed microenvironment. Notably, as little as 0.5Gy irradiation enabled survival of the transplanted cells (2x106 GFP+ healthy whole bone marrow) in non-irradiated side and allowed direct visualization of early clonal expansion in vivo through 16 weeks. Engraftment with the same number of transplanted cells was negligible in non-irradiated mice. With this protocol, for the first time, we showed that hot spots of cell expansion exist in the Tet2+/- murine CHIP model and were able to track Tet2+/- cell interactions with the microenvironment via 60-minute longitudinal imaging with 1-min intervals. Our results showed that Tet2+/- cells are highly mobile (up to 40 microns/hour) and do not form a stable association with the peri-vascular niches. Instead, cells are in direct contact with the autofluorescent cells, which are non-migratory, bone marrow resident F4/80+ cells. In the cases where cells showed close association with vessels, the cells extravasated within the observation period, suggesting that vascular association may be more relevant to cell transmigration to periphery or seeding to the “new soil”, rather than proliferation within the hot spots. The finding suggests the need to analyze local marrow microenvironment; in particular, the macrophage populations.

To capture the highly localized specific niche factors responsible for these hot spots, locations of Tet2+/- dense and sparse bone fragments (0.5 mm x 0.6 mm) in the mouse calvaria were characterized by imaging and harvested for single cell RNA sequencing using 10x genomics. Flow sorting recovered 3042 GFP Tet2+/- positive cells from dense regions with 50 GFP Tet2+/- positive cells from sparse regions, along with their respective niche cells, confirming the effectiveness of image-guided tissue isolation. Preliminary findings from this single cell dataset suggest enrichment of genes associated with inflammation and calcium ion interactions in the hot spots. To further improve the spatial precision of the transcriptomic analyses, we developed image-guided live-cell labeling adapted from the previously published Image-seq protocols9, which allowed recovery of ~10,500 antibody labeled cells with 98% viability from single bone marrow cavities.

In conclusion, we established a working model to visualize expansion of healthy and Tet2+/- hematopoietic cells in vivo. This can be followed by image-assisted live-cell tagging to isolate local microenvironment cells and study cell-niche coordination at high spatial precision. The imaging protocol may also be broadly applied to study microenvironment regulations in non-malignant clonal disorders.

**PAPER #65**

**TITLE:** Characterizing bone marrow interstitial pH by two-photon ratiometric imaging

**PRESENTING AUTHOR:** Melissa MacLiesh

**CO-AUTHOR(S):**

**LAB PI/MENTOR:** Shu-Chi Yeh

**ABSTRACT**

Introduction: Acidic interstitial pH in the bone marrow has been shown to influence metabolic signatures and phenotypes of blood, immune, and leukemic cells (1,2). Using two-photon fluorescence microscopy (TPFM) and ratiometric pH probe, SNARF-1, it is possible to map absolute interstitial pH in live bone marrow at single- cell resolution (3). Mapping pH distribution in vivo will provide unprecedented information that is lost in downstream processing such as tissue sectioning. Here we investigated the acidic pH near macrophages which has been shown to promote their polarization into the immune-suppressive M2 phenotype (1) and drive leukemic transformation (5).

Methods: Dextran conjugated (70kDa), cell-impermeable SNARF-1 was administered retro-orbitally and was subsequently sequestered to the interstitial space. The fluorescence emission spectrum of SNARF-1 undergoes a pH dependent shift from 580nm to 640nm, allowing quantification of the fluorescence ratio to determine relative pH. When addressing the ratio of red (collected in 625 nm-675nm) to green fluorescence (collected in 495 – 605 nm), mathematical corrections need to be applied to account for the increased optical attenuation (from bone and blood) of green fluorescence compared to red in order to retrieve accurate ratiometric measurements in deep tissue. Image segmentation based on the SNARF-1 fluorescence was then performed to retrieve relative pH distribution in the interstitial space. Separately, macrophages were labelled in vivo using pan-macrophage antibodies F4/80 and CD68 (15 µg/mouse), as well as the M2 marker CD206 (15 µg/mouse) in conjunction with Fc-blocker (20 µg/mouse) to prevent nonspecific binding. Image stacks were segmented based on the SNARF-1 fluorescence to retrieve relative pH distribution in the interstitial space. The pH near autofluorescent cells/macrophages was analyzed using a minimum of 3 regions of interest adjacent to each cell.

Results: The methodology revealed a heterogenous pH microenvironment in the bone marrow (pH = 6.7 – 7.5). Additionally, the number of bone marrow autofluorescent cells that were co-labeled with F4/80 antibody revealed that a high percentage of autofluorescent cells express pan-macrophage markers. The acidic microenvironment was found in active bone remodeling sites that have been reported to support the expansion of healthy and leukemic cells (4) and was found surrounding a subpopulation of macrophages (Statistical analyses in progress).

Conclusion: Imaging is a powerful tool to investigate pH in the native bone marrow microenvironment (BMM). We attempted to investigate spatially distinct pH in the BMM, with emphasis on regions of acidic pH near M2 macrophages that are reported to form immune-protective niches in hematological malignancies. To further elucidate how interstitial pH modulates hematopoietic and immune functions, we are optimizing protocols to perform transcriptomic profiling in situ under image guidance as it is unlikely to preserve the pH microenvironment after tissue isolation. We have established protocols to preserve RNA quality in formalin fixed paraffin embedded (FFPE) histology slides and co-register them with 3D in vivo stacks based on vascular architecture, thus allowing subsequent analyses using GeoMx Digital Spatial Profiling and mechanistic studies of healthy and leukemic microenvironments.

References: 1) Wu, H, et al. (2019). 2) Icard P, et al. (2018). 3) Yeh, S-C et al. (2022). 4) Haase, C et al. (2022). 5) Weinhäuser, I et al. (2023).

**PAPER #66**

**TITLE:** Disparities in clinic visit no-show rates at a sports medicine orthopedic clinic

**PRESENTING AUTHOR:** Michaela Malin BA

**CO-AUTHOR(S):** Jonathan Minto MD, Patrick Castle MD, Andrew Jeong MD, William Zhuang BS, Kismat Touhid BS, Sandeep Mannava MD PhD

**LAB PI/MENTOR:** Sandeep Mannava MD PhD

**ABSTRACT**

Background:
Outpatient clinic no-shows are defined as visits that the patient did not attend with no advance notice and not due to physician or clinic cancellations. These include both in person and telehome visits. No-show rate is the number of no-shows a given clinician has out of the total visits scheduled in a given time period. Telehome visits may decrease this no-show rate, especially phone call visits, which utilize widely available technology and do not require internet access. The present study aims to evaluate the sociodemographic factors associated with no show rates and whether this rate varies with in-person or telehome modalities.

Methods:
Retrospective analysis included 1,999 patients seen by a single surgeon during a 6-month period from 9/5/22 to 3/27/23. The inclusion criteria were all patients seen either in person or via telehealth during this period, and exclusion criteria were any patients not seen in a clinic visit during this time. Patients were identified using electronic medical records. Relevant data was collected, including: date of visit, sex, race, ethnicity, age, smoking status, address of primary residence, reason for visit, laterality of injury, whether surgery was performed, date of surgery, procedures conducted, and date of follow-up visit. Descriptive statistical and regression analyses were conducted with chi-squared tests for categorical variables and Kruskal-Wallis for continuous variables.

Results:
A total of 1,797 in-person visits, and 202 telehome visits were included in the analysis. Comparisons between the two groups showed no significant difference in any of the demographic variables between the two groups. The no-show rate in the in-person cohort was 5.06% and 5.45% in the telehome cohort. In both visit types the no-show rate varied across racial groups, with black patients having a 3.7% ($p=0.034$) higher probability of not arriving for their appointment compared to white patients. Medicaid patients did not arrive at a 9.5% ($p < 0.001$) higher rate compared to patients covered by commercial insurance. Visits for patients ultimately received surgical intervention were 7% ($p<0.001$) less likely for the patient to not arrive compared to visits by patients who did not receive surgery. All other variables were not significantly different between no-show and completed clinic visits.

Conclusion:
Discontinuous care is harmful in post-operative recovery and negatively impacts non-surgical interventions and follow-up. Medicaid coverage is used as a proxy for lower socioeconomic status in this study. The higher no-show rate in this subgroup may be indicative of difficulty accessing transportation, childcare, or time off from work, which can all be disproportionate barriers to care for people with lower socioeconomic status. These findings also suggest that no- show rates are consistent across telehome and in-person visits. Future research would be beneficial into the difference in demographic variables between in person and telehome groups to determine if different factors may be influencing these rates. No-show rates are impactful on patient access to orthopaedic care and important for clinicians to identify methods to minimize them.

**PAPER #67**

**TITLE:** In vitro surrogate for vascularization to predict hydrogel mediated allograft healing in tissue engineered periosteum

**PRESENTING AUTHOR:** Alyson March

**CO-AUTHOR(S):** Darien Dennis, Yiming Li, Regine Choe, Danielle S. W. Benoit

**LAB PI/MENTOR:** Danielle S. W. Benoit and Regine Choe

**ABSTRACT**

Bone grafting procedures annually cost over $2.5 billion in the US, with allografts used in approximately one-third of these procedures. Although allografts remain the gold standard for treating critical-size bone defects, approximately 60% fail within ten years. Allograft failure is directly linked to the absence of periosteum, a highly vascularized tissue that promotes bone healing and host tissue recruitment through periosteal paracrine signaling. We have developed a tissue engineered periosteum (TEP) to improve allograft healing, using poly(ethylene glycol) (PEG) hydrogels with encapsulated mouse mesenchymal stem cells (mMSCs) and osteoprogenitor cells (mOPs) to mimic periosteal cell types and subsequent paracrine signaling. However, evaluating TEP efficacy requires in vivo studies, which are low throughput, costly, and time and resource-consuming. In previous studies, we have observed a positive correlation between bone graft vascularization and bone biomechanical strength, motivating our efforts to develop an angiogenic hydrogel to improve bone allograft healing. Therefore, in this work, in vitro surrogates for vascularization were investigated by leveraging a 3D endothelial cell spheroid sprouting assay to predict hydrogel-mediated vascularization in vivo. Spheroids were composed of human umbilical vein endothelial cells (HUVECs) and human mesenchymal stem cells (hMSCs), which act as pericyte-like cells. Hydrogels entrapping spheroids were formed via enzymatically-degradable (DL) or non-degradable (NDL) linkers and functionalized with the cell adhesive peptide RGD or a non-adhesive control RGE. Spheroid sprouting was evaluated using fluorescent microscopy and quantified using the ImageJ ‘Sprout Morphology’ plug-in. Data indicate that hydrogel degradation is necessary for cell sprouting in vitro, as both degradable hydrogels support sprouting over time. In addition, degradable hydrogels functionalized with RGD best supported total network formation overtime, indicating that both hydrogel degradation and RGD functionalization are necessary for cell sprouting in vitro. To further characterize the cell behavior, cell-secreted angiogenesis factors, or angiocrines, were evaluated over time. These data further support the need for hydrogel degradation, as degradable hydrogel groups demonstrated significantly higher secretion of vascular endothelial growth factor-A (VEGF-A) over time than non-degradable hydrogel. However, there was no significant difference observed between the DL RGD and DL RGE group for VEGF-A secretion, and other angiocrines, such as angiopoietin, did not show significant differences between all groups. Hydrogel promotion of bone allograft healing was then evaluated in vivo using our murine femur graft model. Allografts were modified with cell-laden hydrogels fabricated around the bone to mimic the periosteum and implanted into 10-12 week old female C57Bl6/J mice. Bone healing was evaluated at 3-, 6-, and 9-weeks post-implantation with microcomputed tomography (µCT), histology, and biomechanical analysis. At 9-weeks post-implantation, µCT results show a ~3-fold increase in bone callus for TEP-modified allografts compared to unmodified allografts, but no significant difference between hydrogel groups. However, at 9-weeks post-implantation, there is no statistically significant increase in biomechanical strength for TEP-allografts compared to allografts alone. On-going work aims to evaluate bone grafts with immunohistochemistry to evaluate microvasculature and bone formation. This study evaluates the correlations between in vitro cell response in hydrogels to in vivo allograft healing in a TEP system.

**PAPER #68**

**TITLE:** Identification of T cell exhaustion as a biomarker of Staphylococcus aureus chronic osteomyelitis in humanized mice

**PRESENTING AUTHOR:** Katya McDonald

**CO-AUTHOR(S):** Motoo Saito, Javier Rangel-Moreno, John Owen, Edward Schwarz, Stephen Kates, and Gowrishankar Muthukrishnan

**LAB PI/MENTOR:** Gowrishankar Muthukrishnan

**ABSTRACT**

Staphylococcus aureus, a significant human pathogen, continues to be the leading cause of implant-associated osteomyelitis including peri-prosthetic joint infections and fracture-related infections. It is broadly considered incurable due to recalcitrant biofilms and colonization of the osteocyte-lacuno canalicular network (OLCN) of cortical bone, which cannot be eradicated with standards of care short of amputation. However, it is also known that patients can resolve acute infections and live a full life with asymptomatic S. aureus osteomyelitis. Unfortunately, currently available diagnostics to guide conservative vs. aggressive surgical treatment options for patients are very limited. This led the 2018 International Consensus Meeting on Musculoskeletal Infection to conclude that developing a functional definition for acute vs. chronic osteomyelitis is the greatest priority in this field.

To this end, preclinical natural history studies evaluated transitions in host immunity and found that initial robust pro-inflammatory responses in the acute phase of infection transition from Th1 and Th17 to suppressive Treg adaptive immune responses over time. To account for human-specific S. aureus pathology, we developed a humanized mouse model of osteomyelitis and showed that the commencement of persistent osteomyelitis (14 days post-infection) occurs with large numbers of proliferating CD3+/Tbet+ adjacent to purulent abscesses in the bone marrow. This coincided with increased infection and osteolysis, suggesting that human T cell infiltration and proliferation in the bone do not aid bacterial clearance. Subsequent multi-omics studies in an improved humanized NSG-SGM3 BLT model revealed that: 1) human T cells are remarkably heterogenous in gene expression and numbers, and 2) immune checkpoint proteins are upregulated in Th1 and Th17 cells due to infection suggesting an exhaustion phenotype. Moreover, in a clinical pilot study, these proteins were upregulated in the serum of patients with chronic S. aureus osteomyelitis. Remarkably, increased levels of these immune checkpoint proteins were highly predictive of adverse outcomes such as arthrodesis, reinfection, amputation, and septic death in these patients. Our results indicate that T cell exhaustion could be a functional biomarker for persistent S. aureus osteomyelitis and treatment outcome.

**PAPER #69**

**TITLE:** StretchToC: a tendon-on-a-chip platform for studying the impact of mechanical forces in fibrotic adhesions

**PRESENTING AUTHOR:** Hayley Miller

**CO-AUTHOR(S):**

**LAB PI/MENTOR:** Hani Awad

**ABSTRACT**

INTRODUCTION: A common complication of zone II flexor tendon injuries is fibrotic adhesions, in which the tendon fuses to surrounding connective tissues due to the buildup of scar tissue. Prevalent in this process is the main regulator of fibrosis, Transforming Growth Factor-β1, and the downstream protein Plasminogen Activator Inhibitor-1 (PAI-1) [1]. It was previously found that PAI-1 knockout leads to reduced adhesion formation, but not when tendons were immobilized during the healing process. This suggests the importance of physical therapy in conjunction with biologic treatment [2]. The goal of this work is to tailor our pre-existing human tendon-on-a-chip (hToC) platform to include a stretching mechanic, allowing us to apply strain to embedded tissues and study the role of biomechanics in tendon adhesion. Few fabrication methods exist for such devices, with most being costly and time consuming. Therefore, we also aim to create a method by which millimeter-scale, stretchable layers with through-holes can be fabricated at a low barrier of entry.

METHODS: The layer-by-layer StretchToC platform consisted of a membrane containing pillar-like protrusions for anchoring cells. Outside these pillars were vacuum chambers that, once activated, stretched both the membrane and attached anchors. 3D finite element analysis (FEA) was performed to determine if the proposed design was capable of achieving physiological strains of up to 4% [3]. Physical prototypes were produced through a double-casting method. Briefly, physical replicas of each layer were produced by laser cutting acrylic sheets. Each layer was then adhered to the inside of a petri dish. A silicone mold making mix was poured into the dish until the acrylic was fully submersed. Once cured, the silicone negative was treated in an oxygen plasma chamber and exposed to 70% ethanol to create a secondary mold. Each secondary mold was then used to cast individual layers of the StretchToc device using polydimethylsiloxane (PDMS). The components were gently removed and bonded to subsequent layers via oxygen plasma treatment.

RESULTS: FEA yielded a device that stretched uniaxially when a negative pressure was applied to the interior boundaries of the vacuum chambers. A simulated collagen matrix embedded around the pillars showcased strains of up to 30% when utilizing the maximum vacuum pressure attainable by the pump system (-0.08 MPa). The proposed PDMS double-casting method was capable of producing thin (1/16'') layers with feature sizes as small as 1 mm. All materials utilized in the procedure were readily available in the lab or easily obtained. Each secondary mold of the device was capable of being produced within a single work day, and in tandem with the other layers.

DISCUSSION: Each stretchable hToc device maintains the same footprint as our pre-existing static systems, allowing for high throughput analysis of in vitro tendon structures with the novel incorporation of uniaxial strain. Modeling confirms that the design is capable of producing strains within the physiological range without failure. The PDMS-double casting method was successful in rapidly creating StretchToC layers at a low cost. Future incorporation of tenocytes into these systems will unveil the role of mechanical forces in a model of fibrosis, including under potential pharmacologic conditions.

REFERENCES: [1] Farhat, Y., et al., J. Cell. Physiol., 2014. [2] Farhat, Y., PhD Dissertation, 2015. [3] Latash, M. & Zatskiorsky, V., Biomechanics and Motor Control, 2016.

**PAPER #70**

**TITLE:** A novel adoptive dendritic cell targeting delivery of TNF combined with an IAP antagonist to treat breast cancer

**PRESENTING AUTHOR:** Philip Milton

**CO-AUTHOR(S):** Rong Duan, Jun Wu, Xin Liu, Zhenqiang Yao

**LAB PI/MENTOR:** Zhenqiang Yao

**ABSTRACT**

Inhibitor of apoptosis proteins (IAPs) restrain caspase-mediated apoptosis. The IAP antagonist, SM-164, which efficiently degrades IAPs, does not kill cancer cells, but we found that it enabled TNFα to strongly induce breast cancer (BC) cell apoptosis in vitro, and combined with TNFα it significantly reduced the % of leg bones with metastases from heart-injected MDA-MB-231 BC cells in a mouse model (40% vs 88% in vehicle, $p<0.01$). SM-164 alone or a standard chemotherapy (SCT) regimen reduced tumor burden in bone, but not the % of bones with metastases. However, SM-164+TNFα more effectively reduced tumor burden in bone than SM-164 or SCT. Treatment of mice inoculated with MDA-MB-231 cells with a TNF antibody or with clodronate, which depletes macrophages, reduced the inhibitory effect of SM-164 on tumor growth in bone, and clodronate inhibited osteolysis. These findings suggest that TNFα+SM-164 could be an effective therapy to reduce BC bone metastasis. However, systemically administrated TNFα can have serious side effects. Targeted delivery of TNFα+SM-164 would be a promising approach to treat BC. Mucin1, a surface glycoprotein on epithelial cells, is highly expressed on the surface of all BC cells. We induced and expanded dendritic cells (DCs) from human peripheral blood using M-CSF and GM-CSF and engineered them to express TNFα and chimeric CD66b-Mucin1 scFv, which was constructed by linking Mucin1 monoclonal Ab scFv to the extracellular domain of a truncated portion of myeloid cell receptor, CD66b, to target BC. We called these novel engineered DCs Mucin1-directed DCs producing TNFα (M-DCsTNF). Conditioned medium from M-DCsTNF (contains 300 pg/ml TNFα) strongly induced MDA-MB-231 cell death in the presence of SM-164 in vitro; this was blocked by a TNF Ab. Specific binding of M-DCsTNF to MDA-MB-231 cells was confirmed in bones in NSG mice. Importantly, SM-164 given with a one-time injection of M-DCsTNF significantly reduced the growth of human BC from orthotopically-injected Her2+ BT474 BC cells (median tumor wt. 6.25 vs. 98.4 mg in vehicle, $p<0.01$) and patient-derived xenograft (PDX) of triple-negative BC (tumor wt. 0.78+/-0.42 vs. 1.56+/-0.82 g in vehicle, $p<0.05$) in NSG mice. In contrast, SM164 alone did not inhibit BC growth in the PDX model. Our findings suggest that an adoptive cell targeted delivery of TNFα to BC deposits combined with SM-164 may be a novel effective approach to treat breast cancer.

**PAPER #71**

**TITLE:** Characterizing the Achilles tendon mechanoresponse to voluntary wheel running

**PRESENTING AUTHOR:** Samantha Muscat

**CO-AUTHOR(S):** Nolan Sparks, Elsa Lecaj

**LAB PI/MENTOR:** Anne Nichols

**ABSTRACT**

Tendons act as a mechanosensitive bridge that transmit contractile muscle forces to bone that enable movement and maintenance of body posture. While mechanical force is critical to maintaining tendon homeostasis, chronic or repetitive loading puts tendons at risk for tendinopathy and over-use injuries. Previous studies implicate tenocytes as the main facilitators of mechanotransduction, however the cellular mechanisms underpinning this process and how the subsequent tissue-level adaptive or maladaptive mechanoresponse is mediated remain unknown. The goal of the present study was to evaluate voluntary wheel running (VWR) as a model of physiological mechanical load that could be used to identify possible candidates regulating both tendon homeostasis and damage in response to load. Individually housed 10-week-old male C57BL/6J mice were allowed to freely run on the open surface of a slanted plastic saucer shaped wheel inside the mouse cage for 8 or 12 weeks. Control mice were placed in cages with a locked wheel. After 8 and 12 weeks (n=7 per timepoint and exercise regimen), Achilles tendons were isolated, homogenized and total RNA was isolated for bulk-RNA sequencing. Significantly upregulated and downregulated differentially expressed genes were entered into the Database for Annotation, Visualization, and Integrated Discovery (DAVID) for gene ontology analysis. Over the course of the experiment, the 8-week VWR cohort averaged a total run distance of 783.09± 49.0 km and the 12-week VWR cohort averaged a total run distance of 1111.0 ± 131.1 km. VWR mice displayed distinct transcriptional shifts at both 8 and 12 weeks: After 8 weeks of running, 24 genes were upregulated, and 22 genes were downregulated, relative to sedentary controls. After 12 weeks of running, 97 genes were upregulated and 139 genes were downregulated, relative to sedentary controls. GO analysis of DEGs revealed that after 8 weeks of running, VWR Achilles tendons upregulate pathways relating to morphogenesis, embryogenesis and cell adhesion processes,suggesting a developmentally directed adaptation process. No significantly enriched downregulated pathways were observed. By 12 weeks, Achilles tendons shift their transcriptional response to loading: In contrast to the 8 week VWR cohort, processes involving morphogenesis, development and matrix remodeling were downregulated in 12 week VWR mice relative to sedentary controls. Upregulated GO terms include metabolic processes. Together, these results suggest that after 12 weeks of running, VWR Achilles tendons upregulate metabolism related mechanisms to regulate available energy and potentially adjusts towards a homeostatic adaptive response. Numerous studies have implicated tenocytes as the mechanosensitive intermediary in tendon, but little is known about exactly how tendons translate mechanical signals into a tissue-level adaptive response. The results of our study suggest that in response to mechanical loading, the Achilles tendon promotes adaptation via developmentally guided processes after 8 weeks but downregulates similar mechanisms after 12 weeks of physiological load. This may suggest that 8 weeks of mechanical loading is sufficient to promote morphogenesis and drive anabolic adaptation, but after 12 weeks of loading, these processes potentially shift toward a new homeostatic state, indicating homeostatic adaptation by downregulating developmental processes. Together,this suggests that a switch between adaptive anabolic growth and adaptive homeostasis may occur between 8 and 12 weeks of physiological loading. Ongoing functional, structural, and morphological studies will shed light on how these transcriptional responses to VWR affect overall tendon behavior. Ultimately, the goal of future studies will be to use this model to parse out the complex mechanotransduction network that allow tenocytes to coordinate a tissue-level adaptive response.

**PAPER #72**

**TITLE:** High Levels of MSC Efferocytosis Cause Myeloid Skewing

**PRESENTING AUTHOR:** Swachi H. Patel

**CO-AUTHOR(S):** Emily R. Quarato, Yuko Kawano, Noah A. Salama, Ronald Lakony

**LAB PI/MENTOR:** Laura M. Calvi

**ABSTRACT**

Bone marrow mesenchymal stromal/stem cell (MSC) dysfunction impacts not only age-induced bone loss but also dysfunction of the hematopoietic stem cell (HSC) niche in hematologic malignancies like myelodysplastic syndromes (MDS). MDS is a myeloid neoplasm seen primarily in older individuals where the bone marrow produces immature or dysfunctional blood cells resulting in a significant decline of normal mature blood cell production and accumulation of apoptotic cells. MDS is characterized by myeloid skewing and increased risk of transformation to acute myeloid leukemia. We previously demonstrated that in aging, bone marrow-derived macrophages become deficient in their ability to clear apoptotic cells, a process known as efferocytosis, during aging and in MDS. While macrophages act as the primary phagocytic cells of the bone marrow, we have shown that MSCs can contribute to the clearance of apoptotic cells in the bone marrow, which increases with aging. We have previously shown that increased efferocytic activity impacts MSCs' ability to differentiate into bone; however, it is unknown whether efferocytic activity impacts MSCs' ability to support HSCs. Thus, we hypothesized that efferocytic MSCs will not be able to properly support HSC maintenance. To test whether efferocytic MSCs can support HSCs, we induced efferocytosis in vitro and then tested the ability of MSCs to support hematopoietic colony forming unit cell (CFU-C) assay, a measure of hematopoietic stem and progenitor cells. We found that efferocytic MSCs had decreased CFU-C counts compared to non-efferocytic controls which further declined with aging. To determine the impact of high levels of efferocytosis on HSC support in vivo, we developed a mouse model (PrxCrexBai1) which enhances efferocytosis by introducing a new efferocytic receptor specifically in MSCs. We confirmed functionally in vitro that the PrxCrexBai1 model increased MSC efferocytic function (70% vs. 85%). Using flow cytometry analysis on isolated bone marrow, we found that PrxCrexBai1 mice had increased myeloid progenitors (common myeloid progenitors and granulocyte-monocyte progenitors) and short-term HSCs compared to their wild-type controls. This data suggests skewing of the myeloid lineage in mice 12 months of age. Furthermore, complete blood count (CBC) analysis of the peripheral blood found that there was a significant increase in monocytes at 12 months. Collectively, our data supports the idea that during high levels of MSC efferocytosis, myeloid skewing is prevalent. Therefore, increased efferocytosis may preferentially support and could potentially accelerate the development of myeloid malignancies such as MDS. Taken together, we have demonstrated that MSC efferocytosis impacts both bone health and immune support, suggesting that inhibiting MSC efferocytosis may have novel clinical impacts in the treatment of diseases of aging such as MDS.

**PAPER #73**

**TITLE:** The Effect of Racial and Economic Inequity on Complication Rates and Patient-Reported Outcomes Following ORIF of Humeral Shaft Fractures

**PRESENTING AUTHOR:** Urvi J. Patel, MD, MS

**CO-AUTHOR(S):** Melissa R. Holloway, BS, Thomas J. Carroll, MD, Sandeep Soin, MD

**LAB PI/MENTOR:** John P. Ketz, MD

**ABSTRACT**

Background: The purpose of this study was to investigate the role between racial and economic inequity and orthopaedic trauma as determined by the Area Deprivation Index (ADI) on radiographic fracture healing, complication rates and patient-reported outcomes following open reduction and internal fixation (ORIF) of humeral shaft fractures.

Material and Methods: We retrospectively reviewed patients who underwent ORIF of humeral shaft fractures at our Level-I trauma center. The Area Deprivation Index, a comprehensive metric of socioeconomic status, education, income, employment, and housing quality, was used to stratify patients into four quartiles. Statistical analysis was performed on most deprived (top 75thile) and least deprived (bottom 25thile) ADI quartiles. Statistical significance was set at a p-value of $< 0.05$.

Results: A total of 98 patients met the inclusion criteria. The most deprived cohort had 2.29 greater odds of experiencing a post- operative complication (P=0.04). The average arc of elbow motion in the most deprived group was 107±43 degrees versus 135±28 degrees in the least deprived cohort (P=0.04). PROMIS Pain Interference (PI) and Depression (D) scores were higher in the most deprived group as compared to the least deprived group [(64.57±6.9 vs. 55.30±7.6); p<0.01) and (55.90±11.9 vs. 48.35±8.4; P=0.01), respectively]. PROMIS Physical Function (PF) scores were higher in the least deprived group as compared to the most deprived group (40.32±6.3 vs. 35.86±5.3; p<0.01). Patients in the most deprived group were three times more likely to miss a scheduled provider appointment within the first post-operative year than those in the least deprived cohort (n=13 vs. n=n=38; p<0.01), resulting in a no-show rate that was three times greater than the least deprived group (0.31±0.24 vs. 0.09±0.17; p<0.01).

Conclusion: Patients facing greater SDOH had greater odds of post-operative complications, greater post-operative missed appointments, and decreased PROMIS PF scores. Further investigation is warranted to assess the role of racial and economic inequity on access and compliance with follow up, physical therapy and factors affecting post-operative rehabilitation.

**PAPER #74**

**TITLE:** Role of PD-1 in B cell dysregulation in autoimmunity

**PRESENTING AUTHOR:** Melanie Perkins

**CO-AUTHOR(S):** Jennifer Anolik, M.D., Ph.D. and Lisa DeLouise, Ph.D.

**LAB PI/MENTOR:** Jennifer Anolik, M.D., Ph.D.

**ABSTRACT**

Lupus is a prototypical systemic autoimmune disease in which both genetic and environmental factors are implicated. It is well described that exposure to ultraviolet radiation via sunlight, known to activate the aryl hydrocarbon receptor (AhR), can trigger both development and worsening of disease. Additionally, a correlation between the development of lupus and exposure to environmental pollutants known to act as AhR agonists has been observed in previous studies in human populations. Abnormalities in both the innate and adaptive immune system contribute to lupus pathogenesis. In lupus, the B cell compartment is dysregulated, resulting in the generation of autoreactive antibodies and the production of proinflammatory cytokines. This project focuses on whether pathways that normally provide dampening signals to the B cell compartment are abnormal in lupus. One such negative regulatory molecule is the programmed cell death 1 receptor (PD-1), well described to have an inhibitory role in T cells. The expression and function of PD-1 in B cells is less understood. A role for PD-1 in autoimmunity is supported by data demonstrating that PD-1 deficient mice develop lupus-like disease and patients treated with checkpoint inhibitors which block PD-1 signaling can develop autoimmunity. In preliminary data, increased expression of PD-1 was observed in a novel population of B cells previously shown to be expanded in lupus, age-/autoimmune-associated B cells (ABCs). We hypothesize that PD-1 will normally inhibit pro-inflammatory B cell functions, but this will be dysregulated in lupus and driven by exposure to environmental factors. To test this hypothesis, we will utilize in vitro models focusing on B cells isolated from healthy and lupus human peripheral blood. Previously validated flow cytometry techniques will be used to characterize the expression of the PD-1 receptor as well as its ligands, PD-L1 and PD-L2, in B cells. Additionally, we seek to define the effects of PD-1 agonists and antagonists on B cell function in vitro. Future directions include examining the effect of the AhR pathway on PD-1 expressing B cell function, to further examine the effect of exposure to environmental toxicants on B cell function.

**PAPER #75**

**TITLE:** Leveraging a Poly(ethylene glycol) (PEG) biomaterial to guide tenocyte fate

**PRESENTING AUTHOR:** Tiffany-Rae Robinson

**CO-AUTHOR(S):**

**LAB PI/MENTOR:** Alayna Loiselle & Danielle Benoit

**ABSTRACT**

Tendon injuries represent a large clinical burden with 300,000 repair procedures performed annually in the United States. Unsatisfactory outcomes of surgical tendon repair are due to the pathological, scar-mediated manner in which tendons heal, often resulting in impaired restoration of mechanical properties. Yet, how tendon resident fibroblasts (tenocytes) shift the balance from a fibrotic healing response to an enhanced healing remains elusive. Biomaterials have the potential to guide cell fate and behavior by incorporating niche biophysical and biochemical cues. Here, I hypothesize that an engineered extra cellular matrix (eECM) can guide tenocyte phenotype and function towards enhanced healing. Our lab has developed an 8-arm (20kDa) Poly(ethylene glycol) (PEG) platform that is highly tunable through the incorporation of unique peptide epitopes. Peptide epitopes act as either cell adhesive peptides for cell-matrix interactions or as crosslinkers forming the hydrogel network. Therefore, biophysical and biochemical cues can be modulated by altering the type, the amount, and combination of peptide epitopes present within the eECM. This work examines how crosslinker type can influence tenocyte behavior in a PEG hydrogel. Biophysical cues such as stiffness and mesh size can be controlled by altering the PEG wt% or crosslinking % of the eECM, where an increase in either design parameter leads to an increase in stiffness. In a preliminary study (n=2), primary tenocytes (500,000 cells/mL) were encapsulated into soft (~6.5kPa) and stiff (~17.5kPa) hydrogels with 80% crosslinking. At day 11 post encapsulation, the soft hydrogels maintained >90% viability whereas the stiff hydrogels had <5% viability. Therefore, hydrogel design should target a softer modulus (<10kPa) to support tenocyte viability in vitro. Equally important as viability is the ability of the tenocytes to remodel and degrade the eECM. The eECM can be formed with matrix metalloproteinase (MMP) degradable or non-degradable (ND) crosslinkers. To determine the importance of eECM degradability, NIH 3T3 fibroblasts were encapsulated in hydrogels with 80% crosslinking and 2mM RGD (GCGRGDSG) cell adhesive peptide. Cell spreading was analyzed at days 3- and 10- post encapsulation via confocal microscopy (40X) with dapi and phalloidin (Alexa Fluor 568) staining. Fibroblast cell spreading appeared as early as day 3-post encapsulation in hydrogels that contained an MMP degradable crosslinker. Yet, in hydrogels that contained a ND crosslinker cells remained round at day 10-post encapsulation. Data indicated that fibroblasts favor MMP degradable crosslinkers. In the literature, there are different types of MMP degradable crosslinkers that are susceptible to different MMPs as well as have different susceptibility rates. Now, ongoing work aims to evaluate tenocyte spreading by examining three independent MMP degradable crosslinkers (GKKC-GPQG↓IWGQ-CKKG [7367/Ms], GKKC-IPES↓LRAG-CKKG [22,000/Ms], GKKC-VPLS↓LYSG-CKKG [43,500/Ms]) that have different susceptibility rates to MMP2, MMP9, and MMP14. Overall, this work has begun to identify design criteria of an eECM that supports tenocyte viability and spreading. Future studies will continue to refine the biophysical and biochemical cues present within the eECM to guide tenocyte phenotype and functions towards enhanced healing.

**PAPER #76**

**TITLE:** Postoperative Complications of the Hand Following Shoulder Surgery

**PRESENTING AUTHOR:** Andrew Rodenhouse, MD

**CO-AUTHOR(S):** Akhil Dondapati, MD, Thomas Carroll, MD, Constantinos Ketonis, MD, PhD

**LAB PI/MENTOR:** Constantinos Ketonis, MD, PhD

**ABSTRACT**

Hypothesis and/or Background
Shoulder arthroscopy and arthroplasty are increasingly common procedures utilized to address shoulder pathologies. This study sought to evaluate the incidence of hand-related complications, including carpal tunnel syndrome, cubital tunnel syndrome, trigger finger, de Quervain's tenosynovitis, and Dupuytren's disease following shoulder arthroscopy and arthroplasty procedures. We hypothesized that patients undergoing shoulder surgery would have a higher incidence of hand-related complications within one year of surgery compared to controls.

Methods
This was a retrospective analysis of 12,179 patients who underwent shoulder arthroscopy or arthroplasty procedures that were subsequently diagnosed with carpal tunnel syndrome, cubital tunnel syndrome, trigger finger, de Quervain's tenosynovitis, or Dupuytren's disease within one year postoperatively. Relative risk of developing associated hand pathologies following shoulder surgery was compared to controls.

Results
In total, 10,285 patients underwent shoulder arthroscopy procedures during this period, of whom 815 (7.9%) developed an associated hand pathology within one year from their shoulder procedure. Arthroscopic surgery was associated with an increased risk of developing carpal tunnel syndrome (RR 1.57; 95% CI [1.42-1.73]), cubital tunnel syndrome (RR 2.25; 95% CI [1.94-2.61]), trigger finger (RR 1.76; 95% CI [1.53-2.03]), and Dupuytren's disease (RR 2.02; 95% CI [1.54-2.65]), but was not associated with a higher risk of developing de Quervain's tenosynovitis. In total, 1,894 patients underwent shoulder arthroplasty procedures during this period, of whom 188 (9.9%) developed an associated hand pathology within one year. Shoulder arthroplasty was associated with an increased risk of developing carpal tunnel syndrome (RR 2.10; 95% CI [1.72-2.57]), cubital tunnel syndrome (RR 3.29; 95% CI [2.48-4.39]), and trigger finger (RR 1.99; 95% CI [1.47-2.70]), but was not associated with an increased risk of developing de Quervain's tenosynovitis or Dupuytren's disease.

Conclusion
Shoulder arthroscopy and arthroplasty procedures were associated with an increased risk of developing carpal tunnel syndrome, cubital tunnel syndrome, and trigger finger within one year of surgery. Only shoulder arthroscopy procedures were associated with a higher risk of developing Dupuytren's disease. Neither shoulder arthroscopy nor arthroplasty procedures were associated with an increased risk of developing de Quervain's tenosynovitis.

**PAPER #77**

**TITLE:** Association of Medicare Merit-Based Incentive Payment System Quality Scores with Unplanned Hospital Visits after Outpatient Orthopedic Surgery

**PRESENTING AUTHOR:** Derek T. Schloemann, MD, MPHS

**CO-AUTHOR(S):** Danielle M. Wilbur, MD, Paul T. Rubery, MD, Caroline P. Thirukumaran, MBBS, MHA, PhD

**LAB PI/MENTOR:** Caroline P. Thirukumaran, MBBS, MHA, PhD

**ABSTRACT**

Background:
The Medicare Merit-Based Incentive Payment System (MIPS) ties reimbursement incentives to clinician performance with the aim of improving healthcare quality. It is unclear whether the MIPS quality score can accurately distinguish between high- and low-performing clinicians. Our objective was to examine whether surgeon MIPS quality scores were associated with unplanned hospital visits following outpatient orthopedic surgery.
Methods:
We included 37,735 outpatient orthopedic surgical encounters among Medicare beneficiaries in New York State from 2018-2019. Our key independent variable was MIPS quality score percentile (0-19th, 20-39th, 40-59th, or 60-100th). Our main outcome measures were 7-, 30-, and 90-day unplanned hospital visits after outpatient orthopedic surgery.
Results:
For the 37,735 outpatient orthopedic surgeries included in our study, mean (standard deviation) age of patients was 73.18 (6.46) years, 31,550 (83.6%) were White, and 22,071 (58.5%) were women. When compared to patients undergoing surgery with a surgeon in the 0-19th percentile of MIPS quality score (lowest quality score), the adjusted rate of postoperative unplanned hospital visits was lower at 7, 30, and 90 days for patients undergoing surgery with a surgeon in the 20-39th or 40-59th percentile of MIPS quality score (e.g., 0.71% points lower, 95%CI -1.19 to -0.23%, P=0.003 for 20-39th percentile at 7 days;0.48% points lower, 95%CI -0.97 to 0.01, P=0.046 for 40-59th percentile at 7 days).
Conclusions:
Higher MIPS quality scores were modestly associated with lower rates of unplanned hospital visits after outpatient orthopedic surgery, indicating that the reimbursement adjustments associated with these scores may be modestly aligning incentives among key stakeholders and differentiating between high- and low-performing clinicians.

**PAPER #78**

**TITLE:** Association of Patient, Surgeon, and Facility Factors with Unplanned Hospital Visits after Outpatient Orthopedic Surgery

**PRESENTING AUTHOR:** Derek T. Schloemann, MD, MPHS

**CO-AUTHOR(S):** Danielle M. Wilbur, MD, Paul T. Rubery, MD, Caroline P. Thirukumaran, MBBS, MHA, PhD

**LAB PI/MENTOR:** Caroline P. Thirukumaran, MBBS, MHA, PhD

**ABSTRACT**

Background:
Unplanned hospital visits following outpatient surgery are an important marker of healthcare quality. Unplanned hospital visits are costly, with average charges for these encounters as high as $1,869 for pain-related visits and $12,000 for non-pain-related visits. Surgeons and surgical facilities may be unaware of hospital visits as patients may present to emergency departments at other institutions, making it difficult to understand what factors may make patients more or less likely to present to hospitals after surgery. Our objective was to evaluate the association of patient, surgeon, and facility factors with unplanned hospital visits within 7, 30, and 90 days following outpatient orthopedic surgery.
Methods:
We included outpatient orthopedic surgical procedures performed in HOPDs and ASCs in the New York Statewide Planning and Research Cooperative System (SPARCS) database from 2018-2019. We used Medicare's algorithm to determine whether admissions were planned vs. unplanned based on diagnoses and procedures performed during postoperative hospital visits. We estimated multivariable logistic regression models to examine the association of postoperative unplanned visits with patient, facility, and surgeon characteristics.
Results:
There were 476,654 outpatient orthopedic surgeries included in our study. The mean (standard deviation) age was 51.92 (15.82) years, 309,563 (64.9%) were White, 250,400 (52.5%) were women, and 214,438 (45.0%) had private insurance. There were 7,351 (1.5%), 9,703 (2.0%), and 12,967 (2.7%) who had an unplanned hospital visit within 7, 30, or 90 days. ED visits were the most common unplanned visits, representing 97.1%, 95.9%, and 94.2% of unplanned hospital visits within 7, 30, and 90 days, respectively.
After controlling for covariates and facility random effects, and compared with their respective counterparts, the odds of unplanned hospital visits within 7 days of outpatient orthopaedic surgery were higher for racial and ethnic minority patients (e.g. odds ratio for Hispanic [OR] 1.11, 95% confidence interval [CI] 1.02 to 1.21, P=0.02), patients covered by Workers' Compensation (OR 1.17, 95%CI 1.04 to 1.31, P=0.006), self-pay patients (OR 1.66, 95%CI 1.48 to 1.86), and undergoing surgery with a lower volume surgeon (e.g. OR 4.76, 95%CI 4.17 to 5.44, P<0.001 for fourth [lowest] relative to first [highest] quartile). Facility volume was not associated with unplanned hospital visits within seven days. Women gender (OR 0.91, 95%CI 0.86 to 0.96, P<0.001) and undergoing surgery in an ASC (OR 0.22, 95%CI 0.14 to 0.33, P<0.001) were associated with lower odds of postoperative unplanned hospital visits within seven days. Similar results were found for unplanned hospital visits within 30 or 90 days, with the exception being that Workers' Compensation insurance was not associated with unplanned hospital visits at these later time points.
Conclusions:
Postoperative unplanned hospital visits are frequently seen after outpatient orthopedic surgery and represent a substantial cost to payers, patients, and healthcare systems. We found that a number of patient-, surgeon-, and facility-level variables were associated with unplanned hospital visits after outpatient orthopedic surgery. Patients, payers, and facilities may seek out higher volume surgeons to reduce risk for postoperative healthcare utilization. Stakeholders can use this information to better understand the risk for postoperative healthcare utilization following outpatient orthopedic surgery and potentially design interventions to improve patient outcomes and healthcare quality.

**PAPER #79**

**TITLE:** Association of New York's opioid prescribing restrictions with opioid fills following total hip and knee arthroplasty

**PRESENTING AUTHOR:** Derek Schloemann, MD, MPHS

**CO-AUTHOR(S):** Benjamin Ricciardi, MD; Meredith Rosenthal, PhD; Jalpa Doshi, PhD; Kevin Fiscella, MD, MPH; Caroline Thirukumaran, MBBS, MHA, PhD

**LAB PI/MENTOR:** Caroline Thirukumaran, MBBS, MHA, PhD

**ABSTRACT**

Introduction
New York (NY) implemented Section 3331 in July 2016 to limit the prescription of opioids for acute pain to 7 days. Our objective is to examine the association of Section 3331 with the likelihood of opioid fills in the post-total hip/knee arthroplasty (THA/TKA) period for Medicare beneficiaries.

Methods
We used 2014-2019 national Medicare data to identify patients who underwent THA/TKA in NY (treatment group) and California ([CA]; control group-CA did not have a similar opioid restriction legislation). Outcomes were one or more opioid fills in the 15 days before admission to 7 days after discharge ("7-day"), 8 to 30-days after discharge, and 31 to 90 days after discharge. Key independent variables were state (NY/CA), phase (before[2014-2015] or after[2017-2019] Section 3331 implementation), and their interactions. We estimated multivariable hierarchical linear probability models with difference-in-differences (a method for policy evaluation). All models controlled for patient- and hospital-level covariates, and hospital-level random effects.

Results
For 71,565 encounters, the mean age (standard deviation) was 73.77 (5.56) years, 61.55% were female, 94.50% were White, and 8.15% were dually-eligible for Medicare and Medicaid. On multivariable analysis and before Section 3331, opioid fill rates in 7-, 8-to-30- and 31-to-90-day periods were 88.68%, 38.01%, and 29.10% in NY. With Section 3331 implementation, opioid fill rates in the 7-day period increased by 2.74%-points in NY (95% Confidence Interval [CI]: 1.29% to 4.18%, $p<0.001$), whereas the rate decreased by 6.47%-points in CA (95% CI: -7.55% to -5.39%, $p<0.001$) during the same period. Hence, Section 3331-associated increase in the likelihood of opioid fills in NY was 9.21%-points higher than in CA (95% CI: 7.50 to 10.91, $p<0.001$). In the later post-THA/TKA period, trends in NY were not different from those in CA.

Conclusion
NY's Section 3331 was associated with a significant increase in opioid fills in the immediate post-THA/TKA period. Because Section 3331 restricts opioid prescribing to 7 days, higher-than-average opioid prescriptions are being filled during this period. This is an unintended consequence of Section 3331 and needs to be carefully examined to prevent misuse.

**PAPER #80**

**TITLE:** Pharmacological Modulation of Extrinsic Macrophage Recruitment to Facilitate Regenerative Tendon Healing

**PRESENTING AUTHOR:** Gilbert Smolyak

**CO-AUTHOR(S):** Andrew Rodenhouse, Alayna Loiselle

**LAB PI/MENTOR:** Alayna Loiselle

**ABSTRACT**

Introduction: Flexor tendon (FT) injuries of the hand are common and functional restoration after surgical repair represents a challenge. Fibrosis of the healing tendon after repair results in a significant clinical burden and unsatisfactory outcomes. Macrophages have been identified as a potential driver of peritendinous scar formation, and recruitment of circulating monocytes/ macrophages is driven in large part by elevated CCL2 levels at the site of injury, resulting in homing of CCR2+ cells to the healing tendon. Genetic deletion of CCR2 blunts the extrinsic macrophage response to tendon injury, which in turn blunted the myofibroblast response and impaired the healing response. However, this approach was limited by the constitutive loss of CCR2. As such, we hypothesize that using a pharmacological CCR2 antagonist to block CCR2-mediated monocyte/macrophage recruitment in a time-dependent manner will facilitate enhanced healing by blunting the pro-fibrotic feedback loop that typically leads to the formation of a pathologic fibrovascular scar. In addition, this approach will facilitate the delineation between the circulating and tendon-resident CCR2+ populations.

Methods: C57Bl/6J mice will be obtained from Jackson Laboratories and will undergo complete transection and surgical repair of the flexor digitorum longus tendon. Mice will be treated with either the CCR2 antagonist RS102895, or vehicle. Two different treatment regimens, encompassing either the late inflammatory/early proliferative phase of healing, or continuous treatment. Tissue from the tendon repair as well as the contralateral paw will be harvested on post-operative day (POD) 14 for histological and biomechanical analysis. Histological studies will be used to determine the relative levels of CCR2 positive macrophages recruited to the site of injury, morphological assessment, and scar volume of the healing tissue will be conducted. Biomechanical studies will be done in the form of tendon gliding analysis as well as force to tendon rupture to determine the integrity of the repair. All procedures completed in compliance with our UCAR approved protocol.

Anticipated Results: We hypothesize that inhibition of CCR2+ macrophage recruitment will reduce the formation of pathological scaring throughout the healing process. Therefore, we anticipate that there will be reduced volume of scar tissue site of the repair. Tendon gliding studies are anticipated to show increased or similar range of motion to control mice, though, the force to rupture may be lower in treated mice depending on the time point group they are assigned to.

Conclusions: Should the results be congruent with what is anticipated then we can conclude that the CCR2 inhibitor does limit the ability of CCR2 positive macrophages to be recruited to the site of injury. These results would also highlight the different roles of resident macrophages in comparison to recruited peripheral macrophages.

**PAPER #81**

**TITLE:** Optimization of an In Vitro Model of Staphylococcal Abscess Communities to Study Bactericidal Mechanisms

**PRESENTING AUTHOR:** Levy A. Sominsky

**CO-AUTHOR(S):** Karen L. de Mesy Bentley, Youliang Ren, Gowrishankar Muthukrishnan, Chao Xie

**LAB PI/MENTOR:** Edward M. Schwarz

**ABSTRACT**

Staphylococcus aureus, the primary pathogen in bone infections, possesses unique abilities to evade antibiotics. For example, S. aureus forms abscesses within bone marrow or surrounding soft tissue, known as Staphylococcal abscess communities (SACs) (1), which protect the bacteria from antibiotics and host immunity via a fibrin pseudocapsule. While vancomycin, the standard for MRSA infections, is ineffective against SACs, previous studies demonstrate that sitafloxacin, a 2nd-generation fluoroquinolone clinically used in Japan, can kill S. aureus inside SACs in vivo with degradation of the encasing fibrin ring (2). Here, we adapt a previously described in vitro SAC model (3) to compare the efficacy of sitafloxacin vs. vancomycin, and to elucidate sitafloxacin's indirect effects on the fibrin pseudocapsule.

In vitro SACs were grown using S. aureus JAR 06.01.31 as previously described (3) and were overlaid with human serum, serum supplemented with fibrinogen, or plasma. After 24 hours, mature SACs were embedded within 100% epoxy resin, from which 1-micron sections were stained with Toluidine blue to identify the location of SACs within the gel for subsequent thin sectioning at 70 nm and imaging with Hitachi 7650 TEM. In parallel, 5-micron frozen sections were stained with H&E. For antibiotic treatments, mature SACs were overlaid with sitafloxacin and vancomycin at 100x and 1000x their minimum inhibitory concentration (MIC) for 24 hours, after which they were either processed for TEM or homogenized, sonicated, and enumerated for CFUs. Analysis was performed using one-way ANOVA with Tukey's multiple comparisons test ($p<0.05$ considered significant).

While serum alone supported bacterial growth, SACs formed within the gel did not possess a fibrin pseudocapsule. In contrast, SACs grown with serum and fibrinogen had a dense fibrin ring that encased the bacterial community. Heparinized plasma similarly induced pseudocapsule formation, although it did not appear as dense under TEM. To determine if antimicrobial efficacy could be compared within our model, plasma-grown SACs were overlaid with sitafloxacin or vancomycin diluted to 100x or 1000x their relative MIC. At 100x the MIC, only sitafloxacin significantly reduced the total CFUs from each gel, with vancomycin only displaying similar activity at 1000x its MIC. Morphologically, SACs treated with sitafloxacin at 1000x the MIC had degeneration of the pseudocapsule, in addition to antibiotic-killed bacteria, characterized by cell wall remnants and vacuole formation. In contrast, the pseudocapsule of vancomycin-treated SACs remained intact, with little evidence of antibiotic-induced death.

With the current standard of care, vancomycin, having limited efficacy against SACs both in vivo and in vitro, understanding how sitafloxacin kills bacteria within SACs and disrupts the encasing fibrin can improve treatment for bone infection. Since sitafloxacin cannot directly degrade the fibrin ring, it must influence the structure by acting on the encased bacteria. The accessory gene regulator (agr) of S. aureus typically favors dissemination from the SAC once local nutrients are depleted by inducing the secretion of staphylokinase, which activates plasmin to degrade the pseudocapsule. We believe that sitafloxacin uniquely acts on this pathway, leading to digestion of the fibrin ring. In future studies, we will utilize our in vitro model to perform bulk RNA sequencing over the lethal time course of sitafloxacin to define how sitafloxacin activates agr and, in turn, disrupts the fibrin pseudocapsule. This work will delineate mechanisms by which antibiotics influence the structure of the fibrin pseudocapsule that encases SACs, and serves as a screening tool for novel antimicrobials that kill SACs to improve therapy for bone infection.

REFS: 1) Cheng et al. FASEB J 25:3393-404 (2009), 2) Ren et al. Front Cell Infect Microbiol 12:910970 (2022), 3) Hofstee et al. Infect Immun. 88(11):e00293-2

**PAPER #82**

**TITLE:** Impact of Social Deprivation on Cubital Tunnel Syndrome

**PRESENTING AUTHOR:** Janet Tran B.A.

**CO-AUTHOR(S):** Callista Zaronias B.A., Thomas Carroll M.D., Akhil Dondapati M.D., Bilal Mahmood M.D.

**LAB PI/MENTOR:** Dr. Bilal Mahmood, M.D.

**ABSTRACT**

Purpose: Cubital tunnel syndrome (CuTS) is the second most common peripheral nerve compression syndrome in the upper extremity. The Area Deprivation Index (ADI) measures social deprivation using several domains such as education, income/employment, and housing environment based on zip codes. The aim of this study is to investigate the impact of social deprivation on the presenting electrodiagnostic severity of CuTS and on the treatment timeline of CuTS patients undergoing surgery.

Methods: This is a retrospective study evaluating patients presenting to an academic institution who were diagnosed with CuTS and underwent surgical intervention in a 6-year period. Variables including age, gender, BMI, ADI, electrodiagnostic severity classification, and time elapsed between several treatment milestones were obtained from 277 cases. Treatment milestones included referral to and initial evaluation by hand surgery, date of electrodiagnostic studies, surgical decision date, and surgical date. Study inclusion criteria include a ICD-10 code for cubital tunnel syndrome (G56.20) or a CPT code for ulnar nerve decompression (64718) and a valid 9-digit zip code. Patients treated in the setting of trauma, ipsilateral revision, or second contralateral diagnosis were excluded. Patients who obtained EDX studies prior to presentation were excluded in analysis of time elapsed between EDX studies and treatment milestones. Patients were grouped into thirds of ADI national percentiles. Higher ADI percentiles indicate a greater degree of deprivation.

Results: Current data included 383 patients divided by ADI national percentiles from least to most deprived thirds: low (n=30), middle (n=152), and upper (n=201) Patients in the lowest third had significantly shorter time between initial presentation to date of surgery compared to the middle third (116 vs. 196 days, p=0.02) and upper third (116 vs. 204 days, p=0.01) of percentiles. Additionally, patients in the lowest third compared to the highest third of percentiles had significantly shorter time between initial presentation to date of EDX studies (41 vs. 70 days, p=0.02) and surgical decision (47 vs. 107 days, p=0.01). The proportion of electrodiagnostically severe CuTS exhibits a trend of increasing with increasing social deprivation. This does not meet statistical significance at the current sample sizes.

Conclusions: Increasing social deprivation correlates with a prolonged time from presentation to the surgery. Delays in completing different treatment milestones may contribute to this in an additive fashion. We also note a trend towards more advanced disease in the more socially deprived groups. Defining and acting on factors that result in this delayed care represents an area of improvement for healthcare systems.

**PAPER #83**

**TITLE:** Targeting TRPC6 for Discogenic Chronic Back Pain

**PRESENTING AUTHOR:** Janitri Venkatachala Babu

**CO-AUTHOR(S):** Alexandra Sadowska, Addisu Mesfin, Varun Puvanesarajah, Karin Wuertz-Kozak

**LAB PI/MENTOR:** Karin Wuertz-Kozak

**ABSTRACT**

INTRODUCTION: Discogenic chronic back pain (DCBP) arising from the degenerated intervertebral disc (IVD) is a significant contributor that accounts for 42% of back pain cases and is characterized by increased levels of pro-inflammatory cytokines at the degenerated site irritating the ingrowing nerve fibers causing nociception. The existing treatments like physical therapy, oral pain medication, and surgery address the symptoms but not the underlying causes. Identifying effective pharmacological interventions for DCBP is challenging due to a limited understanding of the molecular processes involved. In efforts to identify new drug targets for DCBP, transient receptor potential (TRP) channels are particularly promising. TRP channels are a superfamily of 28 multimodal cation-selective trans-membrane receptors activated by a wide array of stimuli eliciting various cellular responses. In the context of DCBP, the canonical subtype 6 (TRPC6) is noteworthy for its role in regulating inflammation in various tissues. Therefore, we hypothesize that TRPC6 activation in IVD cells through pharmacological modulators will increase catabolism and inflammation, the key characteristics of DCBP. We further hypothesize that pharmacological inhibition of TRPC6 will mitigate inflammation and catabolism in vitro and alleviate pain in vivo, presenting a novel non-opioid pharmacological therapeutic for DCBP.
METHODS: Human IVD samples of degenerated (n=22) and non-degenerated (n=12) discs were used for direct mRNA isolation and TRPC6 expression was analyzed using RT-qPCR. The modulation of TRPC6 channel activity in isolated human IVD cells (n=3) was assessed following treatment with different concentrations of either a pharmacological activator (HYP9) or inhibitor (larixyl acetate) by measuring calcium flux (Flex Station reader, Fura-2 QBTTM Calcium kit). To determine effects of TRPC6 activation on gene expression, human IVD cells (n=7) were exposed to HYP9 (1 µM) for 18 hours, followed by mRNA isolation and qPCR analysis of proinflammatory cytokines. Furthermore, IVD cells (n=3) were treated with a TRPC6 specific inhibitor, larixyl acetate (1 µM or 10 µM for 18 hours) after 2 hours of pre-treatment with HYP9 (1 µM), with subsequent qPCR. Untreated cells and vehicle controls were included. All the statistical tests (normality test, t-tests, one-way ANOVA) were done using GraphPad Prism 10.0.2 for Windows (GraphPad Software).
RESULTS: TRPC6 exhibits significantly elevated expression levels in the degenerated human IVDs compared to healthy controls, with particularly pronounced upregulation in IVDs associated with pain. The pharmacological activation of TRPC6 using HYP9 elicited a dose-dependent influx of calcium ions in human IVD cells, while pharmacological inhibition with larixyl acetate reduced calcium ion influx. TRPC6 activation resulted in a significant increase in mRNA levels of matrix-degrading enzymes, including MMP1 ($p<0.05$), MMP2 ($p<0.05$), and MMP3 ($p<0.05$), as well as neurotrophic factors like NGF ($p<0.05$) and BDNF ($p<0.05$), and inflammatory cytokines such as IL6 ($p<0.05$), IL8 ($p<0.05$), and COX2 ($p=0.053$). The targeted inhibition of TRPC6 reversed the effect by significantly decreasing mRNA expression of matrix-degrading enzymes, including MMP1 ($p<0.01$) and MMP3 ($p<0.05$), as well as neurotrophic factors like NGF ($p<0.05$) and inflammatory cytokines, including COX2 ($p<0.01$).
DISCUSSION: Due to the increased expression of TRPC6 in degeneration, this channel constitutes a potential therapeutic target for DCBP. Our results of pharmacological TRPC6 activation in vitro show an inflammatory response, whereas the use of a pharmacological inhibitor reverses the catabolic inflammatory responses in vitro. These findings highlight the potential of modulating TRPC6 as a molecularly targeted therapy to mitigate degenerative processes in IVDs. Further experimentation in vitro and in vivo will validate the role of TRPC6 in IVD degeneration and pathophysiology.

**PAPER #84**

**TITLE:** Bone increase in mice with global Axl loss of function is not due to changes in embryonic skeletal development

**PRESENTING AUTHOR:** Valerie Voytsekhovskaya

**CO-AUTHOR(S):** Emily R. Quarato, Ronald Lakony, Noah A. Salama

**LAB PI/MENTOR:** Laura M. Calvi, MD

**ABSTRACT**

Osteoporosis, a condition of low bone mineral density and mass, is an increasingly prevalent public health issue affecting 200 million people worldwide. The condition increases risk for injuries, contributing to 1.5 million fractures in the US, and is a financial burden projected to incur over $1.5 billion in cost over the next decade. While it is well known that bone loss is closely linked to aging, the cellular mechanisms behind this process are not well understood. Previous research has shown that mesenchymal stem/stromal cells (MSCs), which can differentiate into bone cells, become senescent with aging. However, the mechanisms that induce MSC senescence are not well characterized. We discovered that MSCs can clear apoptotic cells, a process known as efferocytosis, which increases with aging. This previously unknown function of MSCs led us to hypothesize that excessive MSC efferocytosis may cause cellular senescence; consequently, reducing MSC efferocytic activity could potentially protect their ability to support bone health. Through RNA sequencing and pharmacologic studies, we identified Axl as a key efferocytic receptor of MSCs, and developed a global Axl knockout (Axl KO) mouse model. Compared to their wild type (WT) counterparts, the Axl KO mice were found to have decreased MSC efferocytic activity in vitro and in vivo, a lower rate of cellular senescence, and higher bone mineral density at 3 and 24 months old. Overall, our findings support Axl as a potential therapeutic intervention to maintain or restore bone mass.

Given the increased bone density at 3 months of age in mice lacking Axl, we wanted to test whether increased bone density may already be present at birth, indicating a role for Axl in skeletal development. We hypothesized that if P0 Axl KO and WT pups are born with similar bone anatomy, then differences seen at 3-24 months would not be due to inhibition of Axl and decreased MSC efferocytic activity during embryonal development. To make this assessment, whole mount skeletal staining, using Alcian blue to stain cartilage and Alizarin red to stain ossified bone, was performed on dissected P0 Axl KO and WT pups. The final skeletons were then imaged with a scanner and enhanced using ImageJ. Upon initial analysis, no significant differences were observed visually. Further analysis via ImageJ measuring the lengths and widths of the tibia, femur, spine, ribs, and the area of cartilage found no significant differences in Axl KO and WT pups, regardless of sex. These findings suggest that global inhibition of Axl may have positive late life impacts by accelerating bone development in youth and slowing bone loss in age. Given the reliance of MSC efferocytosis on Axl, this makes Axl a potential therapeutic target for the treatment of bone loss and osteoporosis.

**PAPER #85**

**TITLE:** Achilles Tendon Impingement Elicits Spatially-Dependent Change in Aggrecan Metabolism

**PRESENTING AUTHOR:** Brian Wise

**CO-AUTHOR(S):**

**LAB PI/MENTOR:** Whasil Lee, Mark Buckley

**ABSTRACT**

Tendon impingement generates a unique mechanical strain environment with markedly elevated transverse compressive strain that drives anabolism of glycosaminoglycan (GAG)-rich macromolecules such as aggrecan, yielding a localized fibrocartilage phenotype with compressive load bearing capacity. While this fibrocartilaginous tissue is present in impinged regions of healthy tendon, aberrant proteoglycan metabolism and excessive fibrocartilage formation is a hallmark feature of tendinopathy, which frequently colocalizes to impinged regions. Accordingly, tendon impingement is clinically recognized as an extrinsic factor in tendinopathy pathogenesis. Nevertheless, mechanobiology underlying tendon impingement remains understudied, which obscures our understanding of degenerative disease and impedes the development of superior therapeutic modalities. Prior studies have demonstrated that uniaxial compression of excised tendon explants stimulates aggrecan biosynthesis and regulates proteolytic turnover. This is noteworthy considering altered proteoglycan catabolism has been identified in tendon disease. Despite these observations, aggrecan metabolism within the multiaxial, spatially heterogeneous strain environment generated by tendon impingement has yet to be characterized. In this regard, our lab has developed a novel murine hind limb explant model for studying mechanobiology secondary to impingement of the calcaneus upon the Achilles tendon insertion via passively applied ankle dorsiflexion while maintaining viability across 7 days. By preserving anatomical structures of the impinged region in situ, this model reproduces physiologically relevant strain patterns through controlled prescription of mechanical impingement and can be interfaced with ultrasound/multiphoton imaging to quantify tissue strains. Previously, we reported altered GAG staining and collagen disorganization elicited by impingement within this model, indicative of fibrocartilage formation. Here, we seek to investigate the molecular basis of impingement-driven GAG augmentation, which we hypothesize is attributed to altered aggrecan metabolism within the extracellular and pericellular space. Explants were loaded into our platform to maintain the Achilles tendon insertion under static impingement for 7 days, while contralateral limbs were cultured unloaded. Level-matched tissue sections from contralateral limbs were immunolabeled using anti-Aggrecan antibodies targeting AA610-709, a region present in many GAG-rich fragments generated by constitutive aggrecanase activity that are retained in the tissue during culture. Adjacent level-matched sections were labeled using antibodies targeting AA1177-1326, a region spanning a high-affinity site of aggrecanase proteolysis that remains intact in nondegraded aggrecan. Fluorescence quantification demonstrated spatial change in both GAG-rich aggrecan fragments and nondegraded aggrecan secondary to impingement. Significant accumulation of GAG-rich aggrecan fragments were detected distally, deep within the tendon insertion adjacent to the calcaneus where we have previously measured maximum transverse compressive strain, elevated GAG staining and collagen disorganization, suggesting GAG enrichment driven by impingement may reflect changes in aggrecan metabolism regulated by compressive strain. Additionally, nondegraded aggrecan was confined to the pericellular space and was significantly altered by impingement in proximal and superficial regions, suggesting cells in these regions may adapt to exaggerated magnitudes of compressive strain via increased deposition and/or decreased catabolism of newly synthesized aggrecan within the pericellular matrix. In the future, we will continue to characterize impingement-driven change in aggrecan metabolism using protease-specific neoepitope antibodies and GAG-specific antibodies, with the goal of relating these changes to nanomechanical compressive properties via atomic force microscopy.

**PAPER #86**

**TITLE:** Longitudinal µCT Image Analysis for User-Defined Region of Interest in Critical-Sized Bone Defects

**PRESENTING AUTHOR:** Anthony Yosick and Bei Liu

**CO-AUTHOR(S):**

**LAB PI/MENTOR:** Dr. Hani Awad

**ABSTRACT**

INTRODUCTION: µCT imaging analysis of bone volume is a necessary quantitative tool for studying bone regeneration potential and outcomes within longitudinal in vivo studies. Established methods for bone segmentation utilize Amira software for whole bone uCT segmentation and alignment of complex anatomical structures but are limited in abilities of user-defined region of interest (ROI) analysis. We present a protocol expanding upon these methods to permit user-defined ROI bone volume analysis surrounding a critical sized bone defect for week-to-week longitudinal in vivo rat models.

METHODS: Longitudinal µCT images were collected at weeks 0, 2, 4, 6, 8, and 10 of 3mm critical rat radial defects treated with one of three polycaprolactone (PCL) based scaffold groups (n=9 per scaffold group, 27 animals total): carboxymethyl chitosan-amorphous calcium phosphate nanoparticles (NP), calcium phosphate (CaP), and PCL control. All animal use was performed in accordance with protocols approved by the University of Rochester's Committee on Animal Resources (UCAR). It has previously been established that DICOMs can be segmented in Amira software using a watershed-based segmentation. Amira software alignment modules are used to align and overlay segmentation volumes between weeks. For all scaffold models, regardless of apparent scaffold in µCT images at week 0, variations in the region of radius and ulna captured in µCT images between weeks require a consistent ROI to characterize and consistently compare bone volume changes. To specify a dimensional basis for the segmented volumes within Amira software, µCT slice thickness perpendicular to the long axis of the radius was exploited to establish a consistent ROI. Using the Ortho Slice module in the Amira software, the ROI was determined by locating the furthest slice both proximally and distally at the critical defect of the week 0 segmented image. These slices were adjusted 25 slices away from the proximal and distal ends to encompass the defect region. Given alignment of week 0 and a subsequent week, an additional Ortho Slice module is applied to determine the corresponding slices for the ROI. Provided proper determination of slice numbers for week 0 and the subsequent week, the difference between the slices will be equivalent indicating a consistent ROI between weeks. Through use of an Arithmetic module within the Amira software, the difference in bone volume can be determined between each week.

RESULTS: The current protocol consistently generated ROIs for the NP, CAP, and PCL groups at different experimental time points by selecting proximal and distal slices to encompass the bone defect region. Bone volume in the defect region was quantified and compared between these groups, revealing that new bone formation is significantly greater in the NP group at the 10-week post-operative stage compared to the CAP and PCL groups.

DISCUSSION: This longitudinal µCT image analysis proves particularly advantageous when studying critical-sized bone defects in week-to-week longitudinal in vivo rat models. It overcomes the limitation of comparative analysis between different scaffold groups caused by minor variations in µCT scan locations. Future studies should prioritize the validation of the protocol's repeatability and reproducibility through inter- and intra-user assessments. These efforts will enhance the reliability of this approach and strengthen its effectiveness in bone regeneration research.

SIGNIFICANCE: Established segmentation protocols provide a robust, high-accuracy method for segmentation, alignment, and analysis but present limitations for user-defined ROI. This method leverages the validated process' strengths and allows for a consistent, quantitative process when a variable region of µCT images is present. While this process was designed for analysis of critical bone defects, it can readily be applied to other classifications of bone beyond appendicular long bone studies.

**PAPER #87**

**TITLE:** Sex-dependent Piezo1 and Piezo2 Functional expression in articular cartilage

**PRESENTING AUTHOR:** Yaxin Zhang

**CO-AUTHOR(S):** Alexander Kotelsky, Johann Kintzel, Whasil Lee

**LAB PI/MENTOR:** Whasil Lee

**ABSTRACT**

Osteoarthritis (OA) is a common and incapacitating joint condition that demonstrates sex-dependent impacts on individuals.(Srikanth et al., 2005) Within the realm of molecular investigations into OA, there are increased research attention understanding the role of mechanosensitive ion channels in the pathogenesis of OA. Articular cartilage, the avascular and load-bearing tissue that lines joint surfaces, relies on the intricate interplay of chondrocytes residing in distinct zones to maintain tissue homeostasis. Piezo channels, well-known for their capacity to convert mechanical stimuli into intracellular messages, play a pivotal role in chondrocyte mechanosensory functions, influencing various cellular processes relevant to OA pathogenesis.(Gao et al., 2022) In this study, our goal is to quantify sex-dependent expression of Piezo1 and Piezo2 channels and mechanical susceptibility of articular chondrocytes using murine and porcine knee joints. Ethical approval was obtained by the UCAR committee (Protocol#: 2019-008). Tissue harvest: C57BL6/J mice (12~16-weeks old, N=4/group) were sacrificed and hindlimbs were harvested. Porcine chondrocytes plugs harvested from the femoral condyles of skeletally mature pigs with a biopsy punch. Mechno-death assay: Murine femoral cartilage and porcine cartilage plugs were subjected to mechanical injury using a custom-built injury device Immunohistochemistry: Mouse knee and porcine cartilage plugs were fixed, paraffin-imbeded, sectioned sagittally (7 or 8 μm), labeled with Piezo1 and Piezo2 antibodies (Novus, Inc. NBP2-75617, NBP1-78624), and imaged by Keyence microscope. First, we observed a sex-dependent mechanosensitive in femoral cartilage that female porcine sample presented a wider mechano-cell death after mechanical injury. At the same time, a higher expression level of Piezo1 channel exhibited in female mice and higher expression level of Piezo1&2 channels in female porcine. Meanwhile, Piezo1&2 channel shared a higher positive cell percentage, but lower cell intensity expression in superficial zone of femoral cartilage in female porcine compared with transitional zone. We showed the heterogeneity of sex-dependent mechanosensitivity both in mice and porcine femoral cartilage, demonstrating both a wider mechano-cell death response following mechanical injury and higher expression levels of Piezo1 channels in female. Many studies have announced the mechanical properties and mechanical signaling change in superficial zone of articular cartilage in osteoarthritis, (Panula et al., 1998), and Piezo1&2 channels have been showed that is highly related to the mechano-sensing and osteoarthritis progression in chondrocytes of articular cartilage(Gao et al., 2022; Lee et al., 2014). Our results further indicated that Piezo1 and Piezo2 channels exhibit a distinct spatial distribution within the femoral cartilage of female porcine subjects. Specifically, a higher percentage of cells positive for these channels was observed in the superficial zone; however, in terms of expression levels, Piezo1 and Piezo2 displayed elevated expression levels in the transitional zone. This spatial divergence in Piezo channel distribution and expression suggests that different zones within the cartilage may possess unique mechanosensory mechanisms, which could potentially influence cartilage responses to mechanical stimuli. Harkey and his group study also showed that only female cartilage structure was related to the metabolism at rest and acutely following walking and drop-landing in healthy individuals (Harkey et al., 2021). Further research is warranted to elucidate the functional implications of these spatial variations and their role in cartilage homeostasis and pathology.

**PAPER #88**

**TITLE:** Diversity among academic sports medicine surgeons in the United States

**PRESENTING AUTHOR:** William Zhuang

**CO-AUTHOR(S):** Andrew Jeong, Patrick Castle, Jonathan Minto, Michaela Malin, Kismat Touhid

**LAB PI/MENTOR:** Dr. Sandeep Mannava

**ABSTRACT**

1. Objectives
The purpose of this study was to conduct a cross-sectional analysis on the diversity of academic sports medicine surgeons in the United States.
2. Methods
Surgeons were identified using the American Orthopedic Society for Sports Medicine (AOSSM) membership database, including individuals who had completed fellowship training and are practicing in academia. Demographic data (age and race), academic rank, leadership positions held, years in practice, practice setting (urban vs. rural), and work address were obtained from the AOSSM membership directory and publicly available profession profiles. National area deprivation index (ADI) decile of work addresses as a measure of socioeconomic deprivation was subsequently calculated. Surgeons without a work address in the U.S. or who were still undergoing residency or fellowship training were excluded.
ADI scores were evaluated with linear regression, while years in practice were evaluated with negative binomial regression to account for the skew in distribution. Practice setting and leadership status were assessed using logistic regression. Academic rank was evaluated using ordered logistic regression.
No institutional review board approval was required for this survey study.
3. Results
Of the 554 surgeons who met the inclusion criteria, 86.28% were male and 13.72% were female. 82.67% were white, 11.19% were Asian, 4.69% were black, and 1.44% were Hispanic. 82.13% of surgeons held an academic rank. Of those who did, 0.54% were instructors, 31.95% were assistant professors, 22.02% were associate professors, 27.62% were professors. Under half of the surgeons included did not have at least one leadership position (43.68%). Over half of the surgeons evaluated practiced in an urban setting (57.94%). The average ADI of work addresses was 35.64%. The average years in practice was 13.9 years.
Statistical analysis revealed that neither gender nor race significantly impacted the attainment of academic rank, leadership status, or ADI of work setting. However, male surgeons were found to have a higher probability of practicing in a rural setting compared to their female counterparts (44.40 vs. 27.40, P = 0.002). Black and Hispanic surgeons had a 14.26% lower probability of practicing in a rural setting than their white counterparts, although this was not significant (-29.94, 1.41, P = 0.074). Analysis further revealed that male surgeons on average had more years in practice compared to their female counterparts by 4.16 years (14.46 vs. 10.30, P < 0.001). Asian surgeons on average had 4.58 years less experience than their white counterparts (-7.02, -2.14, P<0.001).
4. Conclusion
The analysis demonstrates that female continue to be underrepresented despite recent increases in females entering the field of orthopedic surgery. White and Asian surgeons are overrepresented while black and Hispanic surgeons are underrepresented. Despite female, black and Hispanic individuals being underrepresented in orthopedic sports medicine, this study's analysis found that there was no correlation between a surgeons gender and their attainment of any level of academic rank. Further analysis is needed to elucidate the reasons behind this phenomenon. The finding that male surgeons are more likely to practice in rural areas suggests that there may be confounding factors influencing the practice setting based on gender or race. Additional studies are needed to understand the opportunities and factors influencing a physician's decisions to enter urban or rural practice. Overall, the results suggest that there are still opportunities to increase the rates of females, black, and Hispanic individuals entering the field of orthopedic sports medicine. Increasing diversity within academic orthopedic sports medicine is much needed as the population of patients in the U.S. continues to become more heterogenous, warranting a pool of physicians that must become equally diverse to meet its needs.

**PAPER #89**

**TITLE:** The Effects of Slit3 on Angiogenesis and Osteogenesis of Bone Marrow Cells Isolated from AplinCreERT2 and BMXCreERT2 Mice

**PRESENTING AUTHOR:** Wendy Zimmerman

**CO-AUTHOR(S):**

**LAB PI/MENTOR:** Xinping Zhang

**ABSTRACT**

The neural network of sensory and sympathetic neurons, which innervate bone through the periosteum, has an influence in directing bone remodeling and skeletal development. Experiments have found evidence to support the direct communication of neurite and osteoblastic cells through in vitro co-culture experiments with murine superior cervical ganglia neurons and MC3T3-E1 osteoblast-like cells and direct neurite and osteoclastic cell communication through in vitro co-culture of murine superior cervical ganglia and mouse osteoclast-like cells, with both experiments using scorpion venom to induce neurite activity. Additionally, femoral and sciatic resection was shown to cause calluses to regain less of their mechanical properties and have worse fracture healing in rats and rabbits with tibial fractures. Among the molecules that regulate the development of both the skeletal and neural systems are Slit and Robo. The Slit family controls axon repulsion and guidance through its binding to Robo receptors, a family of transmembrane proteins within the immunoglobulin superfamilies. Slit/Robo signaling has been shown to promote angiogenesis through experiments such as Slit3 and Robo4 knock-outs, which resulted in a reduction in vessel formation. Both osteoblasts and osteoclasts express Slit2 and Slit3. The genetic deletion of Slit3, which reduced skeletal CD31hlEMCNhl endothelium resulting in a low bone mass due to impaired bone formation, suggests that osteoblasts use Slit3 production to condition their environment to be conductive for bone formation through angiogenesis. Deficiency in Slit3 has also been noted to decrease in bone formation and an increase in bone resorption and Slit3 can be used for therapeutic effects in fracture healing and osteoporosis.
The effect of Slit3 on angiogenesis and osteogenesis on bone marrow cells isolated from Col I (2.3) GFP; AplinCreERT2; Ai14 mice was examined in vitro using electrospun nanofiber membranes with incorporated dosages of 0,0.5, and 5 µg/mL of the Slit3 peptide. It was found that the average percent area of the membrane covered by blood vessels was greater in the 0.5 µg/mL dosage membrane, followed by the 0 µg/mL and 5 µg/mL dosages respectively. The average bone cell nodule area and number of nodules was found to be greater in the 0 µg/mL group, followed by the 0.5 µg/mL and 5 µg/mL groups respectively. Some inconsistencies were observed within the dosage groups due to variations in the thickness of fibers. While the results did not yield conclusive results, they do inform on improvements that can be made for future experiments, specifically, in the making of the electrospun nanofiber membranes to maintain consistency.
An experiment directly administering the Slit3 factor in dosages of 0 and 500 ng/mL was conducted to observe the effects of angiogenesis and osteogenesis in bone marrow cells isolated from Col I (2.3) GFP; BMXCreERT2; Ai14 mice. It was found that in early and later stages of the culture, the wells with 500 ng/mL of Slit3 had a greater average percent of area covered by blood vessels. The wells that had the 500 ng/mL of Slit3 also had a greater number of bone cell nodules and percent area covered, but the 0 ng/mL wells had a greater average maximum bone cell nodule size. Although none of the results are statistically significant, the sample size used was small and further experiments are on the way to elucidate a clearer relationship between Slit3 and its effect on angiogenesis and osteogenesis.

**PAPER #90**

**TITLE:** Disability and Function Outcome Measurements Reports for Patients with Musculoskeletal Disorders

**PRESENTING AUTHOR:** Jose Corredor

**CO-AUTHOR(S):** Lu H, Wong D, Chang I, Guida T, Gilbreath H, Schillinger E, Jablonski J, Tome J, Haddas R

**LAB PI/MENTOR:** Haddas, R

## ABSTRACT

**INTRODUCTION:** Musculoskeletal disorders are a major public health concern that affect the quality of life of people and represent a significant financial burden for both patients and society. Around 1.71 billion people live with musculoskeletal conditions globally [1]. Current methods to assess musculoskeletal disorders include Patient Recorded Outcome Measures (PROMs). While these standardized questionnaires offer a holistic view of the quality of life of the patient, they may fail to correlate with clinical and functional outcomes, and can be subjected to varying interpretations [2,3]. Motion laboratories, which can operate 3D motion capture coupled with pressure plates, electromyography (EMG), electroencephalography (EEG), and other tools, can generate Function Outcome Measurements (DFOMs) and may therefore provide an alternative to obtain quantifiable and objective outcome measures. Therefore, the purpose of the study was to generate reports containing DFOMs for clinical patients suffering from a broad range of musculoskeletal disorders through the use of motion laboratories.

**METHODS:** Batteries of tests were developed for spine, shoulder, hip and foot and ankle patients, and these included basic everyday activities such as gait, balance, timed up-and-go (TUG), lifting and personal care. Data from tests was processed through inverse kinematics and kinetics to convert external forces and trajectories into valuable information of the patient's musculoskeletal health such as internal forces, moments and ranges of motion (ROM). After the data was processed, the key variables needed to assess DFOMs were exported into clinical reports that physicians may readily access to get a multidimensional depiction of the state of their patients. Graphics were used to visualize key DFOMs before and after medical intervention.

**RESULTS:** Spine and shoulder reports with DFOMs were generated for three healthy control patients. In the spine reports, gait, balance, lifting and TUG activities were used to generate these reports with DFOMs. From gait, variables such as cadence, limp index, and peak ankle dorsiflexion were assessed. Balance outputted range of sway, total sway, and peak angles. Symmetric lifting was used to measure ROMs in the sagittal and coronal planes, and maximum trunk and pelvis rotation in the transverse plane were obtained for asymmetrical lifting. In TUG, max angles, timing of liftoff and sit, and peak forces at max trunk flexion were measured effectively. For the shoulder report, the drinking activity was used to obtain key DFOMs of kinematics like the max shoulder flexion, external rotation and completion time, as well as DFOMs of compensation like the max shoulder abduction, max trunk lean and flexion. Key DFOMs were also obtained for the rest of the activities in the shoulder report.

**DISCUSSION**: The proposed clinical reports can be used in clinical environment to quantify outcomes in musculoskeletal and neurological disorders patients. Information related to the electrical activity of muscles (EMG), nerves and brain (EEG) can provide further direct measures in more-detailed evaluations. Additionally, recordings of the activities provided useful visual aids for clinicians and patients to understand their musculoskeletal condition and intervention effects.

**SIGNIFICANCE/CLINICAL RELEVANCE:** Clinical DFOMs reports generated at motion labs are able to provide important information for the tracking of pre- and post-surgery musculoskeletal disorder patients, as it provides objective and quantitative information to assess the musculoskeletal health of patients.

References:

1. "Musculoskeletal Health." *World Health Organization*, World Health Organization, www.who.int/news-room/fact-sheets/detail/musculoskeletal-conditions. Accessed 6 Sept. 2023.
2. *McKeon, M., Manson, N., Abraham, E., Taylor, E., Murray, J., & Albert, W. (2015). Patient-reported disability versus objective physical performance measures in assessing patient recovery. Canadian Journal of Surgery, 58, S46-S47.*
3. *Parker, S. L., Adogwa, O., Paul, A. R., Anderson, W. N., Aaronson, O., Cheng, J. S., & McGirt, M. J. (2011). Utility of minimum clinically important difference in assessing pain, disability, and health state after transforaminal lumbar interbody fusion for degenerative lumbar spondylolisthesis. Journal of Neurosurgery: Spine, 14(5), 598-604.*

**PAPER #91**

**TITLE:** An Objective Assessment of Low Back Disorder Patients' Disability and Function using a Wearable Inertial Measurement Unit

**PRESENTING AUTHOR:** Hansen Lu

**CO-AUTHOR(S):** Corredor J, Guida T, Jablonski J, Tome J, Haddas R

**LAB PI/MENTOR:** Haddas R

## ABSTRACT

**Introduction:** Low back pain and disorders are prevalent musculoskeletal concerns. Limitations in clinician accessibility, patient interaction time, and diagnostic resource availability, hinders understanding of patient motion. Disability and Function Outcome Measurements (DFOMs), which provide objective quantitative evaluations of physical function using tools such as motion capture, electromyography (EMG), and force plates, are gradually finding their place in standard orthopedic and spine care. However, their adoption necessitates elaborate motion capture labs, with considerable expenses and limited accessibility. Spine-specific wearables hold promise for overcoming current limitations on data gathering for DFOMs. This study explores the potential of affordable, wearable Inertial Measurement Units (IMUs) that capture continuous data of a patient's natural movements to assess DFOMs in spine patients and controls.

**Methods:** Spine-specific wearables were placed on T1 to capture movements in 12 Lumbar Degenerative (LD) patients and 12 healthy controls. A movement detection algorithm categorized data by associated tasks. The participants are required to perform tasks including Romberg tests, stair climbing, timed up and go, and walking. Participants wore the device for 72 hours, performing tasks twice daily while completing clinical questionnaires including Patient Reported Outcome Measurements (PROMs), Opioid consumption and psychological assessments.

**Results:** The wearable device captured the activity time intervals and 3D kinematic parameters of the trunk in LD patients and control to measure the DFOMs from routine tasks such as walking, standing, sitting, laying down and driving. Key variables from the wearable includes patient sway, balance effort, and gait parameters. In comparison to the control subjects (walking: 8.9%, standing: 19.1%, sitting: 17.1%, and laying down: 36.2% of the day, trunk flexion: 10.3°; $p<0.05$), LD patients exhibited lower free-living physical function and reduced trunk kinematics (walking: 4.7%, standing: 11.6%, sitting: 25.3%, and laying down: 41.7% of the day, trunk flexion: 15.8°) at their home-based environment. LD patients also demonstrated reduced balance and higher gait sway (balance effort: 25.6°, walking: 0.8 m/s, sway: sagittal: 7.9°, coronal: 7.2°) compared to controls (balance effort: 14.6°, walking: 1.0 m/s, sway: sagittal: 5.8°, coronal: 3.2°). Lastly, DFOMs was found to have strong correlations to the PROMIS scores ($r^2$ >0.55, $p<0.05$).

**Discussion:** This study validates spine specific wearables in assessing movement patterns, identifying distinctions between low back disorder patients and controls. This technology enables the continuous collection of extensive data over prolonged periods, enhances the robustness of the findings. This technology hold the potential to equip PM&R physicians, physical therapists, and athletic trainers with the necessary information to make well-informed decisions regarding patient specific care, while simultaneously empowering patients by granting them access to personalized health data. The incorporation of spine specific wearable devices alongside patient-reported outcomes, psychological status assessment, and medication intake data into patient care regimens has a huge potential to optimize patient specific treatment and elevate the established standard of care conveniently, affordably.

**Significance/Clinical Relevance:** The realm of wearable technology is a rapidly advancing sector, poised to offer crucial health insights to both patients and surgeons. By integrating wearable devices with DFOMs with PROMIS data, and radiographic measurements, a holistic assessment of a patient's spinal health can be achieved. This comprehensive approach enhances the physician's ability to make informed decisions and tailor treatment based on the specific need of the patient.